



This is to certify that the

dissertation entitled

SYNTHESIS AND CHARACTERIZATION OF RIGID POLYMER
SYSTEMS: SUBSTITUTED POLY(p-PHENYLENE)S, POLYACENIC
NETWORKS, AND POLY(TRIMETHYLSILYLPROPYLENE) COPOLYMERS

presented by

Cory J. Ruud

has been accepted towards fulfillment
of the requirements for

Ph.D. degree in Chemistry


Major professor

Date 8/11/99



PLACE IN RETURN BOX to remove this checkout from your record.
TO AVOID FINES return on or before date due.
MAY BE RECALLED with earlier due date if requested.

DATE DUE	DATE DUE	DATE DUE
NOV 15 2007		

**SYNTHESIS AND CHARACTERIZATION OF RIGID POLYMER SYSTEMS:
SUBSTITUTED POLY(*p*-PHENYLENE)S, POLYACENIC NETWORKS, AND
POLY(TRIMETHYLSILYLPROPYNE) COPOLYMERS**

By

Cory J. Ruud

A DISSERTATION

Submitted to
Michigan State University
in partial fulfillment of the requirements
for the degree of

DOCTOR OF PHILOSOPHY

Department of Chemistry

1999

ABSTRACT

SYNTHESIS AND CHARACTERIZATION OF RIGID POLYMER SYSTEMS: SUBSTITUTED POLY(*p*-PHENYLENE)S, POLYACENIC NETWORKS, AND POLY(TRIMETHYLSILYLPROPYNE) COPOLYMERS

By

Cory J. Ruud

The simplest mathematical model of a polymer chain in space is the freely jointed chain. It is defined as a chain having n links, each of length L , joined in a linear sequence with no restrictions on the angles between successive bonds. The model is equivalent to a random walk by a particle where n is the number of jumps by the particle and L is the length of each jump, and can be characterized by the net displacement or its end-to-end distance of the random walk. To characterize a polymer's behavior in solution, it is common to define its characteristic ratio, the ratio of the end-to-end distance of the real polymer to that of a freely jointed polymer of the same molecular weight. Flexible polymers like polyethylene or poly(ethylene oxide) usually have small characteristic ratios because of low barriers of rotation about the polymer backbone, and high degrees of polymerization. Rigid polymers, however, typically have large characteristic ratios. Rigidity in polymers occurs when the backbone is locked into a particular conformation by chemical bonding or by large rotational barriers. Usually, flexible polymers are associated with coiled backbones while rigid polymers in solution have rod-like geometries. This is true in the cases of poly(*p*-phenylene) (PPP) and polyacene. The structure of

PPP consists of a series of aromatic rings connected in a linear 1,4-substitution pattern. Since the carbon atoms in PPP are sp^2 hybridized, bond motion is limited to rotation about the central axis and PPP takes a rigid rod-like conformation. Polyacenes are the long chain members of the family of edge-fused aromatic compounds that includes naphthalene, anthracene, and higher homologs. Bond rotation within the acene backbone is impossible since all of the sp^2 carbons are conjugated forming a fused planar structure. The correspondence between chain rigidity and rod-like conformation apparently breaks down for substituted polyacetylenes like poly[1-trimethylsilyl-1-propyne] (PTMSP). The reported solution properties suggest a stiff polymer chain, yet PTMSP is highly soluble and amorphous with no report of liquid crystalline behavior. Large barriers of rotation about the backbone are caused by the steric interaction of the bulky trimethylsilyl and methyl groups, effectively preventing the polymer from changing its conformation. It is deduced that PTMSP has a rigid but disordered backbone contour, i.e., a rigid random coil conformation. The characteristic ratio of PTMSP is expected to be lower than that of rigid rod-like polymers, therefore the geometries of rigid polymers are not restricted to a particular shape.

The three polymer systems investigated: PPP, polyacene, and PTMSP each possess a set of unique electronic, optical and mechanical properties. However rigid polymers often exhibit poor solubility, which hinders efficient processing. Herein the physical properties and potential applications of these rigid polymer systems will be discussed.

ACKNOWLEDGMENTS

I would like to thank my advisor, Professor Greg Baker, for guiding me through this learning process. His friendship, patience and understanding have meant a great deal to me. I would also like to thank my committee members, Gary Blanchard and Mitch Smith, for their willingness to give “free advice” at a price.

I would like to thank the Baker group members, past and present, for their assistance and support throughout my journey. I would like to extend special thanks to Chun who has become a better chemist by learning from my mistakes. I wish them all happiness and success in the future.

Of course I could not continue without mentioning the excellent staff: Russ and Sam in the machine shop, the glass blowers: Manfred, Scott, and Keki, Ron and Scott in the electronics shop who kept our equipment running, Tom in the stockroom, and Bob who kept our lab livable. I would also like to thank Cindy, Carmen, Ann, Lisa, Cathie, and Diane who were always willing to go out of their way to help me.

Most importantly, I would like to thank my Mom and Sally for their constant support and encouragement.

TABLE OF CONTENTS

List of Tables.....	viii
List of Figures.....	ix

Chapter 1. Introduction

1.1. Structure/Property Relationships of Rigid Polymer Systems.....	1
1.1.1. Poly(<i>p</i> -phenylene)s.....	6
1.1.2. Poly(acene).....	10
1.1.3. Poly(1-trimethylsilyl-1-propyne).....	12
1.2. Syntheses of Rigid Polymer Systems.....	16
1.2.1. Poly(<i>p</i> -phenylene)s.....	16
1.2.2. Poly(acene).....	25
1.2.3. Poly(acetylene)s – Poly(1-trimethylsilyl-1-propyne).....	29
1.3. References.....	32

Chapter 2. Synthesis and Characterization of Ethylene Oxide Substituted Poly(*p*-phenylene)s.

2.1. Introduction.....	39
2.2. Experimental Section.....	42
2.3. Results.....	48
2.4. Discussion.....	69
2.5. Conclusions.....	77

2.6. References.....	78
----------------------	----

Chapter 3. Synthesis and Characterization of Polyacenic Networks.

3.1. Introduction.....	81
3.2. Experimental Section.....	83
3.3. Results.....	89
3.4. Discussion.....	103
3.5. Conclusions.....	107
3.6. References.....	108

Chapter 4. Synthesis and Characterization of Poly[(1-trimethylsilyl-1-propyne)-*co*-(1-(4-azidobutyldimethylsilyl)-1-propyne)] Copolymers.

4.1. Introduction.....	110
4.2. Experimental Section.....	113
4.3. Results.....	119
4.4. Discussion.....	142
4.5. Conclusions.....	150
4.6. References.....	151

Chapter 5. PTMSP as a Permeable Solid Support in Oxygen Sensor Applications.

5.1. Introduction.....	154
5.2. Experimental Section.....	159
5.3. Results.....	163

5.4. Discussion.....	178
5.5. Conclusions.....	181
5.6. References.....	182

LIST OF TABLES

Table		Page
Table 1.1	Solubility of phenylene oligomers in toluene at room temperature.....	7
Table 2.1	Representative molecular weights of polymers 5a-5h	53
Table 4.1	Elemental analyses of poly[(1-trimethylsilyl-1-propyne)- <i>co</i> -(1-(4-azidobutyl)dimethylsilyl)-1-propyne)] copolymers.....	125
Table 4.2	Permeability coefficients of oxygen and the O ₂ /N ₂ separation factor (α) at 23±1 °C of thermally cross-linked poly[(1-trimethylsilyl-1-propyne)- <i>co</i> -(1-(4-azidobutyl)-dimethylsilyl)-1-propyne)] copolymer membranes.....	146
Table 4.3	Permeability coefficients of oxygen and the O ₂ /N ₂ separation factor (α) at 23±1 °C of photo cross-linked poly[(1-trimethylsilyl-1-propyne)- <i>co</i> -(1-(4-azidobutyl)-dimethylsilyl)-1-propyne)] copolymer membranes.....	147

LIST OF FIGURES

Figure	Page
Figure 1.1	A random walk of a freely jointed chain.....1
Figure 1.2	Relationships between the characteristic ratio and rigidity in polymers.....2
Figure 1.3	Structures of a) poly(<i>p</i> -phenylene) and b) polyacene.....4
Figure 1.4	Structure of poly(1-trimethylsilyl-1-propyne).....5
Figure 1.5	Structure of a ladder poly(<i>p</i> -phenylene).....9
Figure 1.6	Possible electronic configurations of polyacene: (a) aromatic, (b) <i>cis</i> -quinoid, (c) <i>trans</i> -quinoid.....11
Figure 1.7	Hypothetical rotational barriers for disubstituted polyacetylenes where 0 degrees corresponds to an eclipsed conformation in which two double bonds are coplanar. (a). <i>trans</i> -polyacetylene, 6 Kcal/mol π barrier; (b) 20 Kcal/mol rotational barrier that simulates significant 1-3 steric interaction; (c) 100 Kcal/mol barrier that simulates polyenes with bulky substituents.....13
Figure 1.8	Polymerization of 1-bromo-4-lithiobenzene.....19
Figure 1.9	Polymerization of diiodoarenes.....20
Figure 1.10	Catalytic cycle of palladium mediated aryl coupling.....22
Figure 1.11	Polymerization of an enediyne.....23
Figure 1.12	Diels-Alder polymerization of biscyclopentadienones.....24
Figure 1.13	Synthesis of PPP via soluble poly(cyclohexadiene) Intermediates.....25
Figure 1.14	Polymerization of poly(ethynyl acetylene).....26
Figure 1.15	Polymerization of Langmuir-Blodgett films of diacetylenes.....27

Figure 1.16	Polymerization of cycloproparenes.....	28
Figure 1.17	Initiation and propagation of acetylene polymerization.....	31
Figure 2.1	Structure/property relationships of ethylene oxide substituted PPP's.....	41
Figure 2.2	Synthetic route to monomers 4a-4h	48
Figure 2.3	Melting points of monomers 4a-4h	49
Figure 2.4	Nickel catalyzed polymerization.....	50
Figure 2.5	Catalytic cycle of nickel mediated aryl coupling.....	51
Figure 2.6	Degrees of polymerization of polymers 5a-5h	54
Figure 2.7	Fluorescence spectra of a solution of polymer 5d in methanol excited at 317 nm.....	56
Figure 2.8	Comparison of the orientation of repeat units in 2,5-disubstituted and 2-substituted PPP's.....	57
Figure 2.9	Thermogravimetric analysis of a) 5b , b) 5c , and c) 5d in nitrogen heated at 10 °C/min.....	59
Figure 2.10	DSC results for polymers 5a-5h	60
Figure 2.11	Glass transition temperatures of polymers 5d-5h	61
Figure 2.12	Schematic representation of rigid rod PPP backbone substituted with flexible ethylene oxide side chains.....	62
Figure 2.13	Melting points of polymers 5g-5h	63
Figure 2.14	Effect of Li ⁺ salt on the Tg of polymer 5d	66
Figure 2.15	Effect of Li ⁺ salt on the Tg of polymer 5e	67
Figure 2.16	Schematic phase diagram of ethylene oxide substituted PPP's 5a-5h	70
Figure 2.17	Synthetic route to exact length ethylene glycol monomethyl ethers.....	71

Figure 2.18	Synthetic route to polymers 5a-5h with uniform backbone length.....	74
Figure 3.1	Polymerization of methoxymethylbenzene.....	89
Figure 3.2	Thermogravimetric analysis of the networks formed from monomers 1-3 heated in nitrogen at 10 °C/min.....	91
Figure 3.3	Thermogravimetric analysis of the networks formed from a) monomer 1 , and b) monomer 3 in a stagnant air environment heated at 10 °C/min.....	92
Figure 3.4	Idealized structures resulting from the polymerizations of the bis(methoxymethyl)benzenes 1-3	94
Figure 3.5	Infrared absorption spectra of the polybenzyl network formed from monomer 1 heated in nitrogen at 10 °C/min to a) 30 °C, b) 380 °C, c) 500 °C, d) 600 °C, and e) 800 °C.....	95
Figure 3.6	Synthesis of 1,4-bis(methoxymethyl)-2,5-dibromobenzene.....	97
Figure 3.7	Synthesis of substituted poly(<i>p</i> -phenylene) 6	98
Figure 3.8	Cross-linking of substituted PPP 6	99
Figure 3.9	Thermogravimetric analysis of a) substituted polymer 6 , and b) cross-linked network 7 in nitrogen heated at 10 °C/min.....	100
Figure 3.10	Infrared spectra of a) polymer 6 , b) network 7 , and c) carbon char of network 7 after thermal treatment at 700 °C.....	102
Figure 3.11	Alkyl substituted polyacene.....	104
Figure 3.12	Synthesis of a soluble polyacene precursor.....	105
Figure 3.13	Chemical dehydrogenation of polyacene precursor.....	106
Figure 4.1	Synthesis of azide-containing PTMSP via allylic bromination.....	119
Figure 4.2	Synthetic route to 1-(4-bromobutyldimethylsilyl)-1-propyne.....	122

Figure 4.3	Synthetic route to copolymers 6a-6g	123
Figure 4.4	FTIR spectra of PTMSP and copolymers 6a-6g	126
Figure 4.5	Integrated azide absorbance intensity at 2100 cm ⁻¹ versus the azide content in copolymers 6a-6g as calculated from the comonomer feed ratios.....	127
Figure 4.6	TGA of a) PTMSP under nitrogen; b) copolymer 6g under nitrogen; and c) copolymer 6g under air.....	129
Figure 4.7	DSC results for copolymers 6a-6g	131
Figure 4.8	Heat evolved during thermal decomposition of azide copolymers 6a-6g measured by DSC.....	132
Figure 4.9	FTIR spectra showing the thermal decomposition of copolymer 6f at 225 °C under vacuum.....	134
Figure 4.10	FTIR spectra showing the thermal decomposition of copolymer 6f at 250 °C under vacuum.....	135
Figure 4.11	FTIR spectra showing the thermal decomposition of copolymer 6f at 275 °C under vacuum.....	136
Figure 4.12	Loss of [N ₃] in copolymer 6f versus time at the indicated temperatures.....	137
Figure 4.13	Arrhenius plot of the rates of thermal decomposition of copolymer 6f	138
Figure 4.14	Swelling of thermally cross-linked films of copolymers 6a and 6f in solvents with different solubility parameters, δ ([J/m ³] ^{1/2} x 10 ⁻³).....	140
Figure 4.15	Swelling of thermally cross-linked films of copolymers 6a-6g in toluene.....	141
Figure 5.1	Structure of (Mo ₆ Cl ₁₂) _n clusters.....	155
Figure 5.2	Stern-Vollmer plot of emission intensity versus [O ₂].....	157
Figure 5.3	The UV/Vis absorption spectra of a) PTMSP and b) Mo ₆ Cl ₁₂ , and the fluorescence spectra of c) Mo ₆ Cl ₁₂	164

Figure 5.4	Synthesis of poly[(1-trimethylsilyl-1-propyne)- <i>co</i> -(1-(4-cyanobutyldimethylsilyl)-1-propyne)].....	166
Figure 5.5	Luminescence spectra from a Mo ₆ Cl ₁₂ /nitrile- PTMSP copolymer composite film in laboratory air (bottom curve) and under Ar (top curve).....	168
Figure 5.6	Observed emission from Fiber 1 in varying oxygen/nitrogen environments.....	171
Figure 5.7	Peroxide induced chain degradation of PTMSP.....	172
Figure 5.8	Observed emission intensity from Fiber 2 in nitrogen and a) 2.1%, b) 4.1%, c) 6.2%, d) 12.4%, and e) 20.6% oxygen containing environments.....	174
Figure 5.9	Observed emission intensity from Fiber 2 in nitrogen and a) 0.1%, b) 0.2%, c) 0.4%, d) 0.6%, e) 0.8% and f) 1.0% oxygen containing environments.....	175
Figure 5.10	Stern-Vollmer plot of emission data from Fiber 2	176

Chapter 1

Introduction

1.1. Structure/Property Relationships of Rigid Polymer Systems

The simplest mathematical model of a polymer chain in space is the freely jointed chain. It is defined as a chain having n links, each of length L , joined in a linear sequence with no restrictions on the angles between successive bonds. The model is equivalent to a random walk by a particle where n is the number of jumps by the particle and L is the length of each jump. A random walk such as that shown in Figure 1.1 for a random walk of 30 steps can be characterized by the net displacement or its end-to-end distance, $\langle r^2 \rangle$, of the random walk.

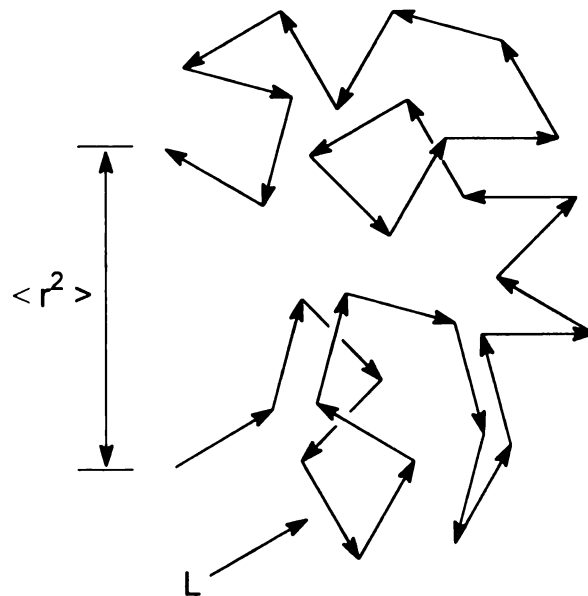


Figure 1.1. A random walk of a freely jointed chain.

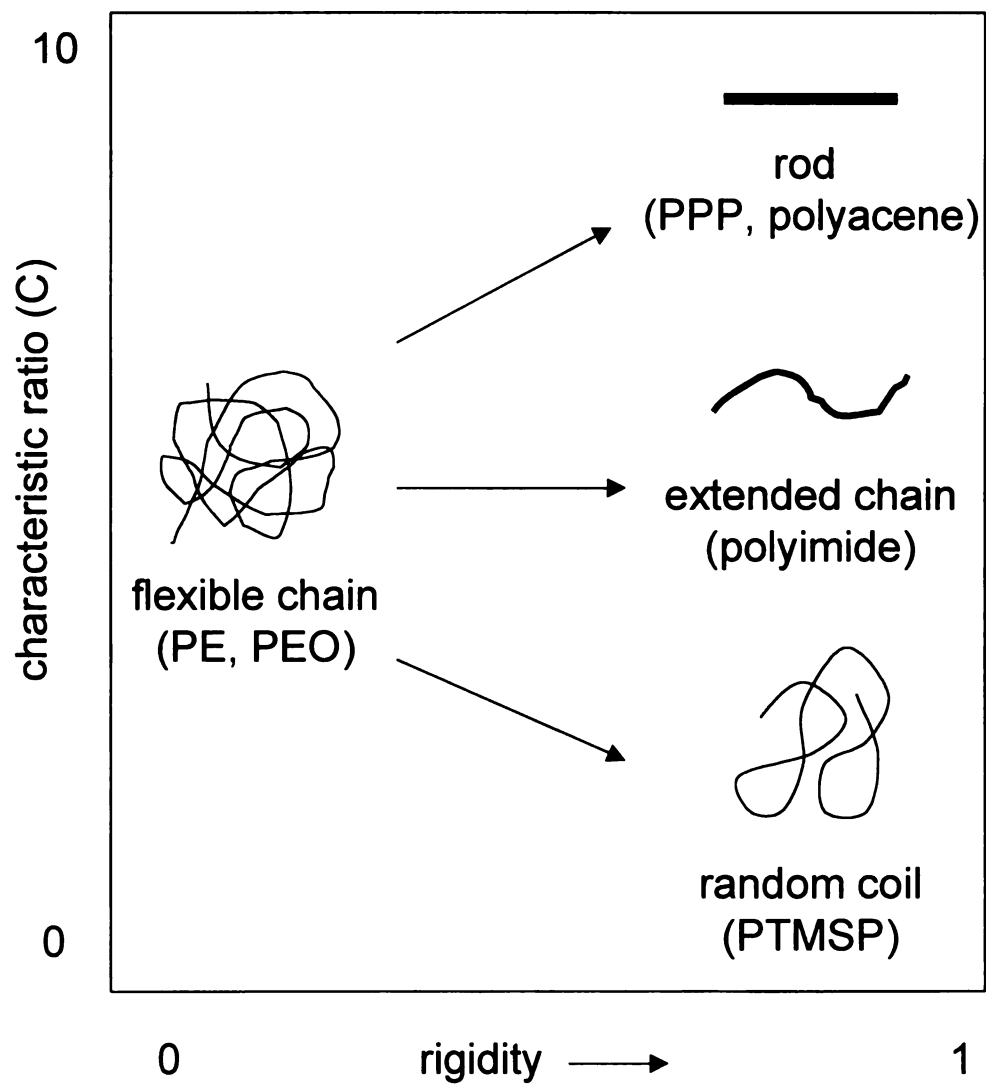


Figure 1.2. Relationships between the characteristic ratio and rigidity in polymers.

To characterize a polymer's behavior in solution, it is common to define its characteristic ratio, C . This ratio (Equation 1) is the ratio of the end-to-end distance of the real polymer to that of a freely jointed polymer of the same molecular weight.¹ As shown schematically in Figure 1.2, flexible polymers like polyethylene (PE) or

$$C = \overline{r^2} / (n \bullet L^2) \quad (1)$$

poly(ethylene oxide) (PEO) usually have small characteristic ratios because of low barriers of rotation about the polymer backbone, and high degrees of polymerization. Rigid polymers, however, typically have large characteristic ratios. Rigidity in polymers occurs when the backbone is locked into a particular conformation by chemical bonding or by large rotational barriers.

Usually, flexible polymers are associated with coiled backbones while rigid polymers in solution have rod-like geometries. This is true in the cases of poly(*p*-phenylene) (PPP) and polyacene. The structure of PPP consists of a series of aromatic rings connected in a linear 1,4-substitution pattern (Figure 1.3 a). Since the carbon atoms in PPP are sp^2 hybridized, bond motion is limited to rotation about the central axis and PPP takes a rigid rod-like conformation. Polyacenes, shown in Figure 1.3 b, are the long chain members of the family of edge-fused aromatic compounds that includes naphthalene, anthracene, and higher homologs. Bond rotation within the acene backbone is impossible since all of the sp^2 carbons are conjugated forming a fused planar structure.

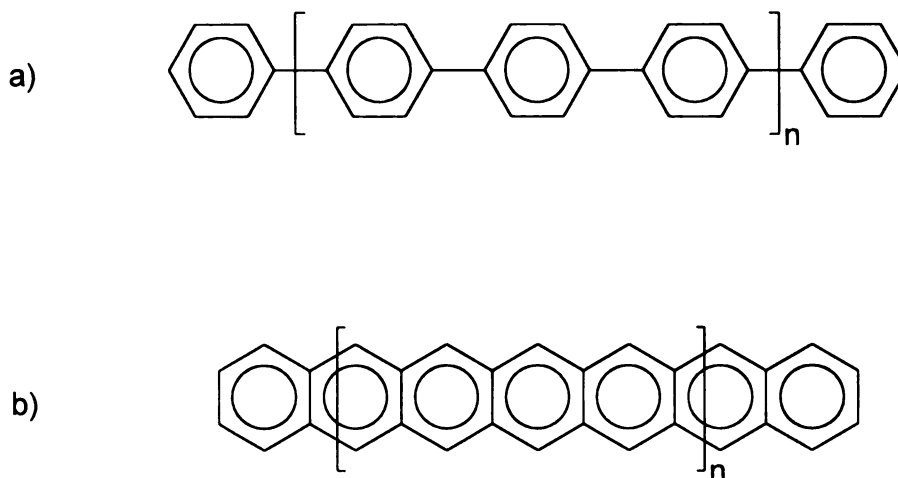


Figure 1.3. Structures of a) poly(*p*-phenylene) and b) polyacene.

The correspondence between chain rigidity and rod-like conformation apparently breaks down for substituted polyacetylenes like poly(1-trimethylsilyl-1-propyne) (PTMSP), shown in Figure 1.4. The reported solution properties suggest a stiff polymer chain, yet PTMSP is highly soluble and amorphous with no report of liquid crystalline behavior. Large barriers to rotation about the backbone are caused by the steric interaction of the bulky trimethylsilyl and methyl groups, effectively preventing the polymer from changing its conformation. It is deduced that PTMSP has a rigid but disordered backbone contour, i.e., a rigid random coil conformation. The characteristic ratio of PTMSP is expected to be lower than that of rigid rod-like polymers, therefore the geometries of rigid polymers are not restricted to a particular shape.

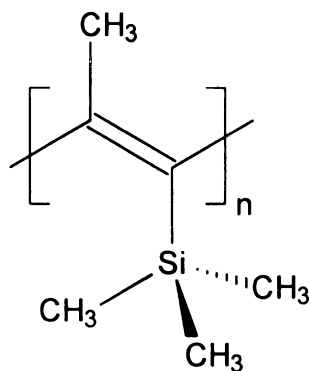


Figure 1.4. Structure of poly(1-trimethylsilyl-1-propyne).


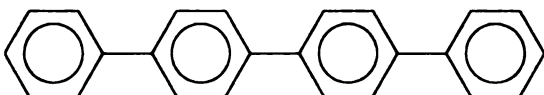
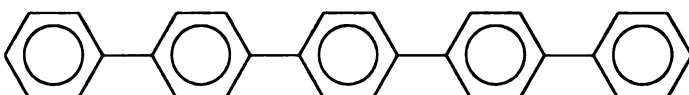
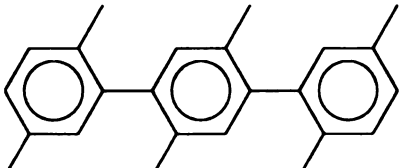
The three polymer systems investigated: PPP, polyacene, and PTMSP each possess a set of unique electronic, optical and mechanical properties. However rigid polymers often exhibit poor solubility, which hinders efficient processing. Herein we describe the physical properties and investigate potential applications of these rigid polymer systems.

1.1.1. Poly(*p*-phenylene)s

PPP's have excellent thermal, oxidative, and electrical stability, and are among the most thermally stable and intractable polymers known. PPP undergoes no glass transitions and decomposes before it melts. Since there are no weak linkages in the polymer backbone, PPP loses only 7% of its mass when heated to 900 °C in an inert atmosphere. Although PPP takes a rigid rod geometry, the polymer backbone is not planar; adjacent rings twist $\sim 23^\circ$ to relieve steric interactions between adjacent *ortho* hydrogens.² The twisting about the central axis limits the extent of conjugation between the rings. PPP's are attractive for applications as electrical conductors, light emitting diodes (LED's), dielectric layers, and luminescent materials.³⁻⁶

The major drawback of PPP is its poor solubility in all organic solvents. As the number of rings in the backbone is increased, the solubility dramatically decreases due to π -stacking of the backbone. As shown in Table 1.1, the solubility of short chain poly(*p*-phenylene) oligomers approaches zero even for low degrees of polymerization.⁷

Table 1.1. Solubility of phenylene oligomers in toluene at room temperature.

Compound	Solubility (g/L)
	8.0
	0.2
	0.01
	30

Recent work has shown that adding side chain substituents⁸ to polyphenylene or connecting the aromatic rings through *ortho* and *meta* linkages increases solubility and processibility.⁹⁻¹¹ Both strategies prevent efficient π -stacking of the backbone, hindering crystallization and therefore increasing solubility. Adding *ortho* and/or *meta* linkages to the PPP backbone however decreases the desired physical properties of the polymer. *Ortho* and *meta* linkages place kinks in the polymer backbone, and the polymer can no longer exist in a rigid rod conformation. Although the solubility of these systems is increased since the polymers take a coiled conformation, polyphenylenes with mixed linkages are not as thermally stable as PPP and tend to be easily oxidized.

There are numerous examples of adding side chains to the PPP backbone to increase its solubility and processibility.¹²⁻¹⁶ It has been reported that when groups are added in the 2,5-positions, the twist angle between adjacent rings increases to $\sim 45^\circ$ to alleviate steric interactions of the adjacent groups. The solubility dramatically increases even for the addition of small side chains. For example, as shown in Table 1.1, terphenyl has a solubility of 8.0 g/L in toluene, while hexamethylterphenyl has a solubility of 30 g/L. It is not quite clear how the added methyl groups improve the solubility of terphenyl. One argument suggests that substitution increases the ring twist and simply creates more disorder in the backbone and hinders crystallization. This argument can not hold true in the case of ladder polyphenylenes however.^{17,18} As shown in Figure 1.5, the aromatic rings in ladder polyphenylenes are fused together

through benzyl linkages, forcing the backbone to become nearly planar. Soluble ladder polyphenylenes have been synthesized by adding side chains to the benzyl positions. In this case, the solubility of these polymers must be due solely to the side chains themselves since ring twisting is impossible. It is proposed that the side chains can act as spacers to disrupt the π -stacking of the polymer backbone, hindering crystallization. The ladder polymers also have a structural source for solubility since the R group can either be above or below the plane of the ladder. This is analogous to tacticity seen in polyolefins.

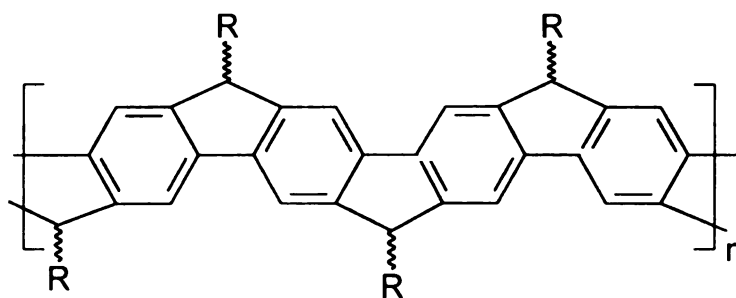


Figure 1.5. Structure of a ladder poly(*p*-phenylene).

Substituted PPP's exhibit interesting properties due to their unique structures. With flexible side chains radiating out from the rigid rod core, soluble substituted PPP's take on a "hairy rod-like" conformation.^{19,20} Liquid crystallinity is often observed in these systems.^{21,22} In Chapter 2, the properties of a substituted PPP will be described. It was observed that the properties of these polymers varied as the volume fraction of the side chain was increased.

1.1.2. Poly(acene)

Polyacene can be viewed as a one-dimensional analog of graphite, a ribbon taken from a single graphene sheet. The structure can also be viewed as a ladder polymer, where the rungs of the ladder connect two *trans*-polyene chains. Since the two polyene chains are locked into a planar conformation, they should possess a very high degree of conjugation. Theory predicts that polyacenes should have very small band gap energies and be promising electrically conductive materials. However, due to the high degree of conjugation, polyacenes are highly reactive and susceptible to oxidation.

Polyacene has long been the object of theoretical interest because it can have several different electronic structures (Figure 1.6), each having a different bandgap energy. Predicted band gap energies range from 0 to 0.45 eV.²³⁻²⁵ The trend of decreasing band gap energy can be seen in the electronic absorption spectra of lower homologs of polyacene. The leading edge of the absorption spectra of anthracene, pentacene, and heptacene decrease in energy as the extent of conjugation is increased. A practical application proposed for polyacenes is their use as optical limiters.^{26,27}

Polyacenic materials, polymer networks that contain a large fraction of acene units, are also materials of great interest. The acene units imbedded in these materials,

usually formed during the high temperature pyrolysis of a suitable precursor, give the materials interesting chemical and electronic properties. Potential applications of polyacenic materials include their use as electrical conductors and electrodes for lithium ion batteries.

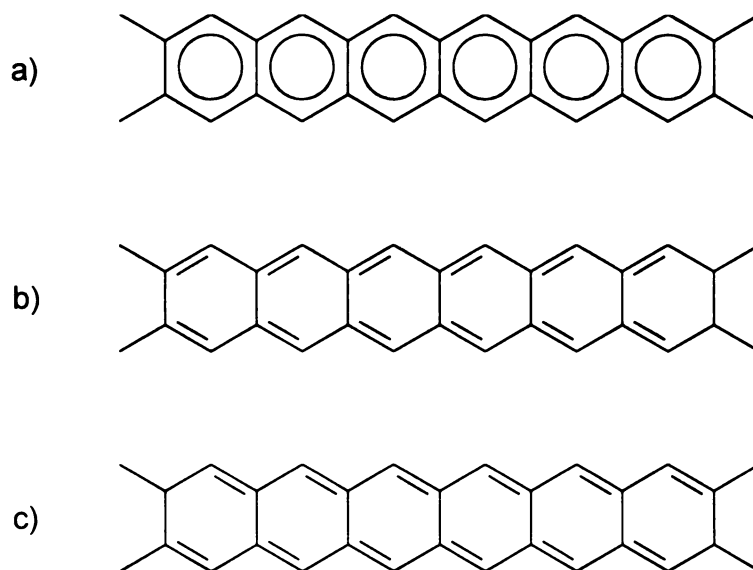


Figure 1.6. Possible electronic configurations of polyacene:
(a) aromatic, (b) *cis*-quinoid, (c) *trans*-quinoid.

1.1.3. Poly(1-trimethylsilyl-1-propyne)

PTMSP is an example of a rigid random coil. For PTMSP, simple molecular mechanics calculations suggest that steric interactions between the substituents on adjacent carbon atoms can cause significant deviations from planarity.²⁸ Because of the shorter distances between carbon atoms in the sp^2 skeleton, the magnitude of the interactions are expected to be much larger than for their saturated analogs and there should be a large barrier to rotation. Plotted schematically in Figure 1.7 is a potential energy diagram for rotation about single bonds in substituted *trans*-polyacetylenes. The rotational barrier can be modeled using two energy terms; one with a $\cos^2\theta$ dependence that accounts for the π contribution to the rotational barrier, and a second term with a $\cos 2\theta$ dependence that corresponds to steric barriers to rotation. Based on experimental results for butadiene,²⁹ the π barrier is set at 6 Kcal/mol. With small substituents, the combination of a small π energy term and limited 1,3 steric interactions leads to a broad shallow potential well with the most stable conformations being those that are nearly planar. As the magnitude of the steric interactions is increased, a double well potential becomes well defined and the π contribution becomes a minor perturbation to the total energy. For large substituents (i.e. *t*-butyl, trimethylsilyl), the barrier to rotation at room temperature may be large enough to make planar conformations so unfavorable that the polymer is driven into one of two sharply defined potential wells. With bulky substituents, the barrier to

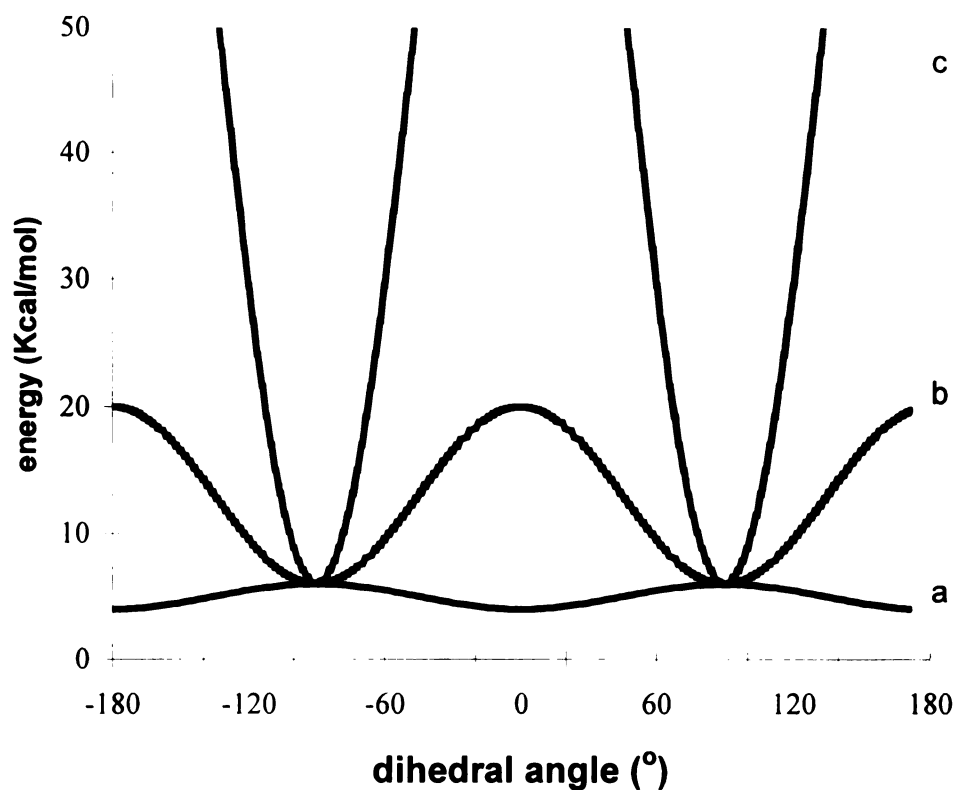


Figure 1.7. Hypothetical rotational barriers for disubstituted polyacetylenes where 0 degrees corresponds to an eclipsed conformation in which two double bonds are coplanar. (a). *trans*-polyacetylene, 6 Kcal/mol π barrier; (b) 20 Kcal/mol rotational barrier that simulates significant 1-3 steric interaction; (c) 100 Kcal/mol barrier that simulates polyenes with bulky substituents.

rotation may become large enough to limit access to a single well. Thus, the polymer conformation is fixed, and overall changes in the shape of the polymer are limited to oscillations within a single well.

Thermal annealing experiments provide an illustration of PTMSP's inability to change conformations.³⁰ Depending on the catalyst used to prepare the polymer, different amounts of *cis* and *trans* double bonds are found in the polymer. For polyacetylene in the solid state, isomerization of *cis* double bonds to *trans* double bonds occurs readily at temperatures above 100 °C. At 180 °C for example, the isomerization of semicrystalline films of *cis*-polyacetylene to the *trans* isomer is completed in one minute.³⁰ Similar experiments on PTMSP show no signs of isomerization.³¹ For annealing at temperatures above 200 °C, ¹³C NMR spectra show that the isomer content is unchanged after 24 hours, and instead random chain scission leads to lower molecular weight polymers with the *cis/trans* ratios preserved. Remarkably, the barrier to isomerization apparently exceeds the energy required to break the polymer backbone. The barrier calculated from molecular dynamics simulations (40 Kcal/mol) is in accord with such behavior. Thus, PTMSP fits well the model of a rigid chain with a highly disordered backbone contour.

Due to its rigid backbone, PTMSP is one of the most unusual polyenes synthesized. In contrast to polyacetylene which is insoluble, appears blue in transmitted light, and can be doped to form highly conducting materials, PTMSP

readily dissolves in a wide range of non-polar solvents, is colorless, and is unreactive toward common chemical dopants. The twisting caused by the steric repulsion of the trimethylsilyl and methyl groups misaligns adjacent π bonds, leading to PTMSP's lack of color. Its lack of absorption above 280 nm in the UV-vis spectrum implies a degree of conjugation as extensive as butadiene. PTMSP is amorphous according to X-ray diffraction and thermal analysis.³²

Amorphous polymers exhibit different physical and mechanical behavior depending on the temperature and the polymer structure. At low temperatures, amorphous polymers are glassy, hard, and brittle. As the temperature is raised, they go through a glass transition (T_g) and enter a rubbery state. However, PTMSP shows no evidence of a T_g to the upper limit of its chemical stability, usually 300 °C. Mechanical measurements³² place the modulus of PTMSP between that of typical glassy and rubbery materials. Due to these unique properties, PTMSP has found practical applications as a material for deep-UV photolithography,^{33,34} and as a highly permeable membrane material for gas³⁵⁻³⁸ and liquid separations.³⁹⁻⁴²

With its rigid backbone structure and the presence of the large bulky substituents, inter-segmental packing is hindered and thus the polymer has a large free volume. Therefore films of PTMSP have many molecular-scale holes just after its preparation which results in a high gas permeability.⁴³ The permeability decays with time however, dropping to 10 % of its original value after 100 days.⁴⁴ One model for the decrease is the slow interdiffusion of polymer coils in the solid state. From solution, the polymer is deposited under kinetic control as an ensemble of

spheres. With time, the chains entangle causing an increase in the density and decrease in free-volume and the permeability. Stabilization of PTMSP in its porous form is needed for PTMSP to be useful.

Cross-linking the polymer should lead to stabilized PTMSP networks in its highly permeable form. Chapter 4 describes a method to stabilize PTMSP by cross-linking. An application for these mechanically stable, highly permeable materials is described in Chapter 5. Cross-linked PTMSP was used as a permeable solid support in a novel oxygen-sensing scheme.

1.2. Syntheses of Rigid Polymer Systems

In order to obtain these rigid polymer systems, controlled synthetic methods are necessary to produce ideal structures. The methods employed must be regiospecific and lead to stable products. Any defects or side reactions can lead to a dramatic decrease in the desired properties. For example, a single flexible link in a rigid rod backbone dramatically reduces the characteristic ratio. A decrease in solubility with increases in the degree of polymerization often must be overcome to lead to high molecular weight products.

1.2.1. Poly(*p*-phenylene)s

PPP has traditionally been a very difficult polymer to synthesize. The struggle to find efficient methods for producing PPP with both a regioregular linear structure and high molecular weight, together with the inherent lack of processibility of the

material, have retarded the development of PPP as a useful material. A successful synthetic approach to poly(*p*-phenylene)s must employ methods that lead to exclusively *para* aromatic linkages and high molecular weights. However, PPP's decreasing solubility as the extent of polymerization increases limits the molecular weight of the product. Degrees of polymerization approaching 50 must be obtained in order for the materials to be classified as polymeric.

The electrochemical coupling of aromatic monomers to give polyphenylenes on inert electrodes (usually Pt) has been reported.^{45,46} Electrochemical methods, namely the oxidative coupling of unsubstituted aromatic monomers and the reductive dehalogenation of halogenated aromatic monomers, only yield small quantities of polymer. Most electrochemical syntheses are designed to produce thin conductive films on electrodes, not bulk amounts. The structures of the deposited polymers are irregular and contain substantial amounts halogens and a mixture of *ortho*, *meta*, and *para* aromatic linkages between the rings, indicating that electrochemical coupling produces lead to materials of uncontrolled structure.

Chemical oxidative coupling of aromatic rings is possible if the catalyst system used can act as a good Friedel-Crafts catalyst and as a good oxidizing agent.⁴⁷ The polymerization of benzene using AlCl_3 and CuCl_2 proceeds under mild conditions to yield a low molecular weight brownish powder, which almost exclusively consists of *para*-linked phenylene rings. Other reagents, such as PbO , MnO_2 , and chloranil,

have been used as co-catalysts with AlCl_3 but result in products with even lower molecular weights and more structural irregularity (branching and high halide content). The polymerization of substituted benzenes resulted in products with higher molecular weights. The increase, however, is not due to an increase in the solubility from the side chains, but instead is a consequence of the increase in the number of mixed linkages (*ortho* and *meta*) that connect the rings.

Some of the earliest reported attempts to synthesize poly(*p*-phenylene) involved the reductive coupling of substituted aromatic compounds. Using the Fittig reaction, dihalo-benzenes were refluxed in diethyl ether with sodium or potassium metal to give brownish oligomers that are soluble in benzene. The relatively low reported melting points ($<300\text{ }^\circ\text{C}$) and structural irregularities, such as chain branching and residual halide content, indicate that the reaction led to low molecular weight products with a less than ideal PPP character.

More recently, an analogous process was developed that involves the polymerization of a 1-bromo-4-lithiobenzene intermediate (Figure 1.8). It was found that the intermediate, generated by the mono lithium-halogen exchange of 1,4-dibromobenzene and *t*-butyllithium, polymerized nearly instantaneously at $-78\text{ }^\circ\text{C}$ upon addition of hexamethylphosphoramide (HMPA) or after 2 hours in tetrahydrofuran at room temperature.^{9,10} The structure of the resulting polymer however contains many non-*para* linkages and has a high bromide content.

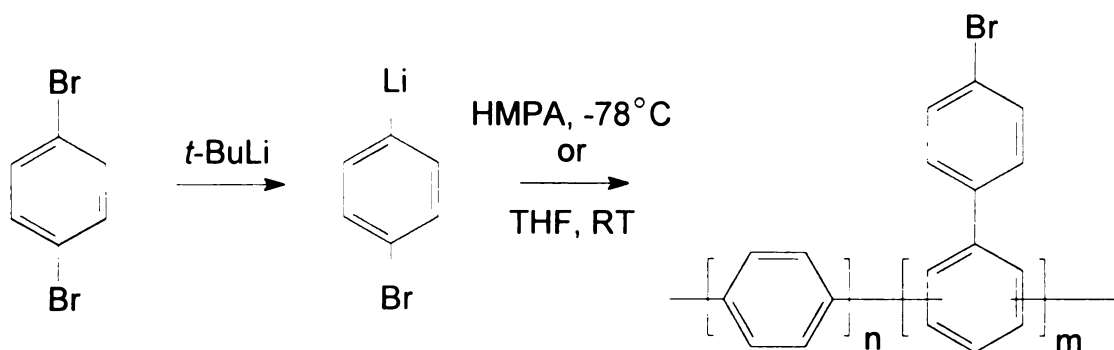


Figure 1.8. Polymerization of 1-bromo-4-lithiobenzene.

Slightly better results are obtained from the Ullmann homocoupling of 1,4-diiodobenzene using activated copper powder.⁴⁸⁻⁵⁰ Starting with the *para* diiodo-substituted benzene ring ensured that the resulting polymer has the correct *para* substitution pattern. As shown in Figure 1.9, exact length poly(*p*-phenylene) oligomers were also synthesized from the coupling of monoiodo biphenyls and terphenyls. The major drawback of Ullmann coupling is the extreme conditions required to promote the reaction. While the Ullmann coupling method has been used in the polymerization of nitro-substituted diiodo-biaryls, the scope of applications for this method is limited since most functional groups can not tolerate the prolonged reaction temperatures of greater than 200°C .

The use of transition metal catalysis allows for milder reaction conditions and greater chemoselectivity leading entirely to *para*-linked polyaromatics when starting with *para*-substituted aromatic monomers.^{8,51-56} High yield palladium

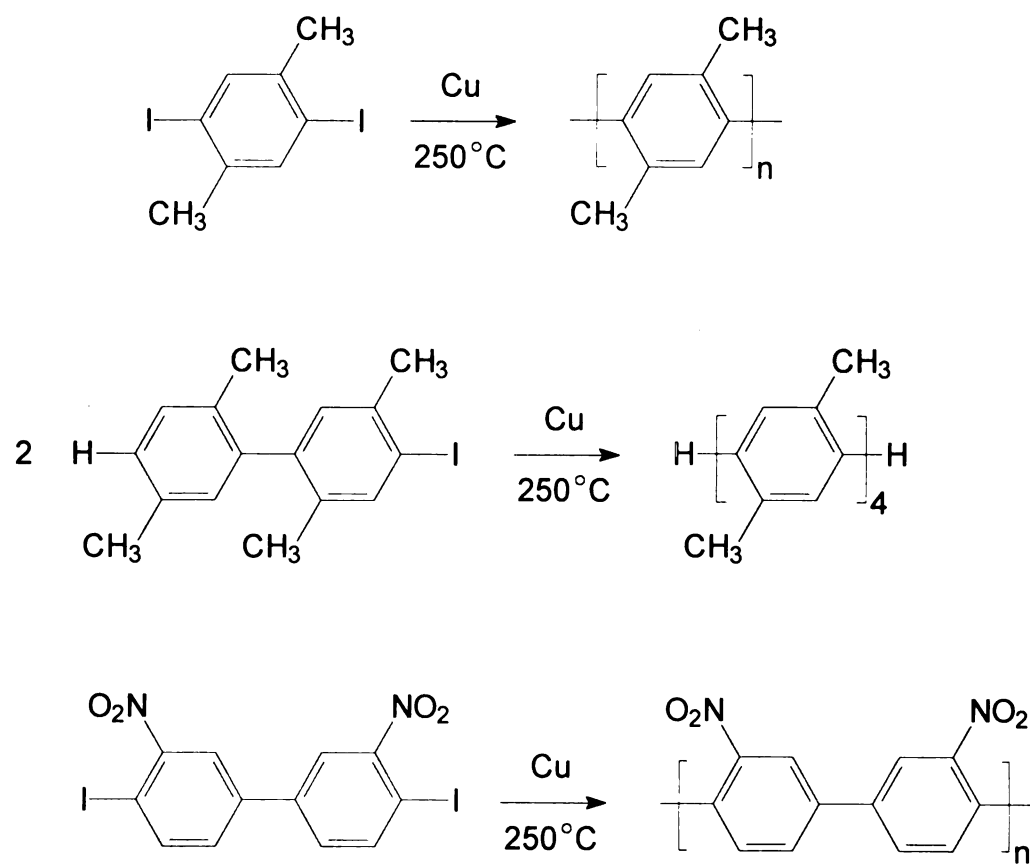


Figure 1.9. Polymerization of diiodoarenes.

and nickel catalyzed aryl coupling reactions were found to be ideal for polymerizations.⁵⁷ Transition metal catalyzed polymerizations are, in general, more tolerant of a wide variety of functional groups. This allows for the synthesis of a gamut of substituted polyphenylenes previously unattainable by earlier methods. The catalytic cycle that most transition metal catalyzed polymerizations follow involves three major steps. A typical palladium catalytic cycle is shown in Figure 1.10. First, a zero valent metal complex, such as *tetrakis*(triphenylphosphine)palladium, undergoes an oxidative addition with a bromo- or iodo-arene. Transmetalation with an electrophilic aromatic species, such as an aryl boronic acid or aryl tin complex, forms a diaryl metal complex. It is proposed that this intermediate rapidly undergoes reductive elimination to yield the coupled product and regenerate the zero valent metal complex. These polymerizations can be run at very low catalyst loadings, i.e. below 5 mol%, due to the efficiency of each step in the cycle. The reactions are very sensitive to impurities however. Since highly reactive zero valent metals are generated during the cycle, great care must be taken to remove all oxygen from the polymerization vessel. Oxidized catalyst usually shows up as an insoluble black powder that precipitates from the polymerization. The specific nickel catalyzed polymerizations used to prepare substituted poly(*p*-phenylene)s will be discussed in more detail in Chapters 2 and 3.

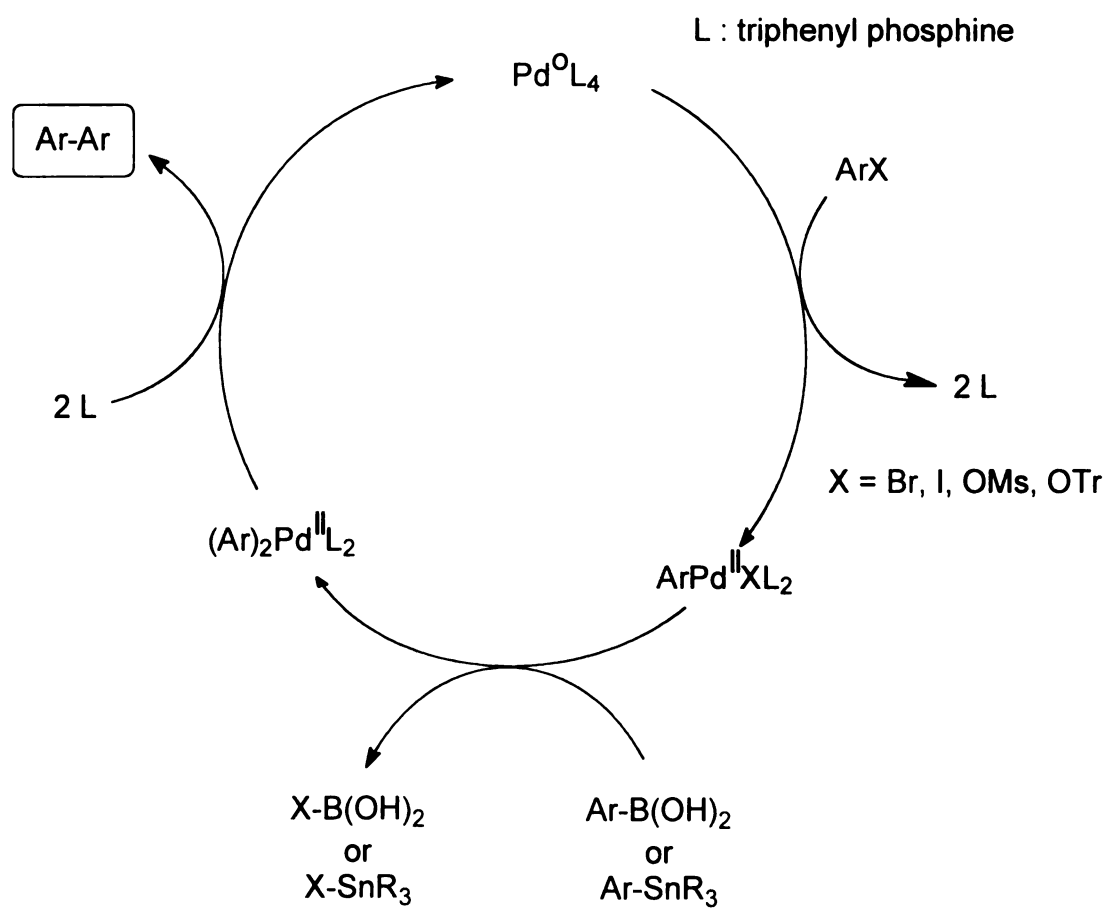


Figure 1.10. Catalytic cycle of palladium mediated aryl coupling.

Synthetic methods other than aromatic coupling have been reported to yield poly(*p*-phenylene)s as well. One example involves the use of Bergman cyclization to thermally generate a benzene 1,4-diradical from an enediyne which then polymerizes (Figure 1.11).⁵⁸ This route is attractive for several reasons. It requires no chemical catalysts or reagents for the polymerization and heteroatomic coupling sites such as halogens are not necessary. The monomers can also be readily prepared with a variety of substitution patterns leading to soluble poly(*p*-phenylene) derivatives.

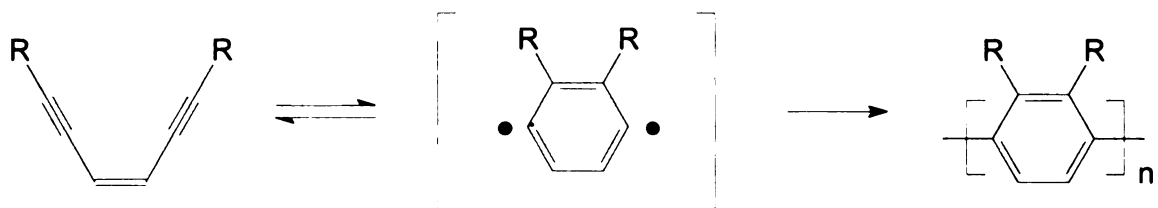


Figure 1.11. Polymerization of an enediyne.

Soluble substituted poly(*p*-phenylene)s have also been prepared via Diels-Alder routes by reacting phenyl-substituted arylene biscyclopentadienones (or arylene bispyrones) with *m*- or *p*-diethynylbenzene (Figure 1.12). The retro Diels-Alder reactions are prevented due to the evolution of CO or CO₂. The polymerizations were conducted in concentrated toluene solutions under pressure at elevated temperatures (200-300 °C). Nearly quantitative yields and satisfactory elemental analyses were obtained. High molecular weights were obtained from the

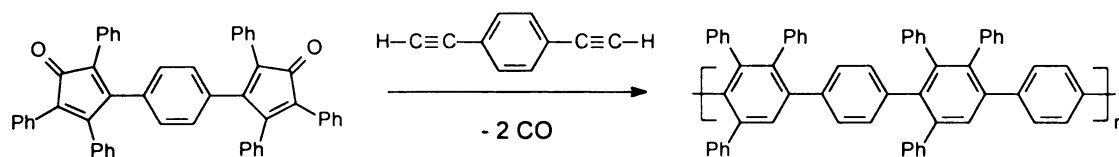


Figure 1.12. Diels-Alder polymerization of biscyclopentadienones.

polymerization using biscyclopentadienones ($M_n > 10,000$), but only low viscosities were obtained for the polymers derived from the bispyrone monomers.

Another novel strategy used to prepare PPP proceeds through soluble poly(cyclohexadiene) intermediates.^{14,59-61} In the first precursor route studied, poly(1,3-cyclohexadiene) was treated with Br_2 , followed by thermal dehydrobromination to form the aromatic polymer. Unfortunately, this method yielded a poorly processible material that underwent only partial conversion to polyphenylene and contained large percentages of *ortho* and *meta* linkages. Slightly improved results were obtained using soluble precursor polymers derived from the radical polymerization of *cis*-5,6-dihydroxy-1,3-cyclohexadiene. These precursors were then converted to PPP by the acid catalyzed elimination of the pendant groups. Although offering high processibility, this route suffered from the low selectivity of the radical polymerization. This resulted in precursor polymers with random tacticity and

regiochemistry, which contributed to thermal depolymerization during the final conversion to PPP. As shown in Figure 1.13, the use of an organonickel catalyst that could stereospecifically polymerize protected hexadiene monomers with the desired tacticity and 1,4-regiochemistry led to structurally regular PPP with high molecular weight after acid catalyzed elimination.

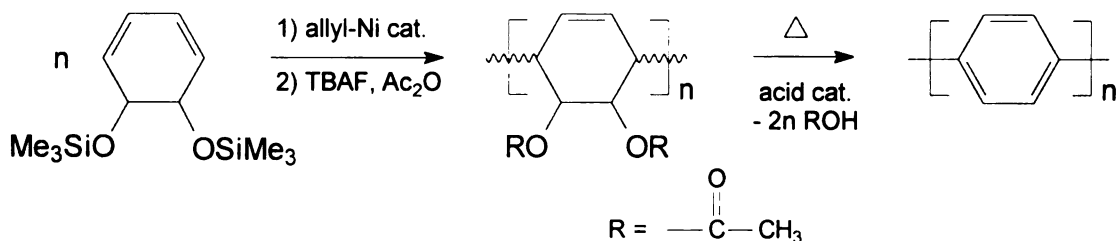


Figure 1.13. Synthesis of PPP via soluble poly(cyclohexadiene) intermediates.

1.2.2. Poly(acene)

To date, well-defined high molecular weight polyacenes have not been successfully prepared and characterized due to their sensitivity towards oxidation and increasing insolubility with increasing chain length. The longest straight chain acene analog that has been prepared is heptacene. Some related structures, however, have been prepared. For example, various planarized polyphenylenes have been synthesized that can be thought of as end-linked fluorene and phenanthrene structures.^{18,62-64} Soluble polyacenequinone structures were synthesized by

repetitive Diels-Alder reactions.⁶⁵ Diels-Alder reactions have also been used to prepare cyclic belt or collar acene-like structures.⁶⁶⁻⁶⁹ Although related structurally, the electronic properties of these materials do not match those expected for the doubly conjugated ladder structure of polyacene.

The synthesis of linear polyacene *via* the step-wise polymerization of a monosilylated diacetylene has been reported.⁷⁰ The first polyacetylene strand was polymerized using a $\text{WCl}_6\text{-Ph}_4\text{Sn}$ mixture. After desilylation of the resulting poly(trimethylsilyl ethynyl acetylene), poly(ethynyl acetylene) was thermally polymerized to form the second polyacetylene strand and yield polyacene (Figure 1.14). The products from this reaction, however, contained substantial amounts of structural defects. The catalyzed polymerization leading to poly(trimethylsilyl ethynyl acetylene) did not result in the required pure *trans* isomer. Bond rotation to relieve steric hindrance in the original polyacetylene strand would also lead to cross-linking between adjacent chains upon thermal treatment.

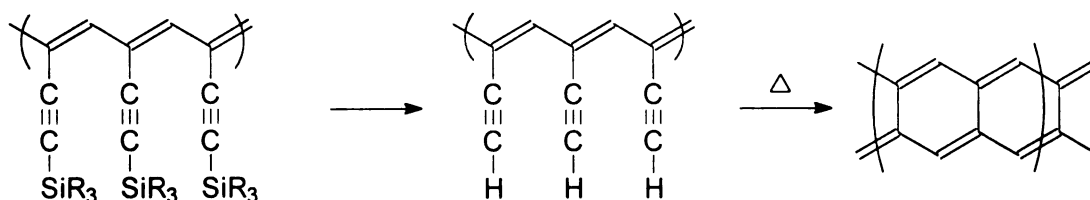


Figure 1.14. Polymerization of poly(ethynyl acetylene).

To overcome this problem, Langmuir-Blodgett (LB) films of the diacetylene monomer were prepared by attaching the monomers to a calcium fluoride surface through short tethers (Figure 1.15).⁷¹ The first polyacetylene strand was photopolymerized by UV irradiation, followed by thermal treatment to form the second. Characterization of the resulting films indicated that only small acenic units were obtained, most likely due to the fact that the LB molecular packing density of the monomer was lower than expected.

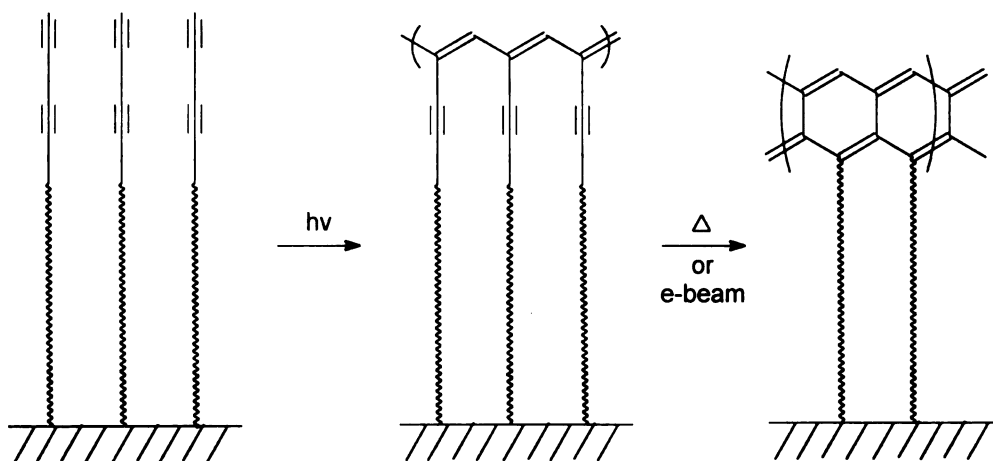


Figure 1.15. Polymerization of Langmuir-Blodgett films of diacetylenes.

Other routes to linear acene materials utilize iterative chain growth reactions. One example, shown in Figure 1.16, exploits the chemistry used to produce 9,10-dihydroacenaphthalene from benzocyclopropene.⁷² Bicycloproparenes were reacted with silver ions in chloroform to yield acene precursors, which upon aromatization

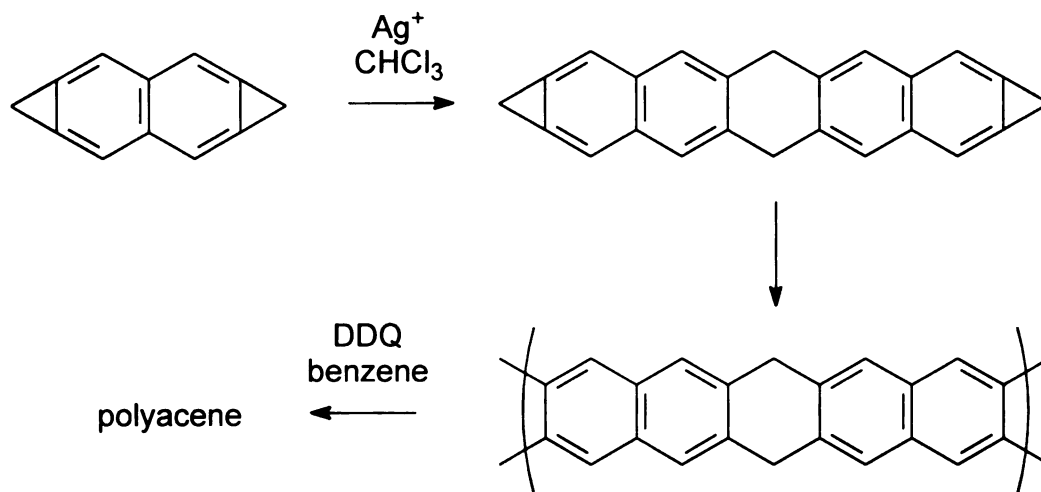


Figure 1.16. Polymerization of cycloproparenes.

using DDQ or other suitable oxidizing agents, affords polyacene. The insolubility of the acene precursors is the major drawback to this method.

The synthesis of polyacenic materials, which are defined as three-dimensional networks that contain some amount of acene units, usually involve the pyrolysis of a suitable precursor. The precursor polymers most commonly used are phenol-formaldehyde and cellulose resins.^{73,74} It is proposed that upon high temperature treatment, the precursors eliminate water and hydrogen to form aromatic materials. A more accurate description of the “curing” process is graphitization since the statistical probability of producing linear acenes is low. The characterization data from the charred materials could also be interpreted as the presence of graphite or three-dimensional aromatic networks.

Using an analogous reaction, we found that bis(methoxymethyl)benzenes undergo acid-catalyzed polymerization to yield network structures. The idealized chemical structure for the polymerization of bis(methoxymethyl)benzenes is a linear polyacene precursor, that after elimination of H₂, should yield polyacenes with an extended p electron system. To obtain the ideal linear acene, the synthetic strategy employed must impart some degree of control over the outcome of the resulting structure. Defects and side reactions quickly lead to less than ideal structures. In Chapter 3, the methods we used to control the structure of the network and the characterization of these materials are described. We also report the preparation of a methoxymethyl-substituted poly(*p*-phenylene) that appears to convert to an acene cross-linked polyphenylene when reacted with concentrated sulfuric acid.

1.2.3. Polyacetylene – Poly[1-trimethylsilyl-1-propyne]

Syntheses of polyacetylene. The most popular synthetic method for preparing linear polyacetylenes with high crystallinity is the polymerization of acetylene with a Ziegler-Natta catalyst.⁷⁵ High quality polyacetylene films are prepared from homogeneous catalyst mixtures consisting of Ti(OR)₄ and R'₃Al. Titanium halides and other metal complexes, such as vanadium-based organometallic compounds, have also been used. Polyacetylene can also be prepared *via* ring-opening polymerization of cyclooctatetraene.⁷⁶ The monomer is polymerized neat using a Grubbs-type catalyst to give free-standing films. This approach has been extended

to the polymerization of trimethylsilyl substituted cyclooctatetraene to afford soluble polyacetylenes which have been used to construct solar cells and layered structures.

Polyacetylene can be obtained through indirect methods as well. Some of the earliest attempts at preparing polyacetylene involved the thermal elimination of small molecules from soluble precursors. Poly(vinyl alcohol) and poly(vinyl chloride) were heated, evolving water and HCl, respectively, to form polyacetylene. However, the thermal elimination was often inefficient and led to irregular structures. The isomerization of poly(benzvalene), prepared through ring-opening polymerization, is an alternative precursor approach to polyacetylene.⁷⁷ The precursor rearranges by heat or light to polyacetylenic materials.

Syntheses of substituted polyacetylenes. Substituted acetylene monomers can be polymerized using suitable transition-metal catalysts.⁷⁵ Metathesis polymerization using Group 5 and 6 transition metal complexes (namely Nb, Ta, Mo, and W) is believed to proceed via metal carbenes. According to the proposed mechanism (shown in Figure 1.17), propagation proceeds through the reaction of a metal carbene with an acetylenic monomer to give a metallocyclobutene, followed by ring opening to regenerate the metal carbene. This mechanism resembles that of the ring-opening metathesis polymerization (ROMP) of cycloolefins. Some of the catalysts that have been effective include: 1) the chlorides of Nb, Ta, Mo, and W; 2) 1:1 mixtures of those metal chlorides with suitable organometallic cocatalysts; and

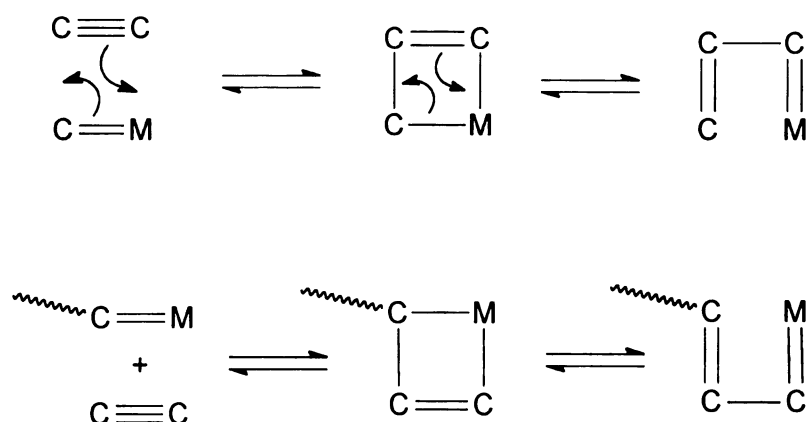


Figure 1.17. Initiation and propagation of acetylene polymerization.

3) catalysts obtained by UV irradiation of CCl_4 solutions of Mo and W hexacarbonyls.

In general, the Group 6 metal complexes (Mo and W) polymerize monosubstituted and less sterically hindered disubstituted acetylenes, while Group 5 metal complexes (Nb and Ta) are used to polymerize sterically hindered disubstituted acetylenes. With proper choice of catalyst and solvent systems, polymers with molecular weights exceeding 10^6 can be obtained from substituted acetylene monomers.

The polymerization of 1-trimethylsilyl-1-propyne, a sterically hindered disubstituted acetylene, was accomplished using a co-catalyst system consisting of tantalum pentachloride and triphenyl bismuth.⁷⁸⁻⁸⁰ Copolymerization of 1-trimethylsilyl-1-propyne with functional acetylenic monomers was also catalyzed by the same co-catalyst system to yield polymers with high molecular weights (Chapter 4).

1.3. References

- 1) Sperling, L. H. *Introduction to Physical Polymer Science*; John Wiley & Sons, Inc.: New York, **1992**.
- 2) Elsenbaumer, R. L.; Jen, K. Y.; Oboodi, R. *Synth. Met.* **1986**, *15*, 169-174.
- 3) Edwards, A.; Blumstengel, S.; Sokolik, I.; Yun, H.; Okamoto, Y.; Dorsinville, R. *Synth. Met.* **1997**, *84*, 639-640.
- 4) Segura, J. L. *Acta Polym.* **1998**, *49*, 319-344.
- 5) Leising, G.; Tasch, S.; Meghdadi, F.; Athouel, L.; Froyer, G.; Scherf, U. *Synth. Met.* **1996**, *81*, 185-189.
- 6) Kim, H. K.; Ober, C. K. *J. Macromol. Sci.-Pure Appl. Chem.* **1993**, *A30*, 877-897.
- 7) Kern, W.; Wirth, H. O. *Makromol. Chem.* **1959**, *31*, 154-164.
- 8) Rehahn, M.; Schluter, A. D.; Wegner, G.; Feast, W. J. *Polymer* **1989**, *30*, 1060-1062.
- 9) Tour, J. M.; Stephens, E. B. *J. Am. Chem. Soc.* **1991**, *113*, 2309-2311.
- 10) Tour, J. M.; Stephens, E. B.; Davis, J. F. *Macromolecules* **1992**, *25*, 499-500.
- 11) Tour, J. M. *Adv. Mater.* **1994**, *6*, 190-198.
- 12) Huber, J.; Scherf, U. *Macromol. Rapid Commun.* **1994**, *15*, 897-902.
- 13) Vahlenkamp, T.; Wegner, G. *Macromol. Chem. Phys.* **1994**, *195*, 1933-1952.
- 14) Gin, D. L.; Conticello, V. P. *Trends Polym. Sci.* **1996**, *4*, 217-223.

- 15) McCarthy, T. F.; Witteler, H.; Pakula, T.; Wegner, G. *Macromolecules* **1995**, *28*, 8350-8362.
- 16) Rehahn, M.; Schluter, A. D.; Wegner, G. *Makromol. Chem., Macromol. Chem. Phys.* **1990**, *191*, 1991-2003.
- 17) Scherf, U.; Mullen, K. *The synthesis of ladder polymers*, 1995; Vol. 123, pp 1-40.
- 18) Kertesz, M.; Houghbanks, T. R. *Synth. Met.* **1995**, *69*, 699-700.
- 19) Petekidis, G.; Vlassopoulos, D.; Fytas, G.; Rulkens, R.; Wegner, G. *Macromolecules* **1998**, *31*, 6129-6138.
- 20) Park, K. C.; Dodd, L. R.; Levon, K.; Kwei, T. K. *Macromolecules* **1996**, *29*, 7149-7154.
- 21) Witteler, H.; Lieser, G.; Wegner, G.; Schulze, M. *Makromol. Chem., Rapid Commun.* **1993**, *14*, 471-480.
- 22) Steuer, M.; Ballauff, M. *J. Polym. Sci. Pol. Chem.* **1993**, *31*, 1609-1619.
- 23) Salem, L.; Longuett-Higgins, H. C. *Proc. R. Soc. London, Ser. A* **1960**, *255*, 435.
- 24) Tanaka, K.; Yata, S.; Yamabe, T. *Synth. Met.* **1995**, *71*, 2147-2149.
- 25) Whangbho, M. H.; Hoffmann, R.; Woodward, R. B. *Proc. R. Soc. London, Ser. A* **1979**, *366*, 23.
- 26) Kojima, Y.; Matsuoka, T.; Sato, N.; Takahashi, H. *Macromolecules* **1995**, *28*, 2893-2896.

- 27)Kojima, Y.; Matsuoka, T.; Takahashi, H. *J. Appl. Polym. Sci.* **1998**, *68*, 129-135.
- 28)Clough, S. B.; Sun, X. F.; Tripathy, S. K.; Baker, G. L. *Macromolecules* **1991**, *24*, 4264-4269.
- 29)Bock, C. W.; George, P.; Trachtman, M.; Zanger, M. *J. Chem. Soc., Perkin Trans.* **1979**, *1*, 26.
- 30)Rolland, M.; Bernier, P.; Lefrant, S.; Aldissi, M. *Polymer* **1980**, *21*, 1111.
- 31)Baker, G. L.; Shelburne III, J. A.; Bates, F. S. *J. Am. Chem. Soc.* **1986**, *108*, 7377.
- 32)Masuda, T.; Tang, B. Z.; Tanaka, A.; Higashimura, T. *Macromolecules* **1986**, *19*, 1459.
- 33)Baker, G. L.; Klausner, C. F.; Gozdz, A. S.; Shelburne, J. A.; Bowmer, T. N. *Adv. Chem. Ser.* **1990**, 663-678.
- 34)Gozdz, A. S.; Baker, G. L.; Klausner, C.; Bowden, M. J. *Proc. SPIE* **1987**, *771*, 18.
- 35)Nagai, K.; Higuchi, A.; Nakagawa, T. *J. Appl. Polym. Sci.* **1994**, *54*, 1207-1217.
- 36)Morisato, A.; Shen, H. C.; Sankar, S. S.; Freeman, B. D.; Pinnau, I.; Casillas, C. G. *J. Polym. Sci. Pt. B-Polym. Phys.* **1996**, *34*, 2209-2222.
- 37)Koros, W. J.; Chern, R. T. *Separation of Gaseous Mixtures Using Polymer Membranes*; Rousseau, R. W., Ed.; Wiley Interscience: New York, 1987.

- 38)Savoca, A. C.; Surnamer, A. D.; Tien, C. F. *Macromolecules* **1993**, 26, 6211-6216.
- 39)Huang, R. Y. M.; Feng, X. *Sep. Sci. Technol.* **1992**, 27, 1583.
- 40)Schmidt, S. L.; Myers, M. D.; Kelley, S. S.; McMillan, J. D.; Padukone, N. *Appl. Biochem. Biotechnol.* **1997**, 63-5, 469-482.
- 41)Robeson, L. M.; Langsam, M. *Sep. Sci. Technol.* **1992**, 27, 1245-1258.
- 42)Masuda, T.; Tang, B.; Higashimura, T. *Polym. J.* **1986**, 18, 565.
- 43)Shimomura, H.; Nakanishi, K.; Odani, H.; Kurata, M.; Masuda, T.; Higashimura, T. *Kobunshi Ronbunshu* **1986**, 43, 747.
- 44)Masuda, T.; Higashimura, T. *Silicon Based Polymer Science*; Ziegler, J. M. and Fearon, F. W. G., Ed.; American Chemical Society: Washington, DC, 1990; Vol. 224, pp 641.
- 45)Arnautov, S. A.; Gavrilenko, V. V. *Synth. Met.* **1997**, 84, 283-284.
- 46)Shimura, T.; Funaki, H.; Nishihara, H.; Aramaki, K.; Ohsawa, T.; Yoshino, K. *Chem. Lett.* **1992**, 457-460.
- 47)Kovacic, P.; Jones, M. B. *Chem. Rev.* **1987**, 87, 357-379.
- 48)Bringmann, G.; Walter, R.; Weirich, R. *Angew. Chem.-Int. Edit. Engl.* **1990**, 29, 977-991.
- 49)Fanta, P. E. *Synthesis* **1974**, 9-21.
- 50)Wirth, H. O.; Herrmann, F. U.; Hern, W. *Makromol. Chem.* **1964**, 80, 120-140.

- 51)Percec, V.; Hill, D. H. *Step-polymerization reactions via nickel- and palladium-catalyzed carbon-carbon bond formation*, 1996; Vol. 624, pp 2-56.
- 52)Percec, V.; Pugh, C.; Cramer, E.; Okita, S.; Weiss, R. *Makromol. Chem., Macromol. Sym.* **1992**, 54-5, 113-150.
- 53)Novak, B. M.; Wallow, T. I.; Goodson, F.; Loos, K. *Abstr. Pap. Am. Chem. Soc.* **1995**, 209, 215-POLY.
- 54)Durairaj, K. *Curr. Sci.* **1994**, 66, 833-838.
- 55)Saa, J. M.; Martorell, G. *J. Org. Chem.* **1993**, 58, 1963-1966.
- 56)Kwiatkowski, G. T.; Colon, I.; Elhibri, M. J.; Matzner, M. *Makromol. Chem., Macromol. Sym.* **1992**, 54-5, 199-224.
- 57)Suzuki, M. *J. Synth. Org. Chem. Jpn.* **1993**, 51, 141-156.
- 58)Tour, J. M.; John, J. A. *Abstr. Pap. Am. Chem. Soc.* **1993**, 206, 43-POLY.
- 59)Gin, D. L.; Conticello, V. P.; Grubbs, R. H. *J. Am. Chem. Soc.* **1994**, 116, 10934-10947.
- 60)Gin, D. L.; Conticello, V. P.; Grubbs, R. H. *J. Am. Chem. Soc.* **1994**, 116, 10507-10519.
- 61)Gin, D. L.; Avlyanov, J. K.; Macdiarmid, A. G. *Synth. Met.* **1994**, 66, 169-175.
- 62)Kertesz, M.; Frapper, G.; Hong, S. Y.; Lee, Y. S.; Kim, O. K. *Synth. Met.* **1993**, 57, 4344-4349.
- 63)Kertesz, M.; Ashertehrani, A. *Macromolecules* **1996**, 29, 940-945.

- 64)Grem, G.; Paar, C.; Stampfl, J.; Leising, G.; Huber, J.; Scherf, U. *Chem. Mat.* **1995**, 7, 2-4.
- 65)Miller, L. L.; Jozefiak, T. H. *Synth. Met.* **1988**, 27, B431-B437.
- 66)Ashton, P. R.; Brown, G. R.; Isaacs, N. S.; Giuffrida, D.; Kohnke, F. H.; Mathias, J. P.; Slawin, A. M. Z.; Smith, D. R.; Stoddart, J. F.; Williams, D. J. *J. Am. Chem. Soc.* **1992**, 114, 6330-6353.
- 67)Ashton, P. R.; Brown, G. R.; Smith, D. R.; Stoddart, J. F.; Williams, D. J. *Tetrahedron Lett.* **1993**, 34, 8337-8340.
- 68)Mayer, A.; Meier, H. *J. Prakt. Chem.-Chem. Ztg.* **1997**, 339, 679-681.
- 69)Graham, R. J.; Paquette, L. A. *J. Org. Chem.* **1995**, 60, 5770-5777.
- 70)Kojima, Y.; Tsuji, M.; Matsuoka, T.; Takahashi, H. *J. Polym. Sci. Pol. Chem.* **1994**, 32, 1371-1376.
- 71)Minakata, T.; Nagoya, I.; Ozaki, M. *Synth. Met.* **1991**, 42, 1501-1508.
- 72)Billups, W. E.; Luo, W. M.; McCord, D.; Wagner, R. *Pure Appl. Chem.* **1996**, 68, 275-280.
- 73)Zheng, T.; Zhong, Q.; Dahn, J. R. *J. Electrochem. Soc.* **1995**, 142, L211-L214.
- 74)Wang, T.; Kang, E. T.; Neoh, K. G.; Tan, K. L. *Synth. Met.* **1997**, 84, 405-406.
- 75)Shirakawa, H. *Synth. Met.* **1995**, 69, 3-8.
- 76)Novak, B. M.; Risse, W.; Grubbs, R. H. *Adv. Polym. Sci.* **1992**, 102, 47-72.

- 77)Gibson, V. C. *Adv. Mater.* **1994**, 6, 37-42.
- 78)Nagai, K.; Higuchi, A.; Nakagawa, T. *J. Polym. Sci. Pt. B-Polym. Phys.* **1995**, 33, 289-298.
- 79)Nagai, K.; Nakagawa, T. *J. Membr. Sci.* **1995**, 105, 261-272.
- 80)Masuda, T.; Isobe, E.; Higashimura, T. *Macromolecules* **1985**, 18, 841.

Chapter 2

Synthesis and Characterization of Ethylene Oxide Substituted Poly(*p*-phenylene)s.

2.1. Introduction

Addition of flexible side chains to rigid polymer backbones has proven to be an extremely effective procedure for obtaining tractable and fusible materials. Not only does this modification enable the utilization of conventional polymer processing methods, side chain substituted polymers often exhibit properties that do not exist in the unsubstituted analogs. Some of these properties include pronounced thermochromism and solvatochromism,¹ thermotropic and lyotropic liquid crystallinity,²⁻⁶ and structural self-assembly.⁷⁻⁹

Most of the side chain containing rigid polymers synthesized to date employ alkyl, alkoxy or phenylalkyl side chains of varying lengths that are chemically anchored at sites along the polymer backbone.^{6,10-16} From a structural standpoint, the most interesting characteristic of these substituted rigid polymers is the presence of two chemically dissimilar building blocks; the non-polar flexible side chains and the stiff π -conjugated main chains. Given the opportunity, these polymers will adopt structures that produce phase separation of the two fundamental units restricted by the chemical linkage that binds them together and any additional steric packing constraints. The net result is that solvent cast films or precipitated powders commonly

form layered, semicrystalline structures whereby the hydrophobic side chains appear as spacers between nested stacks of the main chains.¹⁷⁻¹⁹

Interesting molecular architectures may also be obtained by attaching hydrophilic side chains to the polymer backbone.²⁰⁻²³ Short poly(ethylene oxide) (PEO) side chains have been utilized to increase the solubility of poly(phenylene) and poly(thiophene) systems.^{1,24} An advantage of using polar side chains is that the solubility of the substituted polymers is increased in a wider variety of solvents. The ethylene oxide side chains also increase the functionality of the polymer systems by introducing the ability to coordinate with metal ions. Coordination of Li^+ occurs with the lone pair of electrons on oxygen in the ethylene oxide segments. When lithium salts are incorporated into the flexible side chains, the polymer system may possess a high ionic conductivity.²⁴

We have prepared a series of soluble poly(*p*-phenylene)s substituted with ethylene oxide side chains using a transition metal catalyzed aryl coupling reaction. These substituted rigid rod polymers most likely form comb-like or hairy rod-like structures. As shown schematically in Figure 2.1, we predict that the physical properties of these polymers will vary as the volume fraction of the side chains is increased. Polymers with short side chains should possess properties similar to the parent PPP, while the properties of the polymers with longer side chains should begin to resemble those of poly(ethylene oxide). We also investigated how the addition of lithium salts into the side chains of these polymers affects the physical properties.

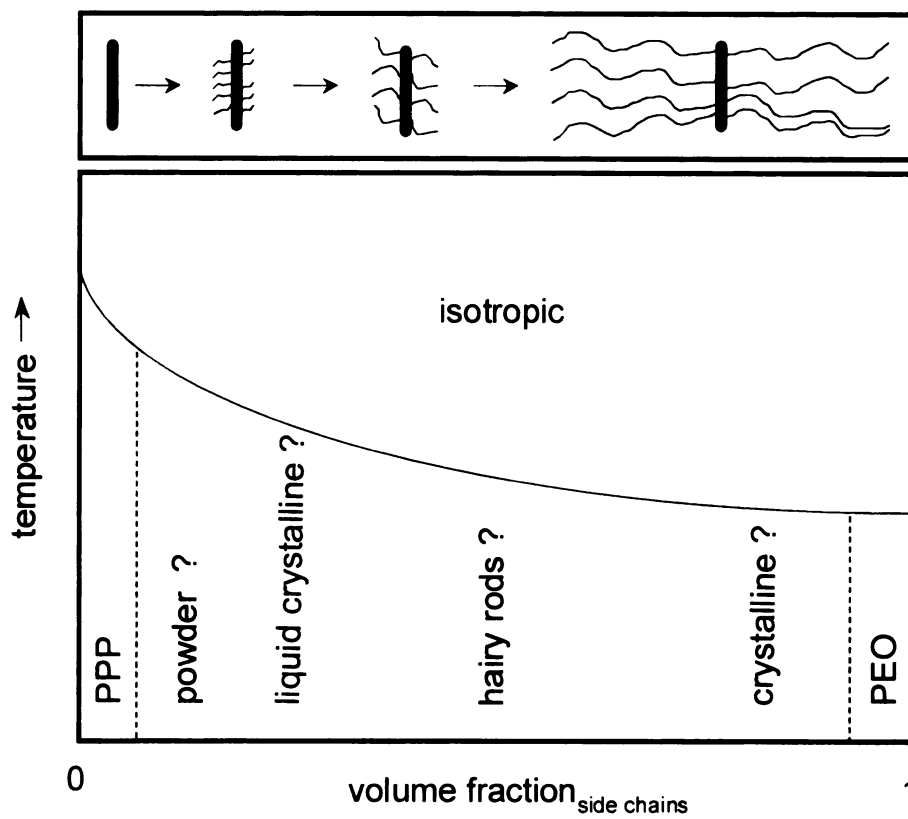


Figure 2.1. Structure/property relationships of ethylene oxide substituted PPP's.

2.2. Experimental Section

Materials. Reagent grade nickel chloride hydrate was heated (250 °C) under vacuum to give a fine, orange powder with constant weight. Triphenylphosphine was purified by recrystallization from hexanes. Powdered zinc was purified by stirring in acetic acid, filtered, rinsed thoroughly with diethyl ether, and dried under vacuum. It was then crushed with a mortar and pestle to increase its surface area. The polymerization solvent, N,N-dimethylformamide (DMF), was stirred over calcium hydride, distilled under vacuum, and stored over 3 Å molecular sieves. Pyridine was stored over 3 Å molecular sieves. Unless otherwise specified, all other ACS reagent grade starting materials and solvents were used as received from commercial suppliers without further purification.

Characterization. Proton nuclear resonance (^1H NMR) spectra were measured using a Varian Gemini-300 spectrometer at 300 MHz. All samples were run at room temperature in CDCl_3 . Chemical shifts were calibrated using residual CHCl_3 and are reported in ppm (δ) relative to tetramethylsilane. Infrared spectra of polymers were obtained under nitrogen at room temperature on a Nicolet Magna-IR 550 Fourier Transform IR spectrometer. A Hitachi U-4001 UV-visible spectrometer was used to obtain the UV-visible spectra of polymer solutions. Molecular weights of polymers were determined by gel permeation chromatography (GPC) using a PLgel 20m Mixed A column and a photodiode array detector at room temperature with THF as eluting solvent at a flow rate 1 mL/min. Monodisperse polystyrene standards

were used to calibrate the molecular weights. The concentration of the polymer solutions used for GPC measurements was 1 mg/mL. Differential scanning calorimetry (DSC) data were obtained under a He environment using a Perkin-Elmer DSC 7 instrument at a heating rate of 10 °C/min. The DSC 7 temperature was calibrated with an indium standard. DSC results of the polymer samples are the first heating scan, taken after flash cooling the sample from an isotropic state. Thermogravimetric analyses (TGA) were performed under nitrogen and air atmospheres at a heating rate of 10 °C/min on a Perkin-Elmer TGA 7 instrument. Elemental analyses were performed using a Perkin-Elmer 2400 Series II Analyzer.

2,5-Dichlorobenzoyl chloride (2). A stirred suspension of 2,5-dichlorobenzoic acid (**1**) (19.02 g, 99.01 mmol) in thionyl chloride (SOCl₂, 100 mL) was refluxed overnight. The excess SOCl₂ was removed by distillation at atmospheric pressure. The crude product was purified by vacuum distillation at 70-74 °C/40 mtorr to yield 18.94 g (90%) of 2,5-dichlorobenzoyl chloride (lit.²⁵ bp 81 °C/2 torr). ¹H NMR δ: 7.4 (d, 2H), 8.0 (t, 1H).

Monomer synthesis: General Procedure. The alcohol (**3a-3h**, 37 mmol) and acid chloride **2** (5.16 g, 24.6 mmol) were dissolved in pyridine (50 mL) and gently heated overnight. Upon cooling, methylene chloride (100 mL) was added and the solution was washed three times with 50 mL of 1N HCl (aq) and once with 50 mL of H₂O. The organic layer was collected, dried with magnesium sulfate, filtered, and the solvent removed with a rotary evaporator. The compounds were purified by

recrystallization (**4a**), vacuum distillation (**4b-4d**), or column chromatography (**4e-4h**). The monomers were passed through a short pad of activated alumina inside a drybox prior to use.

Methyl-2,5-dichlorobenzoate (4a). Compound **4a** was purified by recrystallization from methanol to yield 4.74 g (94%). mp 35 °C (DSC) (lit.²⁶ mp 37-40 °C). ¹H NMR δ: 3.9(s, 3H), 7.4(d, 2H), 7.8(t, 1H).

3-Oxybutyl-2,5-dichlorobenzoate (4b). Compound **4b** was purified by vacuum distillation at 105 °C/80 mtorr to yield 5.63 g (92%). ¹H NMR δ: 3.4(s, 3H), 3.7(t, 2H), 4.45(t, 2H), 7.4(d, 2H), 7.8(t, 1H). Anal. Calcd. for C₁₀H₁₀Cl₂O₃: C, 48.22; H, 4.05; Cl, 28.47; O, 19.27. Found: C, 48.26; H, 4.03.

3,6-Dioxyheptyl-2,5-dichlorobenzoate (4c). Compound **4c** was purified by vacuum distillation at 170 °C/130 mtorr to yield 5.98 g (83%). ¹H NMR δ: 3.4(s, 3H), 3.55(t, 2H), 3.7(t, 2H), 3.85(t, 2H), 4.5(t, 2H), 7.4(d, 2H), 7.8(t, 1H). Anal. Calcd. for C₁₂H₁₄Cl₂O₄: C, 49.17; H, 4.81; Cl, 24.19; O, 21.83. Found: C, 49.01; H, 4.50.

3,6,9-Trioxydecyl-2,5-dichlorobenzoate (4d). Compound **4d** was purified by vacuum distillation at 195 °C/200 mtorr to yield 6.55 g (79%). ¹H NMR δ: 3.35(s, 3H), 3.5(t, 2H), 3.65(m, 6H), 3.8(t, 2H), 4.45(t, 2H), 7.4(d, 2H), 7.8(t, 1H). Anal. Calcd. for C₁₄H₁₈Cl₂O₅: C, 49.87; H, 5.38; Cl, 21.03; O, 23.72. Found: C, 49.75; H, 5.39.

Monomer 4e. Compound **4e** was purified by column chromatography (silica gel) with hexane/ethyl acetate (2:1) as the eluting solvent to yield 11.06 g (86%). ^1H NMR δ : 3.35(s, 3H), 3.5(t, 2H), 3.65(b, 22H), 3.8(t, 2H), 4.45(t, 2H), 7.4(d, 2H), 7.8(t, 1H). Anal. Calcd. for $\text{C}_{22}\text{H}_{34}\text{Cl}_2\text{O}_9$: C, 51.47; H, 6.67; Cl, 13.81; O, 28.05. Found: C, 51.08; H, 6.68.

Monomer 4f. Compound **4f** was purified by column chromatography (silica gel) with hexane/ethyl acetate (2:1) as the eluting solvent to yield 15.12 g (85%). ^1H NMR δ : 3.35(s, 3H), 3.5(t, 2H), 3.65(b, 42H), 3.8(t, 2H), 4.45(t, 2H), 7.4(d, 2H), 7.8(t, 1H). Anal. Calcd. for $\text{C}_{32}\text{H}_{54}\text{Cl}_2\text{O}_{14}$: C, 52.39; H, 7.42; Cl, 9.66; O, 30.53. Found: C, 51.15; H, 7.17.

Monomer 4g. Compound **4g** was purified by column chromatography (silica gel) with hexane/ethyl acetate (2:1) as the eluting solvent to yield 18.39 g (81%). ^1H NMR δ : 3.35(s, 3H), 3.5(t, 2H), 3.65(b, 58H), 3.8(t, 2H), 4.45(t, 2H), 7.4(d, 2H), 7.8(t, 1H). Anal. Calcd. for $\text{C}_{40}\text{H}_{70}\text{Cl}_2\text{O}_{18}$: C, 52.80; H, 7.75; Cl, 7.79; O, 31.65. Found: C, 51.04; H, 7.15.

Monomer 4h. Compound **4h** was purified by column chromatography (silica gel) with hexane/ethyl acetate (2:1) as the eluting solvent to yield 32.07 g (60%). ^1H NMR δ : 3.35(s, 3H), 3.5(t, 2H), 3.65(b, 174H), 3.8(t, 2H), 4.45(t, 2H), 7.4(d, 2H), 7.8(t, 1H). Anal. Calcd. for $\text{C}_{98}\text{H}_{186}\text{Cl}_2\text{O}_{47}$: C, 53.81; H, 8.57; Cl, 3.24; O, 34.38. Found: C, 53.80; H, 8.73.

Nickel Catalyzed Polymerization: General Procedure. Inside a helium atmosphere drybox, the monomer (1.33 mmol), NiCl_2 (8.6 mg, 0.067 mmol), bipyridine (10.4 mg, 0.067 mmol), triphenyl phosphine (34.9 mg, 0.134 mmol), zinc powder (0.27 g, 4.12 mmol), and DMF (1 mL) were added into a 100 mL round bottomed flask. The flask was then fitted with a reflux condenser capped by a rubber septum. After removal from the drybox, the system was connected to an argon bubbler through the rubber septum and placed in an oil bath. The solution was stirred magnetically and the mixture was heated to 80 °C. The green solution became brown after 10 minutes, eventually turning deep red-brown after 30 minutes. The mixture was stirred overnight. Upon cooling, the solution was transferred into a flask containing 200 mL of 2N HCl/MeOH (1:1) and stirred until the excess zinc dissolved. The polymer was extracted from the HCl/MeOH mixture with methylene chloride (3 x 50 mL). The combined organic layers were dried with MgSO_4 , filtered, and the solvent removed under reduced pressure to yield a pale yellow film.

Preparation of polymer/lithium salt composites. Polymer/ Li^+ composites were prepared from polymer and lithium perchlorate (LiClO_4). Acetonitrile (6-8 mL) was added to a vial containing the polymer sample (0.5 g) and the appropriate amount of LiClO_4 . The mixture was stirred until a homogeneous solution was obtained. The solution was concentrated by solvent evaporation at 70 °C, followed by drying under vacuum for 24 h. The composites were further dried under high

vacuum at 120 °C for 2h. Polymer composites from **5d** and **5e** were prepared with O:Li ratios of 64:1, 32:1, 16:1, 8:1, 4:1, and 2:1 for each polymer. The polymer composites were stored in a dry, inert atmosphere.

2.3. Results

Monomer synthesis. The monomers are easily synthesized from the readily available 2,5-dichlorobenzoic acid in ~85% yields (Figure 2.2). This route offers the flexibility of preparing a series of monomers by simply interchanging various ethylene glycol monomethyl ethers. All of the alcohols used are commercially available, however the oligomeric alcohols **3e-3h** used to prepare monomers with long side chains are not monodisperse, which leads to sets of monomers with slightly differing side chain lengths. The series of monomers was purified by different methods depending upon their physical properties. While monomer **4a** was recrystallized from methanol, short side chain monomers **4b-4d** with lower boiling points were vacuum distilled to yield clear oils. Since the monomers with longer side chains thermally decomposed before distilling, monomers **4e-4h** were purified by column chromatography.

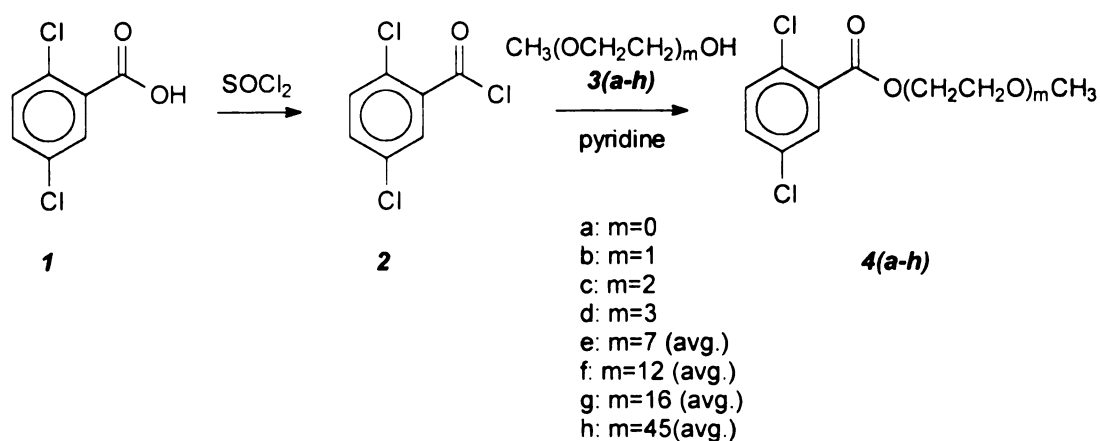


Figure 2.2. Synthetic route to monomers **4a-4h**.

The melting points of the series of monomers as measured by DSC are shown in Figure 2.3. Short side chain monomers (**4a-4c**) exhibited higher melting points, presumably dominated by the p-stacking of the aromatic moiety. For monomer **4d**, no melting point was observed above $-150\text{ }^{\circ}\text{C}$, the low temperature limit of the DSC apparatus. As the lengths of the side chains are increased, the observed melting

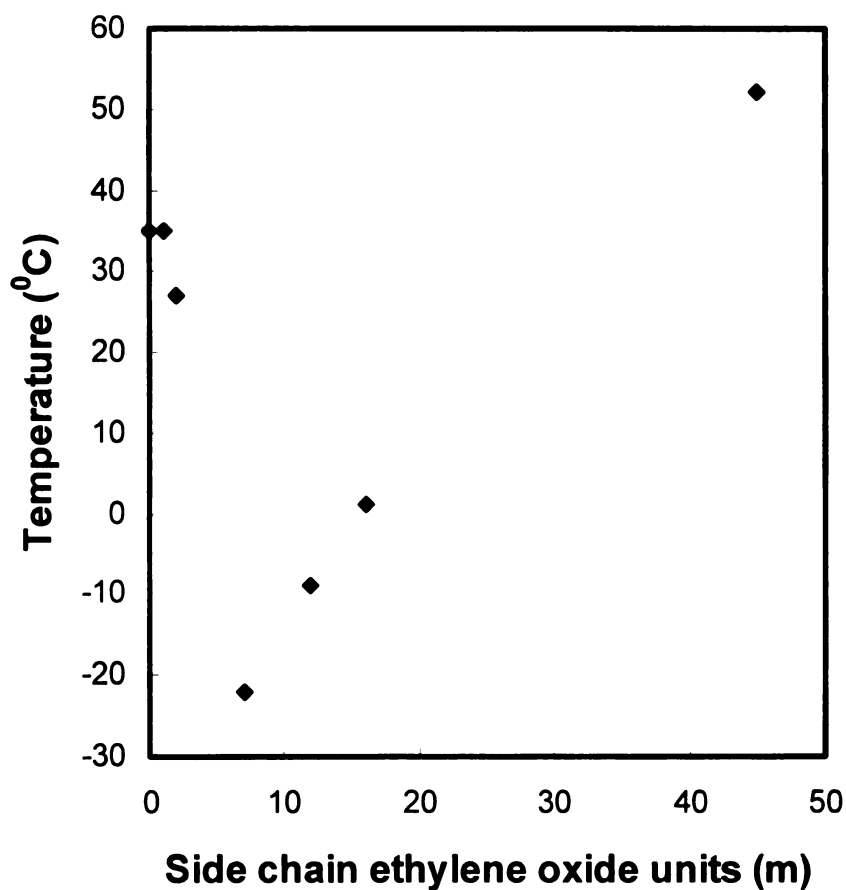


Figure 2.3. Melting points of monomers **4a-4h**.

points increase to where the melting point of monomer **4h** nearly approaches that of PEO. The trend in the melting points of monomers **4a-4h** is a strong indication that increasing the side chain lengths attached to the substituted polyphenylenes should affect the physical properties of the polymers.

Polymerization. The monomers were polymerized utilizing a nickel-catalyzed aryl coupling reaction to yield substituted poly(*p*-phenylene)s **5a-5h** (Figure 2.4). This coupling reaction was originally proposed as an inexpensive aryl coupling reaction to produce substituted biphenyls.²⁷ Due to the reported high yields, lack of terminating side reactions, and tolerance to a variety of functional groups, it was

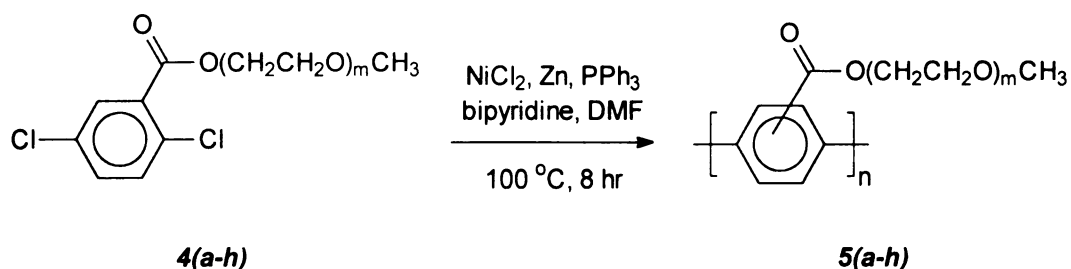


Figure 2.4. Nickel catalyzed polymerization.

also found to be an efficient method for the polymerization of dichloro aromatic compounds.²⁸⁻³¹ The desired all *para* ring linkages in the resulting polymers are ensured by starting with *para* dichloro-substituted aryl monomers. The proposed catalytic cycle is shown in Figure 2.5. The active catalytic species (Ni^0) is generated

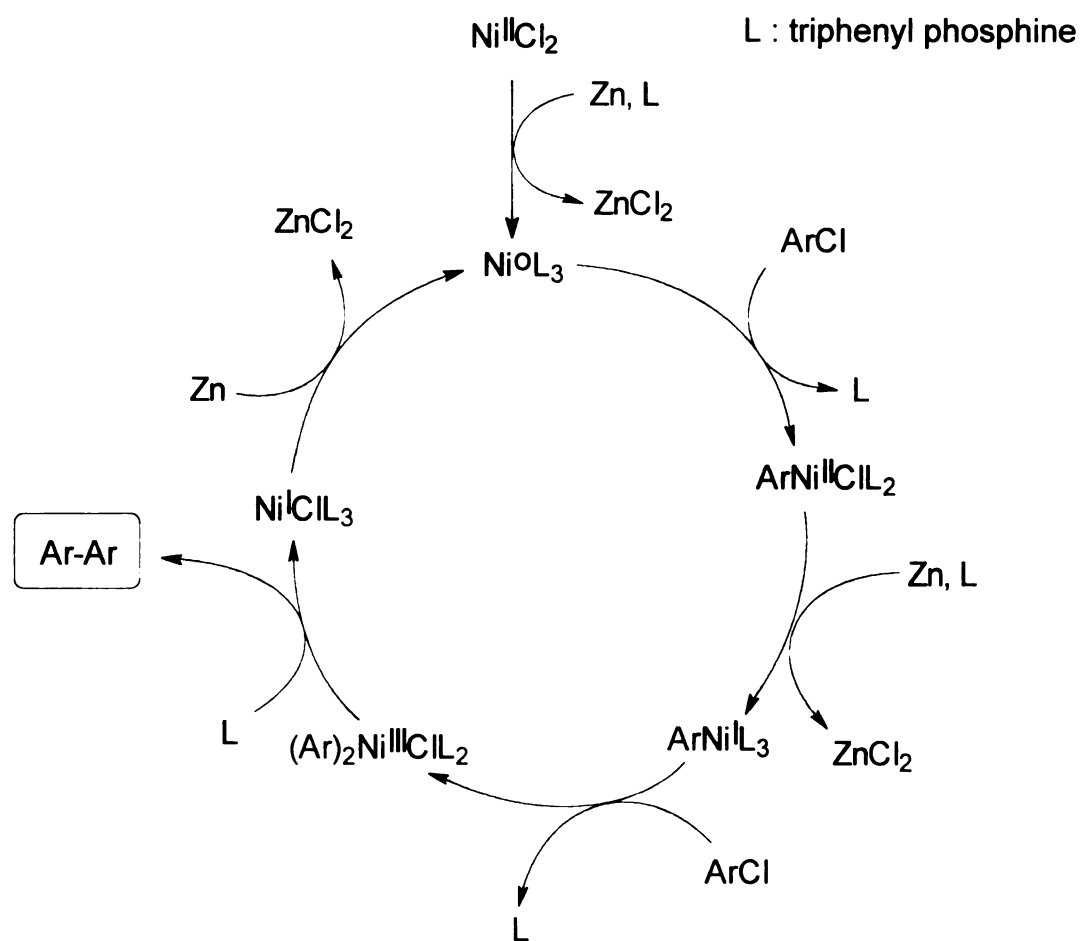


Figure 2.5. Catalytic cycle of nickel mediated aryl coupling.

by the reduction of nickel(II) chloride using powdered zinc. The Ni^0 species then undergoes an oxidative addition with an aryl chloride followed by transmetallation with another monomer unit to form a diaryl nickel(II) complex. In order for reductive elimination to occur and form the coupled product, the aryl ligands must take a *cis* conformation on the square planar nickel complex. The bipyridine acts as a bidentate ligand that forces the aryl groups into a *cis* orientation to facilitate reductive elimination. The catalyst is then regenerated by zinc in the highly reducing environment.²⁷

The condition of the catalyst can be monitored as the reaction proceeds due to a built-in indicator. The reaction takes on a blood red color shortly after heating due to the formation of Ni^0 . Contamination of the polymerization by oxygen and proton sources must be prevented. The active Ni^0 species is consumed by oxidation forming black NiO , and proton sources reduce the growing polymer, terminating the chain. Either contaminant leads to the loss of the deep red reaction color. Potential proton sources in this reaction are moisture absorbed in the solvent (DMF) and monomers, and high boiling alcohols contaminating the monomer after esterification. The solvent was dried by passing it through a pad of oven-dried silica gel inside the dry box and storing it over 3Å molecular sieves. Any possible contamination of residual alcohol in the monomers was removed by running monomer solutions through a short pad of oven dried silica gel using toluene as solvent inside the dry box. The toluene was then removed under reduced pressure and the monomers were stored inside the dry box.

Polymer characterization. The physical properties of the resulting polymers ranged from powders to tacky solids depending upon the side chain length and degree of polymerization. The molecular weights of the polymers as measured by GPC relative to polystyrene standards are shown in Table 2.1. The obtained degrees of

Table 2.1. Representative molecular weights of polymers **5a-5h**.

polymer	Mn	Mw	PDI	DP (n)
5a	4700	8900	1.9	35
5b	17500	46600	2.6	98
5c	15000	41000	2.7	68
5d	14600	63000	4.3	55
5e	18200	59500	3.3	40
5f	14000	26000	1.9	22
5g	18000	35000	1.9	21
5h	9400	23300	2.5	5

polymerization for the series of polymers were not consistent however (Figure 2.6). The molecular weights of the short side chain polymers are limited by insolubility at higher degrees of polymerization, while the molecular weight of the polymers with longer side chains are limited by either steric hindrance, or a reduction in monomer concentration as the aryl ring becomes a smaller part of the monomer. GPC traces also indicate an extremely high molecular weight fraction for polymers **5e-5h**. It is believed that these polymers are lightly cross-linked aggregates. The long chain alcohols used to prepare the monomers most likely contained some diol that when reacted with 2 equivalents of acid chloride, formed a cross-linkable monomer. It is difficult to analyze for the presence of this contaminant since its amount is small and

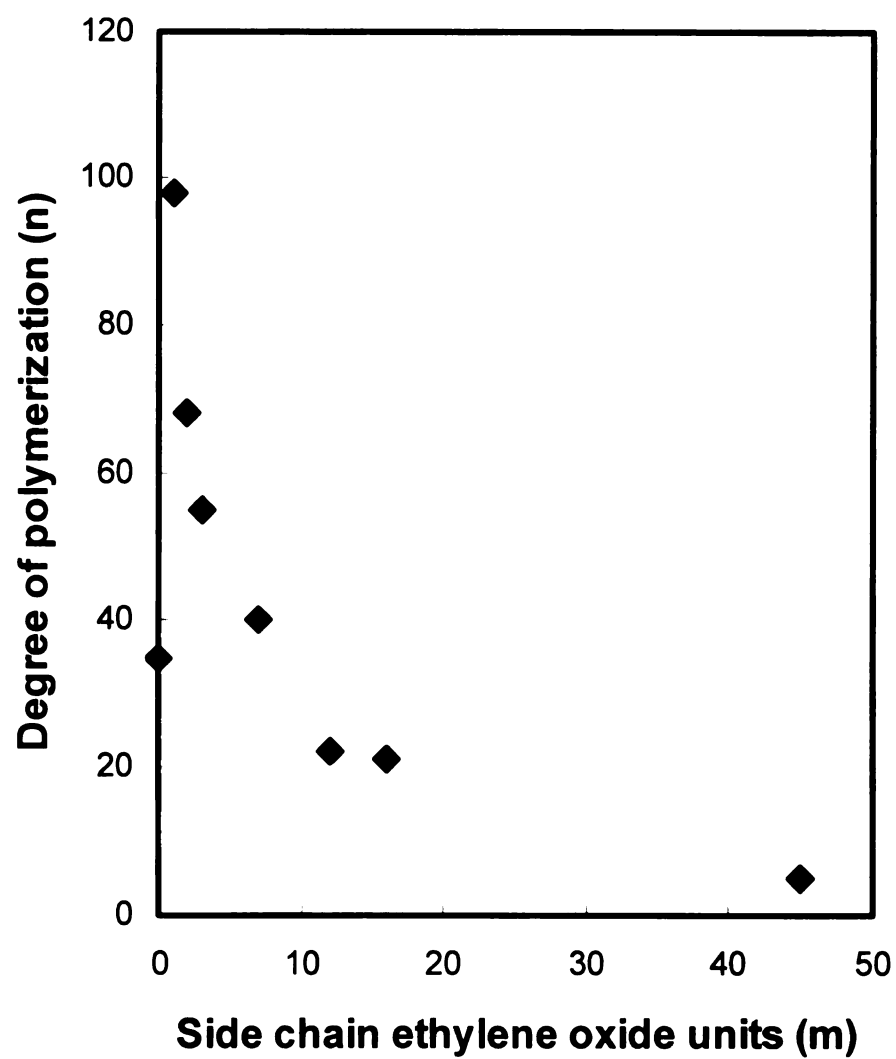


Figure 2.6. Degrees of polymerization of polymers **5a-5h**.

it can not be readily distinguished from the monomer by ^1H NMR integration. The amount of solvent used in the polymerizations also affected the resulting molecular weight of the product. Since dilute polymerizations yielded lower molecular weight polymers than concentrated polymerizations, the minimum amount of solvent was used to dissolve the monomer and catalytic reagents.

The conformation of the aromatic rings in the polymer backbone can be determined from the UV/Vis absorption spectra. Twisting of the rings as a result of steric interactions of the side chains limits the π -conjugation of the phenylene backbone. This is evident by the λ_{max} observed for the polymers. Regardless of molecular weight or length of side chain, the polymers' maximum intensity wavelength absorption was at 317 nm, corresponding to the benzoyl chromophore. With twisting of the rings, the side chains randomly extend outward from the rotated backbone creating comb-like or hairy rod structures. As shown in Figure 2.7, polymer solutions excited at 317 nm strongly fluoresce from 350 to 450 nm. The iridescent blue emission can also be seen when polymer films are irradiated with a black lamp.

There is a multitude of effects directly related to the side chain placement and chemical architecture that have a tremendous impact on the final structural ordering and phase behavior of these polymers (Figure 2.8). For example, it has been observed that varying the degree of regioregularity of the monomeric repeat units can alter many physical properties. In the case of 2,5-disubstituted poly(*p*-phenylene)s, there are considerable steric interactions that frustrate the formation of

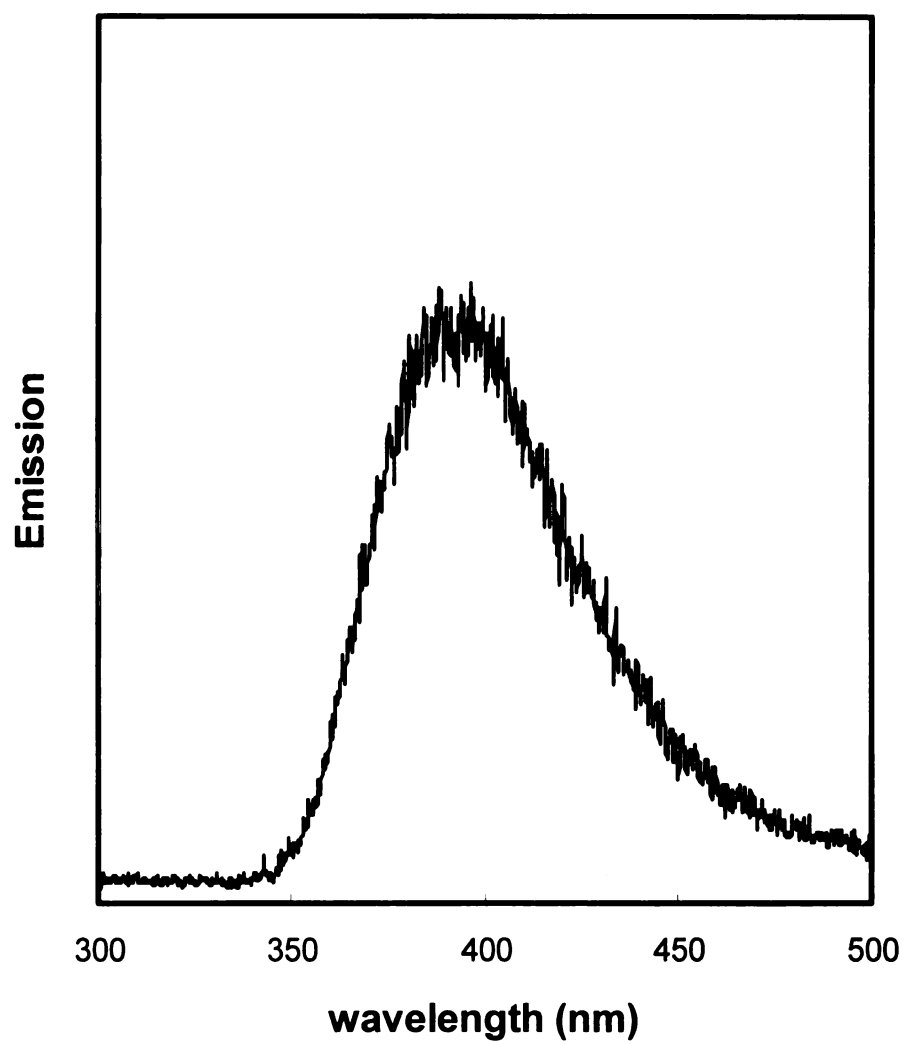


Figure 2.7. Fluorescence spectra of a solution of polymer **5d** in methanol excited at 317 nm.

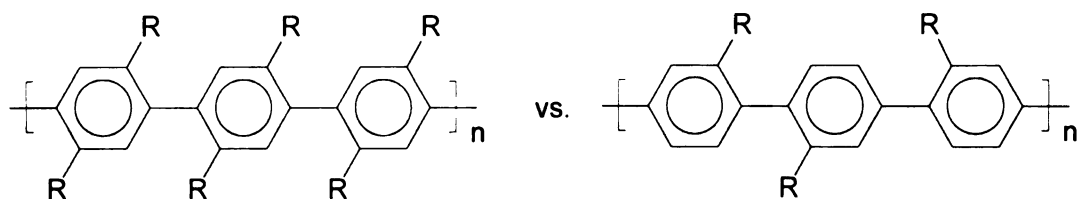


Figure 2.8. Comparison of the orientation of repeat units in 2,5-disubstituted and 2-substituted PPP's.

a planar main chain conformation. Due to the twisting of adjacent aromatic rings to relieve steric interactions between substituents, these polymers are not extensively π -conjugated.³² Since the monomer unit is symmetric, these polymers can organize by stacking and tend to form ordered structures. However, the repeat units in monosubstituted polyphenylenes, such as **5a-5h**, can be coupled in three distinct orientations: head-to-tail, head-to-head, and tail-to-tail. Although the orientations of the repeat units in the resulting polymers may be random or highly regular, considerably less steric interaction exists between adjacent rings and the degree of twisting is less than that in 2,5-disubstituted PPP's. We believe that polymers **5a-5h** form more disordered structures due to randomness of the ring twisting and the positions of the side chains attached to the polymer backbone.

Thermogravimetric analyses of the series of polymers under nitrogen show the onset of a weight loss around 300 °C due to the decomposition of the side chains. Depending upon the volume fraction of polyphenylene backbone in the original sample, degradation results in a 10-50 % char yield at 600 °C. As shown in Figure 2.9, the temperature at which volatile by-products begin to evolve is dependent upon the length of the side chain. Since the polymers with short side chain substituents do not melt before decomposing, it is also possible that these solid samples tend to degrade at slightly higher temperatures.

The phase transitions of the series of polymers were measured by DSC. The thermograms shown in Figure 2.10 are the first heating scans taken after flash cooling the sample from 250 °C. DSC measurements on polymers **5a-5c** show no thermal transitions below the decomposition temperature (< 300 °C). Polymers **5d-5g** with longer side chains exhibit glass transitions (T_g). Plotted in Figure 2.11, the measured glass transition temperatures approach the T_g of PEO, ~ -60 °C, indicating that the properties of the substituted polymers are approaching those of PEO. By definition, a glass transition occurs when molecular motion within a polymer is no longer restricted and results in a second order transition, softening the sample. As shown schematically in Figure 2.12, the T_g 's of these polymers occurs when the side chains become flexible enough to allow the hairy rods to pass back and forth across each other. This is analogous to the feel of a wire bristled brush versus a soft paint brush.

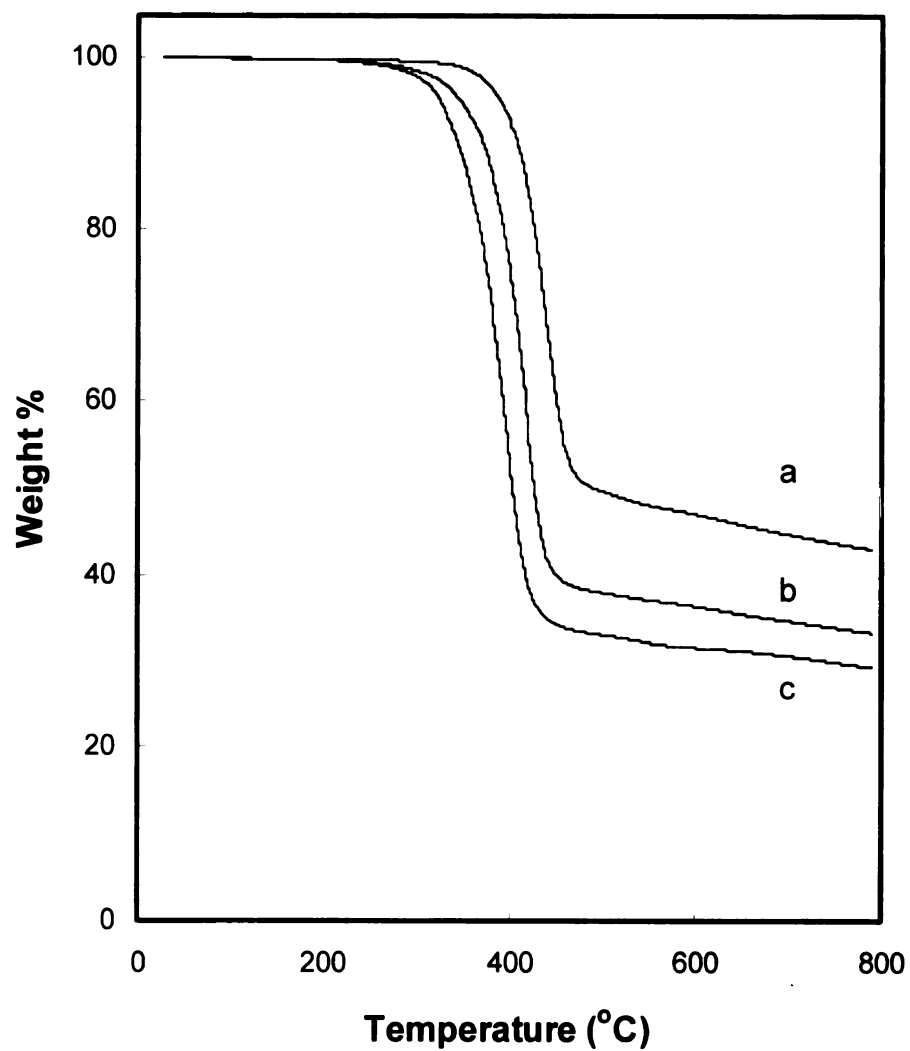


Figure 2.9. Thermogravimetric analysis of a) **5b**, b) **5c**, and c) **5d** in nitrogen heated at 10 °C/min.

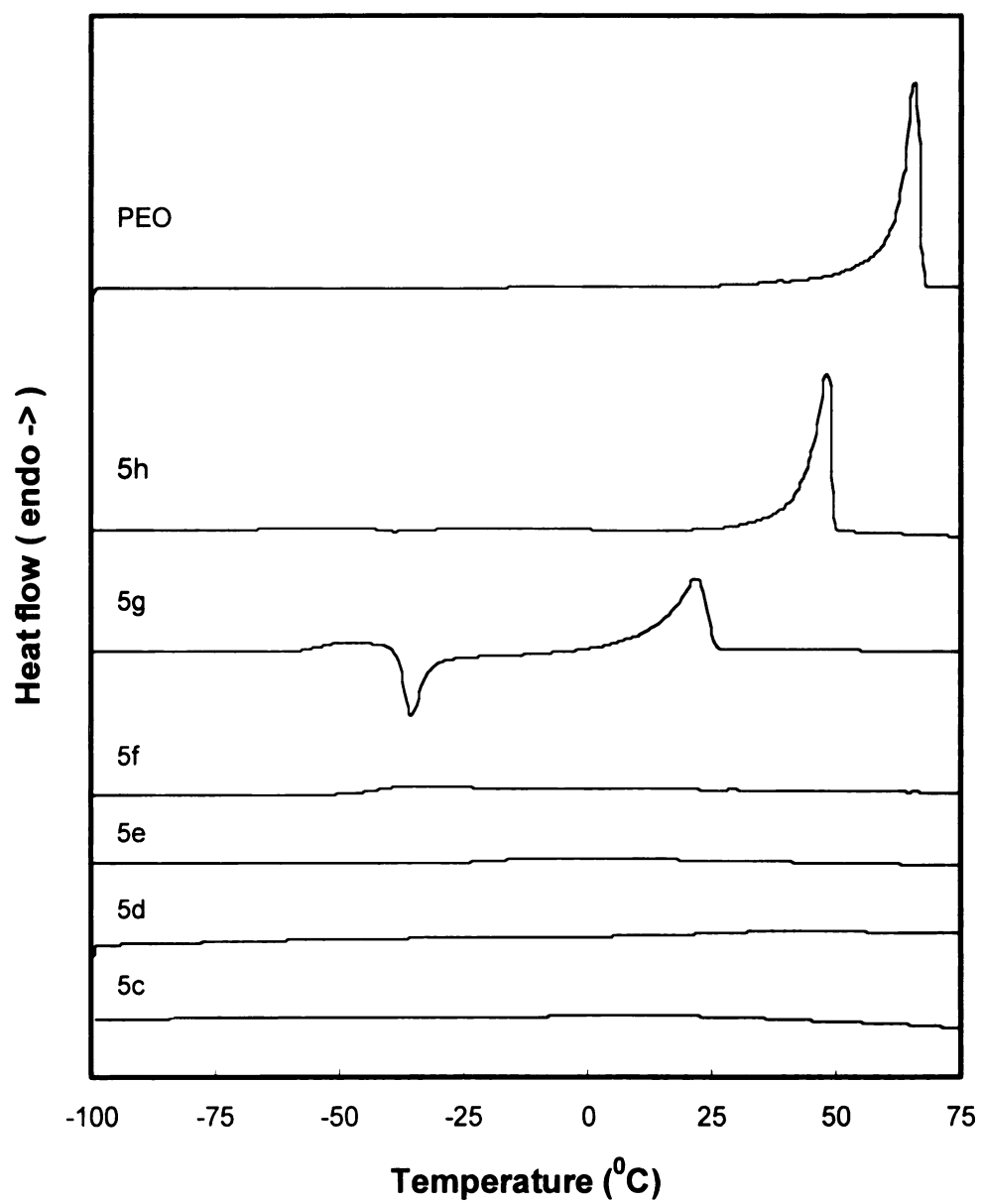


Figure 2.10. DSC results for polymers **5c-5h**, and PEO.

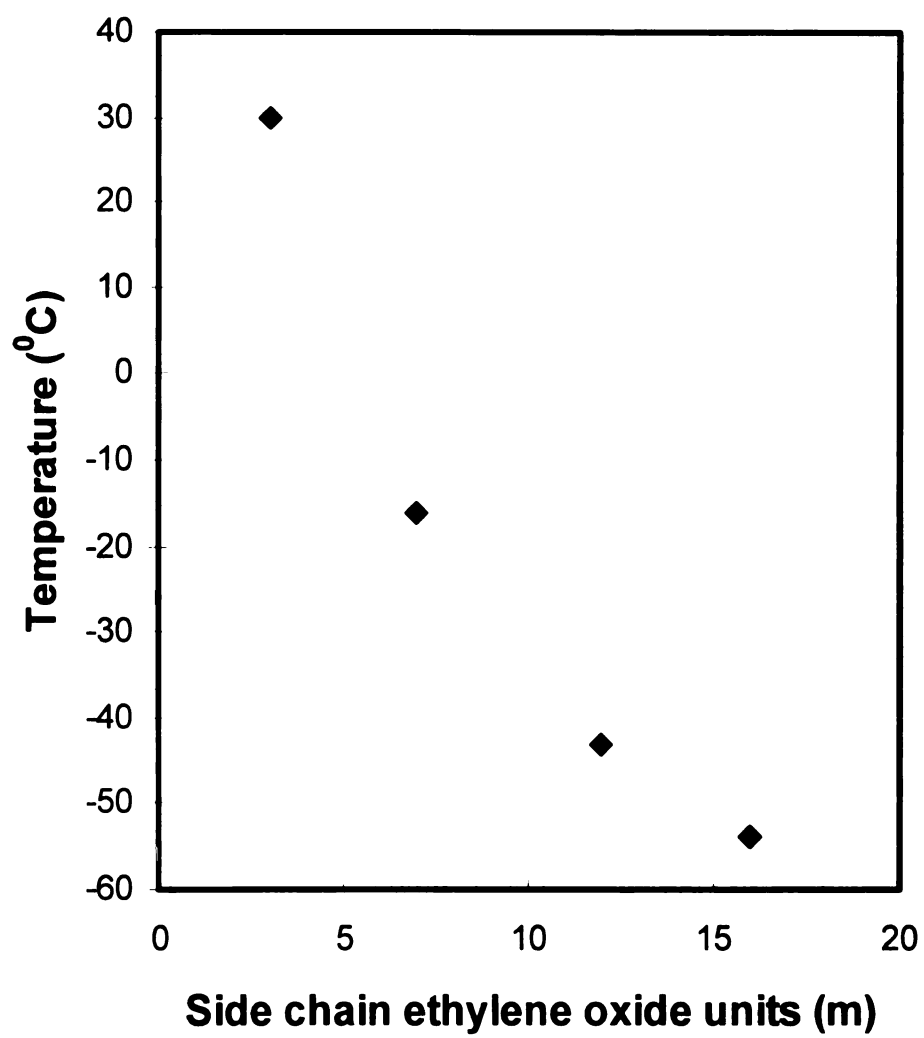


Figure 2.11. Glass transition temperatures of polymers **5d-5h**.

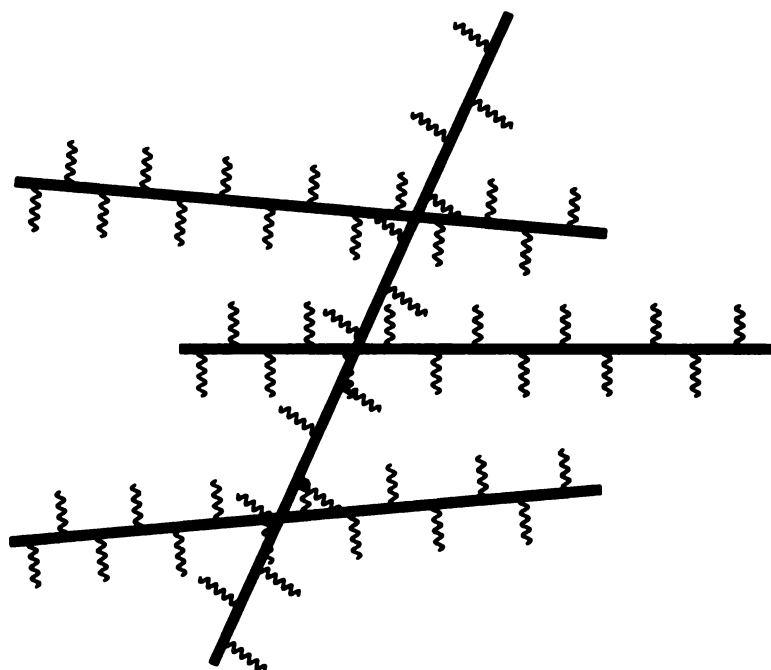


Figure 2.12. Schematic representation of rigid rod PPP backbone substituted with flexible ethylene oxide side chains.

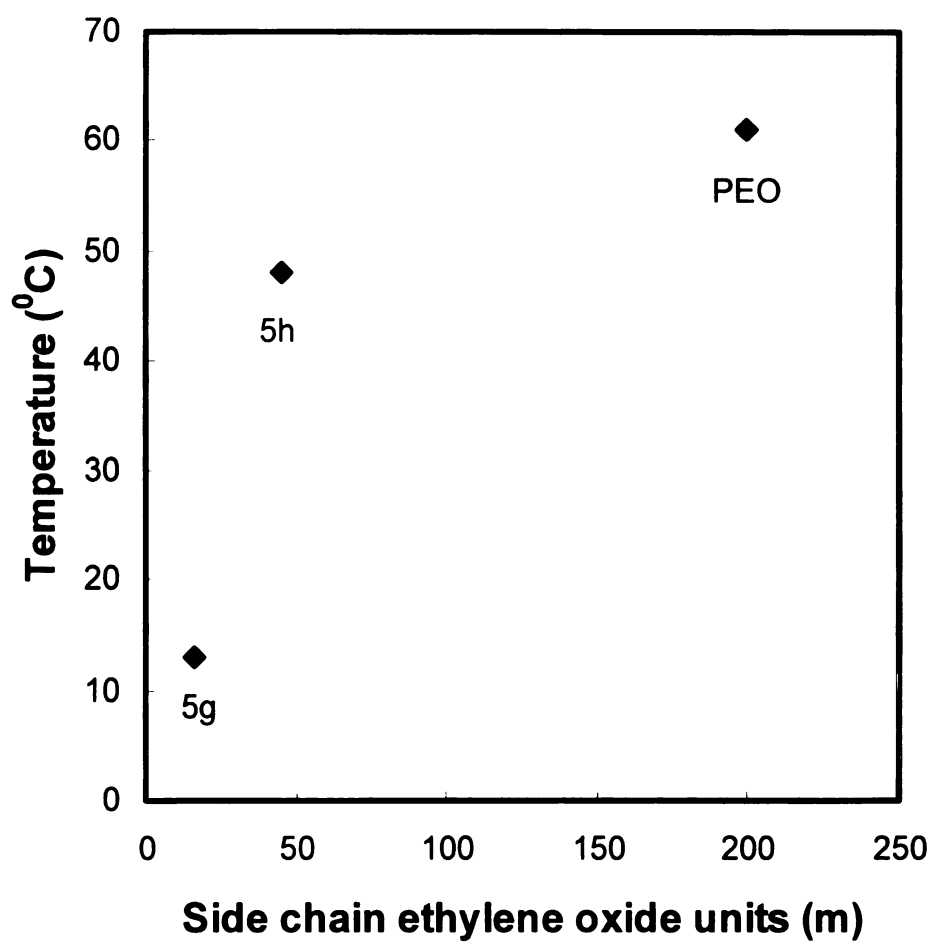


Figure 2.13. Melting points of polymers **5g-5h**, and PEO.

Crystallization of the side chains is observed in polymers **5g** and **5h**. It is likely that the non-uniform side chain lengths for the polymers with $m > 7$ hinder crystallization. Plotted in Figure 2.13, the observed melting points appear to approach that of PEO. The crystallinity was also detected by observing birefringence using polarized optical microscopy.

Liquid crystalline behavior was observed for polyphenylenes **5b-5f**. The term *liquid crystal* refers to the phase that lies between the rigidly ordered solid phase where mobility of individual molecules is restricted and the isotropic phase where molecular mobility and a general lack of molecular order exists. When the rod-like polymer molecules are aligned either through mechanical or other means, the sample will polarize light in the ordered domains. Rod-shaped organic molecules typically align in a nematic phase. The molecules within a nematic mesophase are organized in one dimension, with the chains lying parallel to each other at equilibrium. Polymers **5b** and **5c** exhibited liquid crystalline behavior when the samples were mechanically sheared at elevated temperatures. These polymers however began to thermally degrade before becoming isotropic. Polymers **5d** and **5e** exhibited liquid crystallinity at room temperature when mechanically sheared, but became isotropic when heated slightly. Polyphenylene **5f** showed signs of temporary liquid crystallinity immediately after mechanical shearing at room temperature, but returned to an isotropic state within a few seconds indicating that the interactions aligning the rod-like molecules are not as strong as those for short side chain polymers. When the

crystalline polymers **5g** and **5h** were melted, they showed no signs of liquid crystalline behavior when mechanically sheared. Because the low degrees of polymerization for polymers **5f-5h** may not be high enough to think of the polymer molecules as being truly rod-like, it is likely that the polymers' ability to align in a nematic domain is greatly hindered.

The effect of lithium salts on the physical properties of ethylene oxide side chain substituted PPP was studied by adding various amounts of lithium perchlorate to polymers **5d** and **5e**. In PEO, Li^+ coordination with the oxygen atoms in adjacent polymer chains acts as transient cross-linking, increasing the T_g of the polymer as the amount of added lithium salt is increased. The coordination stabilizes the networks, therefore more energy is needed to overcome the cross-linking. The opposite appears to be happening in the case of the composites prepared with polymer **5d**. As the amount of lithium perchlorate added into the polymer is increased, the measured T_g 's decrease as shown in Figure 2.14. Since the short $m=3$ side chains are relatively rigid without any added lithium salts, we believe that the lithium perchlorate essentially dilates the network lowering chain-chain interactions. Interestingly, another trend is seen in the T_g 's of the composites prepared from polymer **5e** (Figure 2.15). At low Li^+ loadings, the observed T_g 's initially increase, indicating that the added lithium perchlorate presumably organizes the chains through coordination and transient cross-linking. At higher Li^+ loadings however the same trend as seen in Figure 2.14 appears. At these high loadings the increased amount of

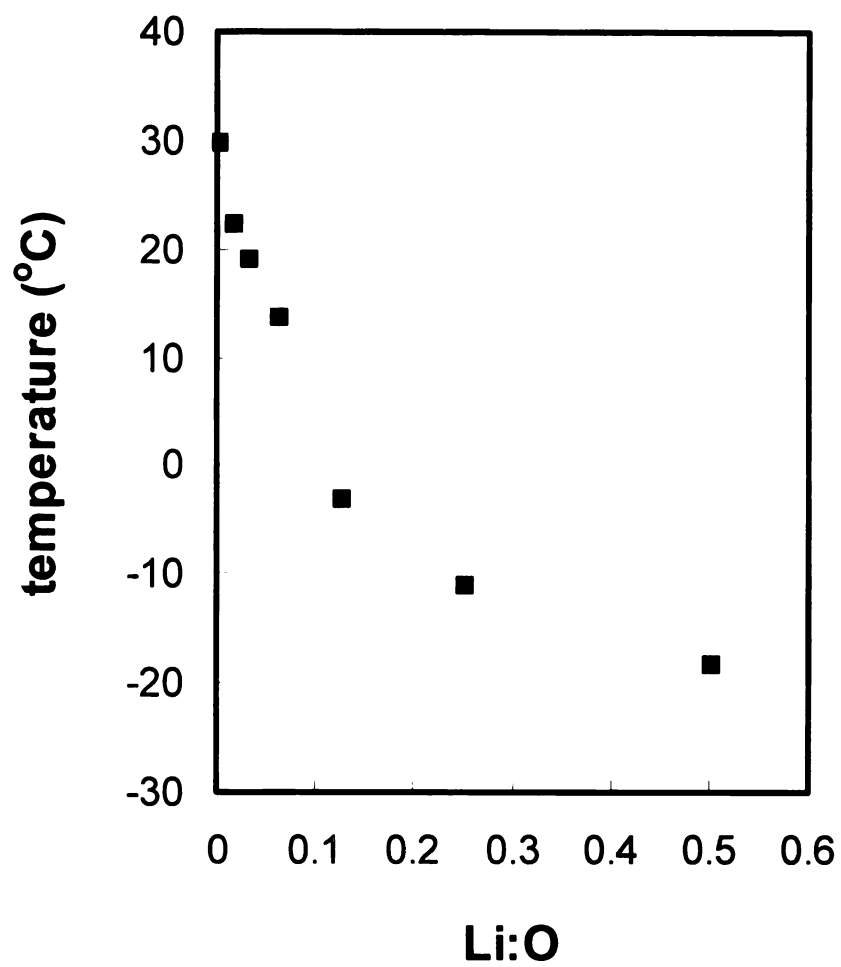


Figure 2.14. Effect of Li^+ salt on the Tg of polymer **5d**.

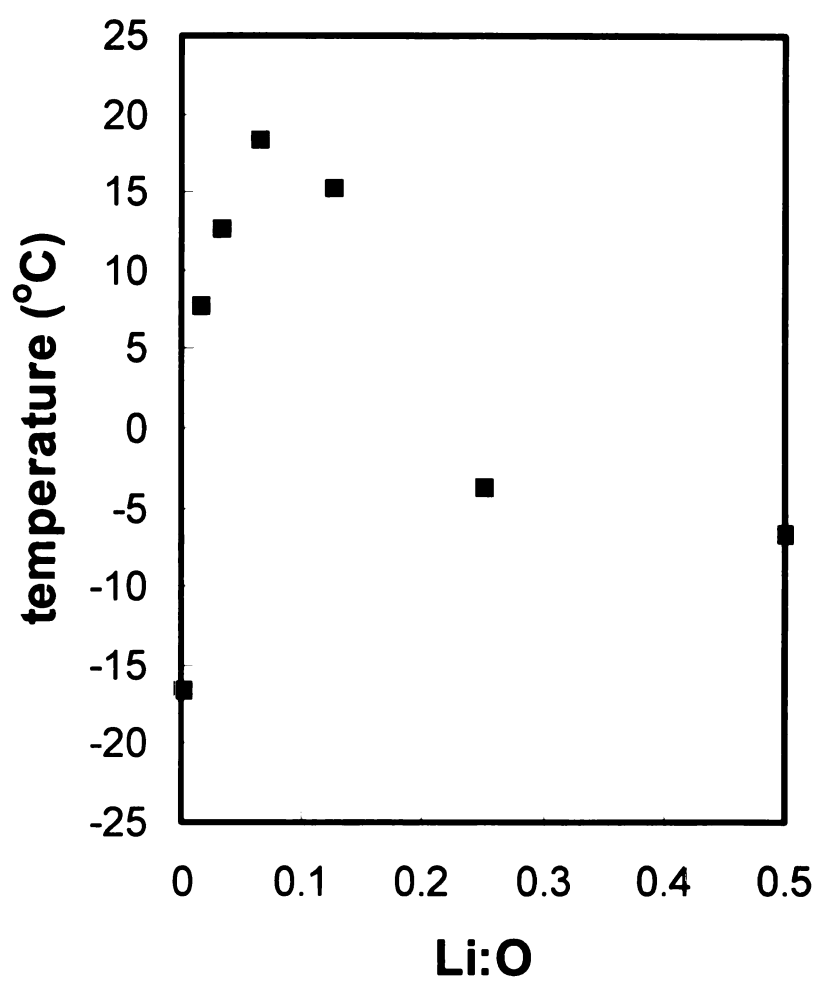


Figure 2.15. Effect of Li^+ salt on the T_g of polymer **5e**.

lithium salt again induces disorder, lowering the T_g . In this sense, high loadings of lithium perchlorate can be thought of as a plasticizer in the polymer sample. If a set of composites were prepared from a high molecular weight sample of polymer **5h**, one would expect the observed T_g 's to increase similarly to PEO since the properties of the polymer **5h** begin to mirror those of PEO.

2.4. Discussion

Structure/property relationships. As predicted, the physical properties of polymers **5a-5h** exhibit a strong dependence upon the length of the oxyethylene side chains attached to the polymer backbone. The structure/property relationships are summarized in the schematic phase diagram shown in Figure 2.16. The side chains in polymers **5a-5h** can be thought of as ropes attached to a wall. The chemical connectivity of the chain to the PPP backbone limits the mobility of the side chains. It was observed that the short chains could not aggregate, and only the longest side chains showed signs of order. Presumably the long chains are less affected by the limited mobility.

The random orientation of the repeat units in the rigid polymer backbone also prevents organization. Whereas stereoregular polymers, which usually have symmetric repeat units, exhibit reasonably well-ordered structures, stereoirregular polymers typically exhibit relatively poor degrees of order. The position of the side chain relative to that of another on an adjacent ring and the degree of twisting along the polymer backbone resulting from the steric repulsion of the ring substituents creates a disordered “hairy rod-like” structures. Therefore, ordering of the side chains could only be expected for longer side chains which are not affected by the chemical connectivity.

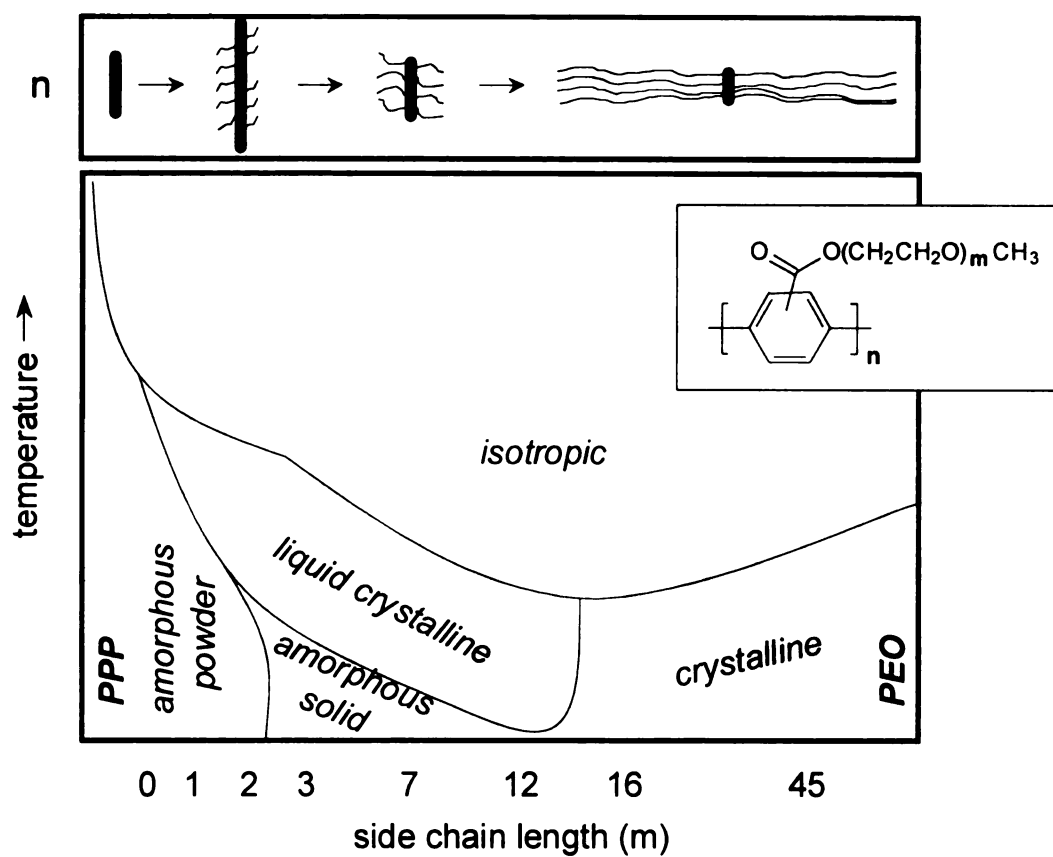


Figure 2.16. Schematic phase diagram of ethylene oxide substituted PPP's **5a-5h**.

A drawback to the assessment of the role of side chain length on the overall properties of the series of substituted polymers is the inconsistency of side chain length for polymers **5e-5h**. The long chain alcohols used in the synthesis of monomers **4e-4h** are not of uniform length. Phase transitions such as crystallization may be hindered due to variance in the side chain lengths. A proposed synthesis of exact length long chain ethylene glycol monomethyl ethers is suggested in Figure 2.17. This route involves the iterative coupling of short chain ethylene glycol monomethyl ethers and deprotonated tetraethylene glycol, protected with a tetrahydropyran (THP) group. The first step involves tosylation of the commercially available, exact length ethylene glycol monomethyl ethers **3a-3d**. Tetraethylene glycol can then be mono-protected by reaction with dihydropyran and deprotonated by reaction with sodium hydride. A Williamson-type ether synthesis gives a coupled product that after

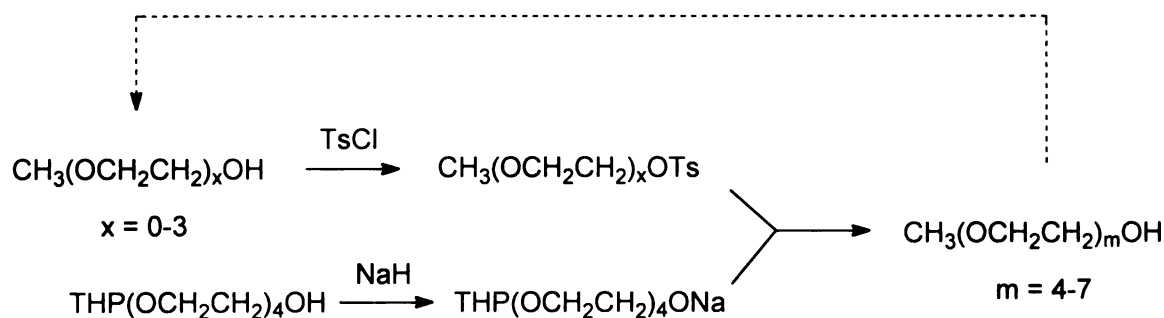


Figure 2.17. Synthetic route to exact length ethylene glycol monomethyl ethers.

deprotection, yields the exact length alcohols with $m = 4-7$. To obtain chain lengths greater than seven ethylene oxide repeat units, the products from the first coupling can be recycled back into the reaction sequence to yield alcohols with 8 to 11 ethylene oxide units. It may be challenging to purify the alcohols however. Since the boiling points of the products are greater than 300 °C, it is likely that the alcohols will thermally degrade before distilling. The differences in polarity of the alcohols and diols could be useful in the separation and purification by column chromatography or HPLC.

Another major problem hampering the evaluation of the effects of side chain length on the properties of polymers **5a-5h** is the inconsistency of the degrees of polymerization between samples. Not only are the side chain lengths being increased, but the backbone lengths are generally decreasing in size. We believe that the degrees of polymerization vary for several reasons. First, the addition of short side chains to the polyphenylene backbone initially results in higher degrees of polymerization due to the increased solubility of the substituted polymer. However, as the side chain length is increased, the molecular weights steadily decline. Initially we believed this to be due to electronic effects caused by the side chains coordinating to the catalytic sites. Addition of diglyme to the polymerization mixture did not result in lower molecular weights however. Another possibility is the steric blocking of the catalytic site by the side chains. The results from this effect should eventually become constant; beyond some side chain length, the total length of the chain becomes

irrelevant. It appears that the decrease in the measured molecular weights is actually due to a dilution of the reactive aryl chloride sites in the monomers as the length of the side chain is increased. Although the monomer/catalyst ratio was held constant, the amount of aryl chloride sites in the polymerization decreased as the total volume remained constant. Even polymerizations of monomer **4h** attempted using a minimum amount of added solvent resulted in low molecular weight products.

A potential route to a series of polymers with uniform backbone lengths involves the large scale synthesis of a pre-polymer. As shown in Figure 2.18, a butoxy-substituted monomer capable of yielding high molecular weight polymer could be polymerized in high yield. After hydrolysis of this polymer, a carboxylic acid substituted pre-polymer could be obtained. Portions of this polymer could then be re-esterified by two possible routes. The first route involves the reaction of the carboxylated polymer with thionyl chloride, followed by esterification with the desired alcohol (**3a-3h**). The other route involves the direct esterification of the pre-polymer with the desired alcohol. These routes do present several challenges however. The insolubility of the pre-polymer could hinder high reaction yields. Presumably as the amount of side chains grafted unto the polymer backbone is increased, the solubility should also increase. Steric hindrance caused by the attached side chains may limit the conversion of esterification. It may also be difficult to determine the extent of reaction by standard means.

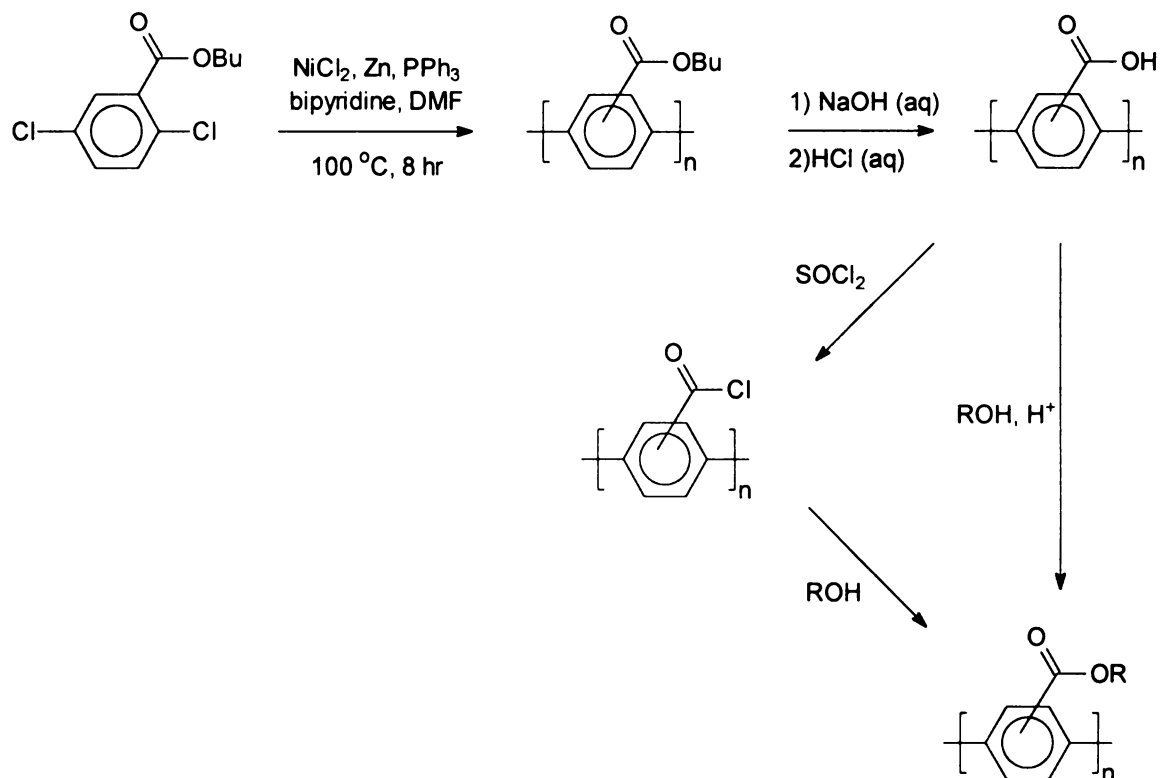


Figure 2.18. Synthetic route to polymers **5a-5h** with uniform backbone lengths.

Applications. Mixtures of PEO with lithium salts have been researched in hopes of developing solid polymer electrolytes (SPE) for rechargeable lithium batteries. In such a device, the SPE has to work as an ion conducting medium as well as a separator preventing direct contact between both electrodes. To do this, the polymer electrolyte requires considerable mechanical strength. One way to achieve this is to form PEO networks. Another possibility is to build molecular composites from rigid rod polymers with ethylene oxide side chains attached to the backbone. The reinforcing effect of the main chains on the disordered ethylene oxide side chains should give materials with distinctly improved mechanical properties compared to pure amorphous PEO systems.²⁴

The UV-visible absorption spectrum of neutral conjugated polymers can be modified by varying their conformational structure. In most cases, these optical changes have been attributed to planar/non-planar conformational transitions of the conjugated backbone. The nature of the side chains and the environment surrounding the polymer affect the electronic properties of the polyphenylene backbone. The strong dependence upon the position and the bulkiness of the substituents seems to indicate that side chain disorder could be the driving force of these optical effects. Non-covalent interactions between alkali metal ions and oxyethylene side chains could also modify the conformation of the side chains and induce a twisting of the main chain. These features are particularly promising for the development of novel affinitychromic and photochromic sensors³³ based on the series of polymers **5a-5h**.

Due to the electronic nature of the rigid backbone and the metal ion coordinating ability of the side chains, these polymers may also have applications as energy transfer materials. Luminescent inorganic salts, such as terbium or europium halides, possess a strong absorption band within the range of the observed fluorescence of polymers **5a-5h**. The emission from the polymer backbone could excite the inorganic salts coordinated to the side chains, resulting in a second lower energy emission (~ 600 nm). The materials could be tuned to emit specific wavelengths by utilizing any number of luminescent inorganic complexes, making it an interesting material for LED devices.

2.5. Conclusions

We have prepared a series of substituted polyphenylenes from ethylene oxide substituted 2,5-dichlorobenzoates utilizing nickel-catalyzed coupling reactions. The number average molecular weights of the polymers ranged from 3000 to 30,000 g/mol. Polymers with short side chains are pale yellow powders, but high molecular weight samples with longer side chains are tacky solids. Thermal analyses and polarized optical microscopy show that the polymer side chains crystallize, and in some cases form liquid crystalline phases. The results of the characterization performed on the title series of substituted poly(*p*-phenylene)s indicate that the physical, thermal, and optical properties observed show a strong dependence on the length of the pendant side chain and on the length of the rigid backbone. The thermal stability of the polymers is limited to the stability of the side chains. An intriguing property of the polymers is the liquid crystalline nature observed after mechanical shearing at elevated temperatures. Due to the physical properties of these polymers, they may have practical applications as LED's, materials for sensing devices, and rigid building blocks for molecular architectures.

2.6. References

- 1) Levesque, I.; Leclerc, M. *J. Chem. Soc., Chem. Commun.* **1995**, 2293-2294.
- 2) Chang, S.; Han, C. D. *Macromolecules* **1997**, *30*, 1670-1684.
- 3) Steuer, M.; Ballauff, M. *J. Polym. Sci. Pol. Chem.* **1993**, *31*, 1609-1619.
- 4) Majnusz, J.; Lenz, R. W. *Eur. Polym. J.* **1989**, *25*, 847-855.
- 5) Majnusz, J.; Catala, J. M.; Lenz, R. W. *Eur. Polym. J.* **1983**, *19*, 1043-1046.
- 6) Stern, R.; Ballauff, M.; Lieser, G.; Wegner, G. *Polymer* **1991**, *32*, 2096-2105.
- 7) Steiner, U. B.; Caseri, W. R.; Suter, U. W.; Rehahn, M.; Rau, I. U. *Langmuir* **1994**, *10*, 1164-1170.
- 8) Delnoye, D. A. P.; Sijbesma, R. P.; Vekemans, J. A. J. M.; Meijer, E. W. *J. Am. Chem. Soc.* **1996**, *118*, 8717-8718.
- 9) Kato, T.; Kihara, H.; Uryu, T.; Fujishima, A.; Frechet, J. M. J. *Macromolecules* **1992**, *25*, 6836-6841.
- 10) Rodriguez-Parada, J. M.; Duran, R.; Wegner, G. *Macromolecules* **1989**, *22*, 2507-2516.
- 11) Schrauwen, C.; Pakula, T.; Wegner, G. *Makromol. Chem., Macromol. Chem. Phys.* **1992**, *193*, 11-30.
- 12) Chen, T. A.; O'Brien, R. A.; Rieke, R. D. *Macromolecules* **1993**, *26*, 3462-3463.
- 13) Chen, S.-A.; Ni, J.-M. *Macromolecules* **1992**, *25*, 6081-6089.
- 14) Rughooputh, S. D. D. V.; Nowak, M.; Hotta, S.; Heeger, A. J.; Wudl, F. *Synth. Met.* **1987**, *21*, 41-50.

- 15)Corish, J.; Morton-Blake, D. A.; Beniere, F.; Lantoine, M. *J. Chem. Soc.-Faraday Trans.* **1996**, *92*, 671-677.
- 16)Segura, J. L. *Acta Polym.* **1998**, *49*, 319-344.
- 17)Moore, J. S. *Curr. Opin. Solid State Mat. Sci.* **1996**, *1*, 777-788.
- 18)Fahlman, M.; Rasmusson, J.; Kaeriyama, K.; Clark, D. T.; Beamson, G.; Salaneck, W. R. *Synth. Met.* **1994**, *66*, 123-127.
- 19)Duran, R.; Ballauff, M.; Wenzel, M.; Wegner, G. *Macromolecules* **1988**, *21*, 2897-2899.
- 20)Lauter, U.; Meyer, W. H.; Wegner, G. *Macromolecules* **1997**, *30*, 2092-2101.
- 21)Allcock, H. R.; O'connor, S. J. M.; Olmeijer, D. L.; Napierala, M. E.; Cameron, C. G. *Macromolecules* **1996**, *29*, 7544-7552.
- 22)Pei, Q.; Yang, Y. *J. Am. Chem. Soc.* **1996**, *118*, 7416-7417.
- 23)Aliotta, F.; Di Marco, G.; Fontanella, M. E.; Lanza, M. *J. Phys. Condes. Matter* **1998**, *10*, 545-556.
- 24)Lauter, U.; Meyer, W. H.; Enkelmann, V.; Wegner, G. *Macromol. Chem. Phys.* **1998**, *199*, 2129-2140.
- 25)Cambie, R. C.; Coulson, S. A.; Mackay, L. G.; Janssen, S. J.; Rutledge, P. S.; Woodgate, P. D. *J. Organomet. Chem.* **1991**, *409*, 385-409.
- 26)Chaturvedi, V.; Tanaka, S.; Kaeriyama, K. *Macromolecules* **1993**, *26*, 2607-2611.
- 27)Colon, I.; Kwiatkowski, G. T. *J. Org. Chem.* **1986**, *51*, 2627.

- 28) Colon, I.; Kwiatkowski, G. T. *J. Polym. Sci. Pol. Chem.* **1990**, 28, 367-383.
- 29) Kwiatkowski, G. T.; Colon, I. *Contemporary Topics in Polymer Science* **1992**, 7, 57-74.
- 30) Kwiatkowski, G. T.; Colon, I.; Elhibri, M. J.; Matzner, M. *Makromol. Chem., Macromol. Sym.* **1992**, 54-5, 199-224.
- 31) Kwiatkowski, G. T.; Colon, I. *Abstr. Pap. Am. Chem. Soc.* **1991**, 201, 167-POLY.
- 32) Pasco, S. T.; Baker, G. L. *Synth. Met.* **1997**, 84, 275-276.
- 33) Levesque, I.; Leclerc, M. *Chem. Mat.* **1996**, 8, 2843-2849.

Chapter 3

Synthesis and Characterization of Polyacenic Networks

3.1. Introduction

Perhaps the most important application of acene-like materials is their use as anodes in lithium ion batteries.¹⁻⁵ These rechargeable batteries consist of a metal oxide cathode (typically CoO_2 , MnO_2 or V_2O_5) and a graphitized carbon anode, both being able to reversibly intercalate lithium ions into their structure. The anode materials are derived from petroleum pitches or phenolic resins pyrolyzed at high temperatures to give partially graphitized structures.⁶ A charged cell corresponds to high lithium content in the carbon anode, with the discharge reaction corresponding to the transfer of lithium ions from the anode to the metal oxide cathode.

An important parameter of lithium ion cells is their capacity, which is limited by the amount of lithium that can be inserted reversibly into the carbon. Until recently, it was thought that the limiting stoichiometry for lithium insertion into graphitized carbon was C_6Li , the value obtained with highly ordered graphite. Recent work⁷⁻¹⁰ using carbons heat treated at low temperatures has shown that the C_6Li ratio can be exceeded. It is unclear if the excess capacity corresponds to cluster-like lithium doping that fills the void space in the disordered carbon,¹¹ or if the excess lithium is located at the edge of the graphene sheets.^{12,13} Recent experimental evidence and calculations indicate that the increased capacity is correlated with the hydrogen content

of the electrode.¹⁴ Therefore, it is important to be able to prepare acene-like structures with a substantial fraction of edges in large quantities.

The high temperatures needed for the pyrolysis allows little control of the acene-like structural elements that are the precursors to graphite. If elements of the acene structure can be designed into the starting material, it should be possible to obtain partially graphitized structures at low temperatures that retain some memory of the chemical structure before pyrolysis. In principle, polyacenes could be prepared that require no thermal treatment for them to be useful electrode materials.

The primary goal of this work is to devise and execute the synthesis of well-defined polyacenes and acene-like materials. We investigated two types of polyacene syntheses based on acid catalyzed electrophilic aromatic substitution reactions. The first targets simple routes to acene-like materials that contain a substantial fraction of acene subunits. Materials resulting from this work are relevant to applications like electrical conductors, anti-static agents, and carbon electrodes, where it is important to be able to supply large amounts of material at relatively low cost. The second route targets the synthesis of a methoxymethyl substituted poly(*p*-phenylene) that when chemically cross-linked, should form a two-dimensional network closely resembling a graphite sheet. It is believed that this precursor can be converted to highly ordered graphite at much lower temperatures than previously obtained.

3.2. Experimental Section

Materials. Tetrahydrofuran (THF) and toluene were distilled from powdered calcium hydride under nitrogen, and then from sodium benzophenone ketyl under nitrogen. N,N-dimethylformamide (DMF) was stirred over powdered calcium hydride, distilled under reduced pressure and stored over 3Å molecular sieves. Reagent grade NiCl_2 was treated with SOCl_2 and then dried at 220°C under vacuum. Triphenylphosphine (PPh_3) was purified by recrystallization from hexanes. Granular zinc was stirred with glacial acetic acid, filtered, rinsed thoroughly with diethyl ether, dried under vacuum, and crushed with a mortar and pestle to increase surface area. All other chemicals were purchased from commercial sources and were used without further purification except as noted.

Characterization. ^1H and ^{13}C NMR spectra were measured using a Varian Gemini-300 spectrometer at 300 MHz. All samples were run at room temperature in CDCl_3 . The chemical shifts were calibrated using residual CHCl_3 and reported in ppm (δ) relative to tetramethylsilane. Infrared spectra were obtained from KBr pellets under nitrogen at room temperature on a Nicolet Magna-IR 550 Fourier Transform IR spectrometer. A Hitachi U-4001 UV-visible spectrometer was used to obtain the UV-visible spectra of cyclohexane solutions of the polymers. Polymer molecular weights were determined by gel permeation chromatography (GPC) using a PLgel 20 μ Mixed A column with THF as the eluting solvent at a flow rate of 1 mL/min, a Waters R401 Differential Refractometer detector at room temperature, and a Varian

2050 Variable Wavelength detector set at 254 nm. Monodisperse polystyrene standards were used to calibrate the molecular weights. The concentration of the polymer solutions used for GPC measurements was 1 mg/mL. Thermogravimetric analyses (TGA) were performed in nitrogen and air atmospheres at a heating rate of 10 °C/min on a Perkin-Elmer TGA 7 instrument. Elemental analyses were performed using a Perkin-Elmer 2400 Series II Analyzer.

Synthesis of bis(methoxymethyl)benzenes. A mixture of hexanes/MeOH (1:1, 50 mL) was added dropwise to a slurry of sodium hydride (NaH, 1.4 g, 57 mmol) that had been rendered oil-free by washing with hexanes. The solution was stirred at room temperature until all of the NaH reacted. The sodium methoxide solution was transferred *via* cannula to a solution of bis(bromomethyl)benzene (6.0 g, 23 mmol) in hexanes (100 mL). The mixture was gently refluxed for 3 hr, during which the color of the solution turned slightly tan. After cooling, the solution was washed with water (3 x 50 mL). The organic layer was passed through a short pad of Celite, and dried with MgSO₄. The solvent was removed under reduced pressure and the products were purified by vacuum distillation to yield clear oils.

1,2-Bis(methoxymethyl)benzene (1). Compound **1** was prepared in 91% yield (3.45 g); bp 98 °C/25 mm Hg (lit.¹⁵ 40-45 °C/2 mm Hg). ¹H NMR: δ 3.35 (s, 6H), 4.5 (s, 4H), 7.2-7.35 (m, 4H).

1,3-Bis(methoxymethyl)benzene (2). Compound **2** was prepared in 85% yield (3.21 g); bp 110 °C/25 mm Hg (lit.¹⁵ 125-130 °C/2 mm Hg). ¹H NMR: δ 3.35 (s, 6H), 4.4 (s, 4H), 7.25-7.4 (m, 4H).

1,4-Bis(methoxymethyl)benzene (3). Compound **3** was prepared in 89% yield (3.36 g); bp 105 °C/25 mm Hg (lit.¹⁵ 55-60 °C/2 mm Hg). ¹H NMR: δ 3.35 (s, 6H), 4.4 (s, 4H), 7.4 (s, 4H).

Polymerization of the bis(methoxymethyl)benzenes. A 100 mL round bottomed flask was charged with the bis(methoxymethyl)benzene (1.0 g) and cooled in an ice bath. Concentrated sulfuric acid (3 mL) was added, and the mixture was stirred at 0 °C for 36 hr. The resulting suspension was washed with 20 % (w/w) sodium hydroxide solution (3 x 25 mL), water (3 x 25 mL), and rinsed with ether (3 x 50 mL). The collected solid was dried overnight at 120 °C under vacuum to yield 0.44 g (72%) of a finely powdered, tan solid.

Chemical dehydrogenation of polyacenic networks. The tan powder (0.270 g) from the acid catalyzed polymerization of the bis(methoxymethyl)benzene, 2,3-dichloro-5,6-dicyano-1,4-benzoquinone (DDQ, 1.20 g, 5.3 mmol), and xylenes (60 mL) were added to a 100 mL round bottomed flask. The yellow DDQ immediately turned dark violet. The flask was fitted with a water condenser and purged with nitrogen. After refluxing for 48 hrs, the suspension was collected *via* filtration and the solid was repeatedly washed with benzene, ethanol, water, and acetone until the filtrate was colorless. The solid was dried at 120 °C under vacuum for 3 hrs to give 0.25 g of a tan powder.

1,4-Bis(bromomethyl)-2,5-dibromobenzene (4). Into a 500 mL round-bottom flask was added 2,5-dibromo-*p*-xylene (20.0 g, 0.076 mol), N-bromosuccinimide (28.41 g, 0.160 mol), a catalytic amount of benzoyl peroxide (10 mg), and carbon tetrachloride (CCl₄, 250 mL). The flask was fitted with a water condenser and the system was flushed with argon. The reaction was initiated by a 250 W sunlamp. The solution was gently refluxed until the succinimide floated atop the mixture (1-2 hours). Upon cooling, the succinimide was removed by filtration and rinsed thoroughly with CCl₄. The combined organic layers were washed with water (3 x 50 mL) and dried with MgSO₄. Filtration and evaporation of the solvent *in vacuo* resulted in a slightly yellow solid. Repeated recrystallization from ethanol yielded 10.57 g (33%) of 1,4-bis(bromomethyl)-2,5-dibromobenzene as a fine white powder. mp 156-157 °C (lit.¹⁶ 161-162 °C). ¹H NMR: δ 7.65 (s, 2H), 4.50 (s, 4H).

1,4-Bis(methoxymethyl)-2,5-dibromobenzene (5). Over a period of one hour, anhydrous methanol (5 mL) and hexanes (10 mL) were added dropwise *via* a pressure equalizing addition funnel to an argon filled 100 mL round bottomed flask containing a stirred solution of oil-free sodium hydride (2.1 eq, 0.051 mol) in 25 mL hexane. After the addition was complete, the flask was fitted with a reflux condenser and the solution was gently refluxed for an additional hour until all of the sodium hydride reacted. Upon cooling, the solution was transferred via cannula to an argon filled 250 mL round bottomed flask containing **4** (10.30 g, 0.024 mol) dissolved in warm hexanes (150 mL). The mixture was gently refluxed for 3-4 hours. The cooled

reaction mixture was poured into a separatory funnel containing 100 mL dilute HCl (1N) and extracted with dichloromethane (CH_2Cl_2). The combined organic layers were dried with magnesium sulfate, filtered, and the solvent evaporated under reduced pressure to yield the crude product as a yellow solid. Recrystallization from ethanol yielded 6.64 g (84%) of 1,4-bis(methoxymethyl)-2,5-dibromobenzene as a pale yellow crystalline solid. mp 68.5-70 °C (lit.¹⁷ 71-72 °C). ^1H NMR: δ 7.61 (s, 2H), 4.44 (s, 4H), 3.45 (s, 6H).

Nickel catalyzed polymerization of 1,4-bis(methoxymethyl)-2,5-dibromobenzene (6). Inside a helium atmosphere drybox, NiCl_2 (8.6 mg, 0.067 mmol), bipyridine (10.4 mg, 0.067 mmol), and zinc powder (0.27 g, 4.12 mmol) were added into a 100 mL round bottomed flask fitted with a reflux condenser capped by a rubber septum. After removal from the drybox, the system was connected to an argon bubbler through the rubber septum and placed in an oil bath. DMF (1 mL) was added to the flask and the solution was stirred magnetically. The mixture was then heated to 80 °C. The green solution became brown after 10 minutes, eventually turning deep red-brown after 30 minutes. The 1,4-bis(methoxymethyl)-2,5-dibromobenzene (0.43 g, 1.33 mmol) was dissolved in DMF (4 mL) in an argon filled 50 mL round bottomed flask and transferred *via* cannula to the catalyst mixture. The solution returned to its original green color upon addition of the monomer but turned deep red-brown after 15 minutes. The mixture was refluxed overnight. Upon cooling, the solution was poured into a flask containing 200 mL of 2N HCl/MeOH

(1:1) and stirred until the excess zinc dissolved. The yellow precipitate was collected by filtration and was repeatedly washed with distilled water and methanol. The polymer was dried under vacuum at 110 °C overnight to yield 0.194 g (88%) of a fine, pale yellow powder that was insoluble in common organic solvents. Anal. Calcd. for $(C_{10}H_{12}O_2)_n$: C, 73.17; H, 7.32; O, 19.51. Found: C, 69.85; H, 7.19; O, not determined.

Cross-linking of methoxymethyl substituted PPP (7). The bis(methoxymethyl) substituted PPP **6** (0.035 g) and concentrated sulfuric acid (3 mL) were mixed in a scintillation vial and cooled in an ice bath. Stirring at 0 °C was continued for 36 hr. The suspension was washed with 20 %(w/w) sodium hydroxide solution (3 x 25 mL), water (3 x 25 mL), and rinsed with ether (3 x 50 mL). The collected solid was dried overnight at 120 °C under vacuum to give 0.009 g (30%) of the cross-linked polymer as a tacky, black solid.

3.3. Results

Polyacenic materials. A simple route to acene-like materials is suggested by the acid catalyzed condensation of alkoxyethyl substituted benzenes. As shown in Figure 3.1, methoxymethylbenzene undergoes electrophilic aromatic substitution to give polybenzyl. While most reported syntheses of polybenzyl are polycondensations utilizing benzyl halides and various Lewis acids (AlCl_3 , TiCl_4 , and SnCl_4), similar results are obtained using benzyl methyl ether and concentrated

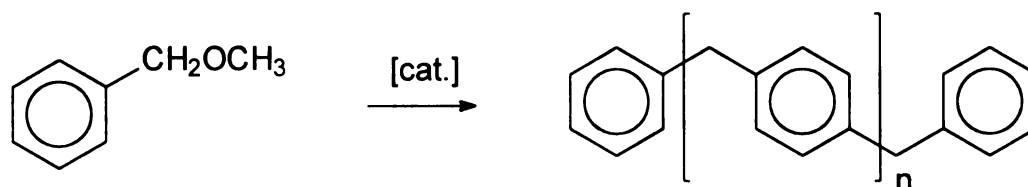


Figure 3.1. Polymerization of methoxymethylbenzene.

sulfuric acid. The polymerization yields a slightly soluble, tan solid that exhibits a glass transition at $180\text{ }^\circ\text{C}$ to form a glassy resin. Thermal analysis indicates the polymer is thermally stable to $400\text{ }^\circ\text{C}$, at which temperature the benzyl linkages connecting the aromatic rings are broken and volatile by-products are evolved.

If this chemistry were applied to bis(methoxymethyl)benzenes, the resulting networks should contain large amounts of fused aromatics, that upon elimination of hydrogen would yield materials with high acenic content. To test this idea, we

prepared the *ortho*-, *meta*-, and *para*- isomers of bis(methoxymethyl)benzene (**1-3**) and polymerized them using acid catalysis. In all cases, the addition of sulfuric acid to the monomer led to the rapid formation of yellow or brown solids, which precipitated from solution. Structural characterization of these materials is difficult. Not only are they insoluble, but the structural differences between polybenzyl and the acene precursor are subtle and not readily detected by NMR, IR, and other standard spectroscopic techniques. However, thermal analysis studies provide circumstantial evidence that the *ortho* isomer tends to form acene-like structures, while the *para* and *meta* isomers yield predominantly polybenzyl architectures.

The networks formed from the acid catalyzed polymerization of the corresponding bis(methoxymethyl)benzenes exhibit surprisingly high thermal stability in a nitrogen atmosphere. As shown in Figure 3.2, after losing a small weight fraction near 400 °C, presumably due to the loss of a low molecular weight fraction or residual unreacted methoxymethyl groups, the polymers derived from the disubstituted monomers are thermally stable past 700 °C resulting in ~70% char yields. When run in air, all the polymers were easily oxidized and completely degraded by 500 °C.

An interesting observation was made however during a thermal analysis experiment in which the environment around the samples was not continuously purged. Figure 3.3 shows the TGA scans of the polymers taken in a stagnant environment containing a small percentage of oxygen. The initial weight loss with an onset near 400 °C was again observed for all the samples. However, for the *para*

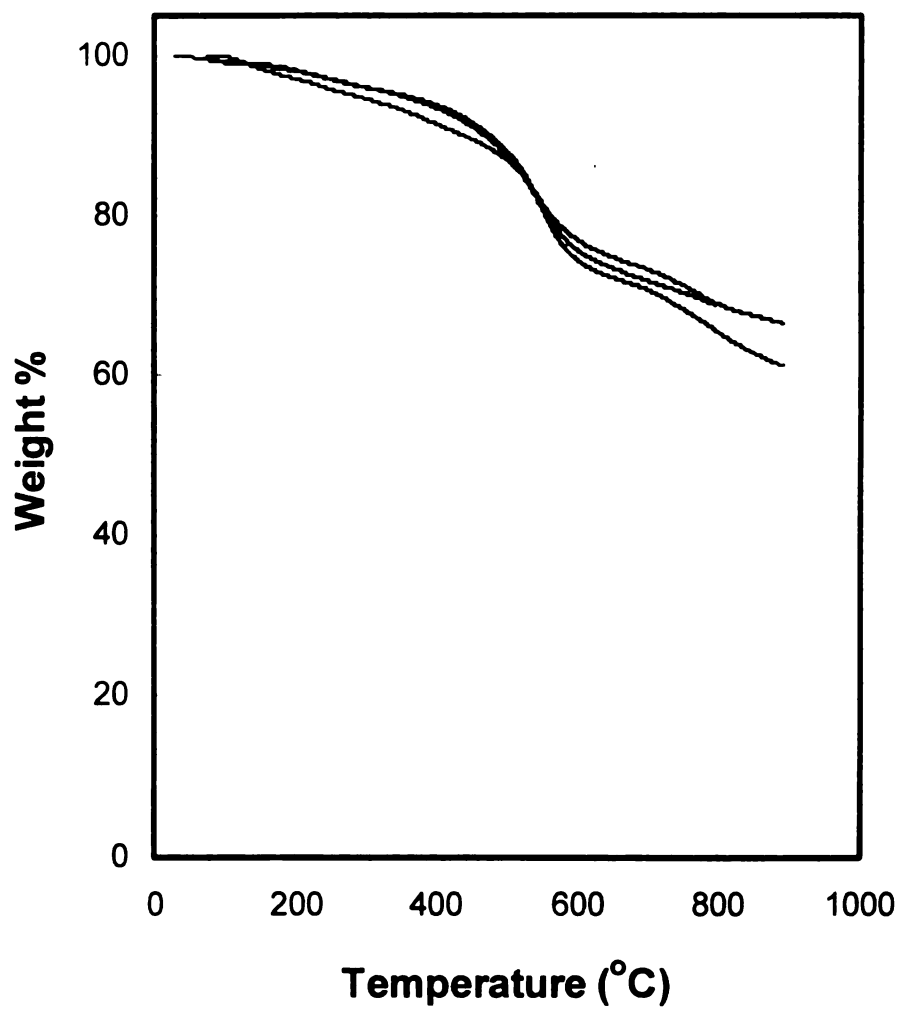


Figure 3.2. Thermogravimetric analysis of the networks formed from monomers 1-3 heated in nitrogen at 10 °C/min.

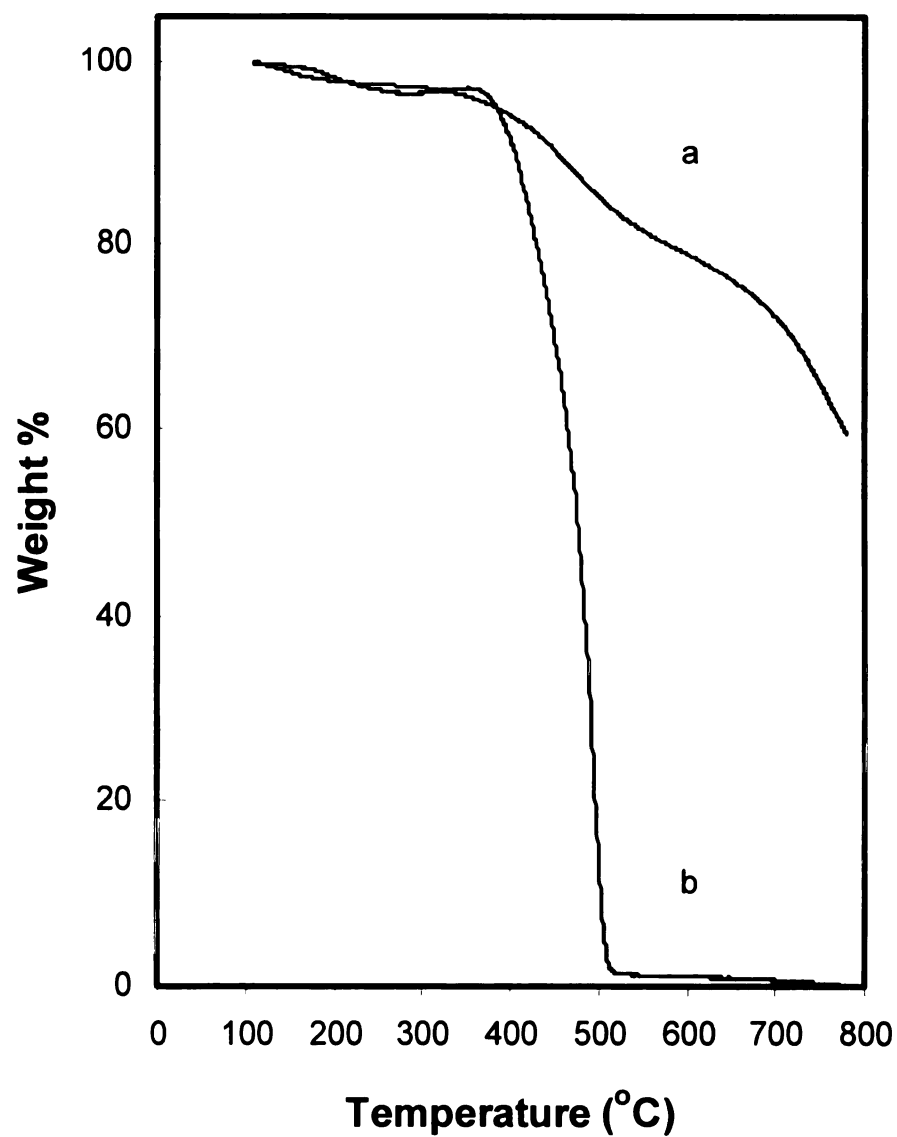


Figure 3.3. Thermogravimetric analysis of the networks formed from a) monomer 1, and b) monomer 3 in a stagnant air environment heated at 10 °C/min.

and *meta* derivatives, low degrees of oxidation led to chain scission and the complete degradation of the samples. In contrast, the *ortho* sample shows the same remarkable stability as it did in a nitrogen environment, a property we attribute to the formation of a substantial proportion of fused rings during polymerization. It appears that the substitution pattern on the benzene ring leads to different structures, with *ortho* substitution favoring cyclization while the *meta* and *para* derivatives yield a predominately polybenzyl network as shown in Figure 3.4. For materials with ladder-like structures, the scission of a single chain does not necessarily lead to the severing of the chain, but chain scission in a single strand polymer like polybenzyl, breaks the polymer chain into smaller pieces. The prediction is that the polymers derived from the *ortho* substituted monomer contain polyacene-like precursors that are thermally stable and are able to dehydrogenate at temperatures above 600 °C.

To better understand the structural changes occurring in the polymer derived from the *ortho* substituted monomer, polymer samples were heated in N₂ to various temperatures in a TGA apparatus and the residues were analyzed using infrared spectroscopy. The spectra, shown in Figure 3.5, show the progressive chemical structure evolution from that of a standard polymer with a high proportion of aliphatic C-H bonds, to an intermediate structure with predominantly aromatic C-H bonds. Assuming the *ortho* precursor contains a large fraction of edge-fused rings, the samples taken at 500 °C should contain an appreciable fraction of polyacenes. One signature of polyacenes would be the appearance of materials with a relatively low bandgap,

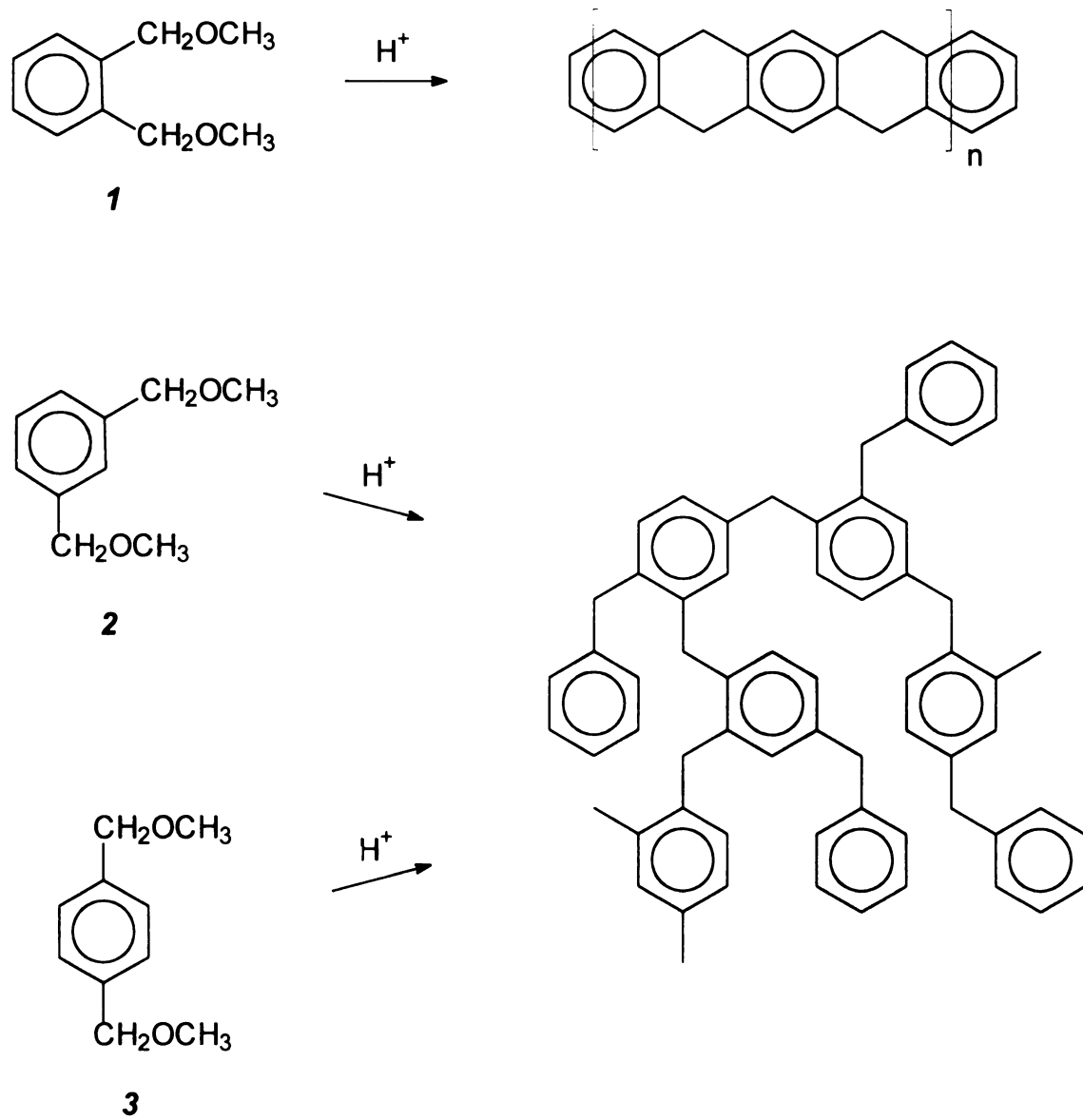


Figure 3.4. Idealized structures resulting from the polymerizations of the bis(methoxymethyl)benzenes **1-3**.

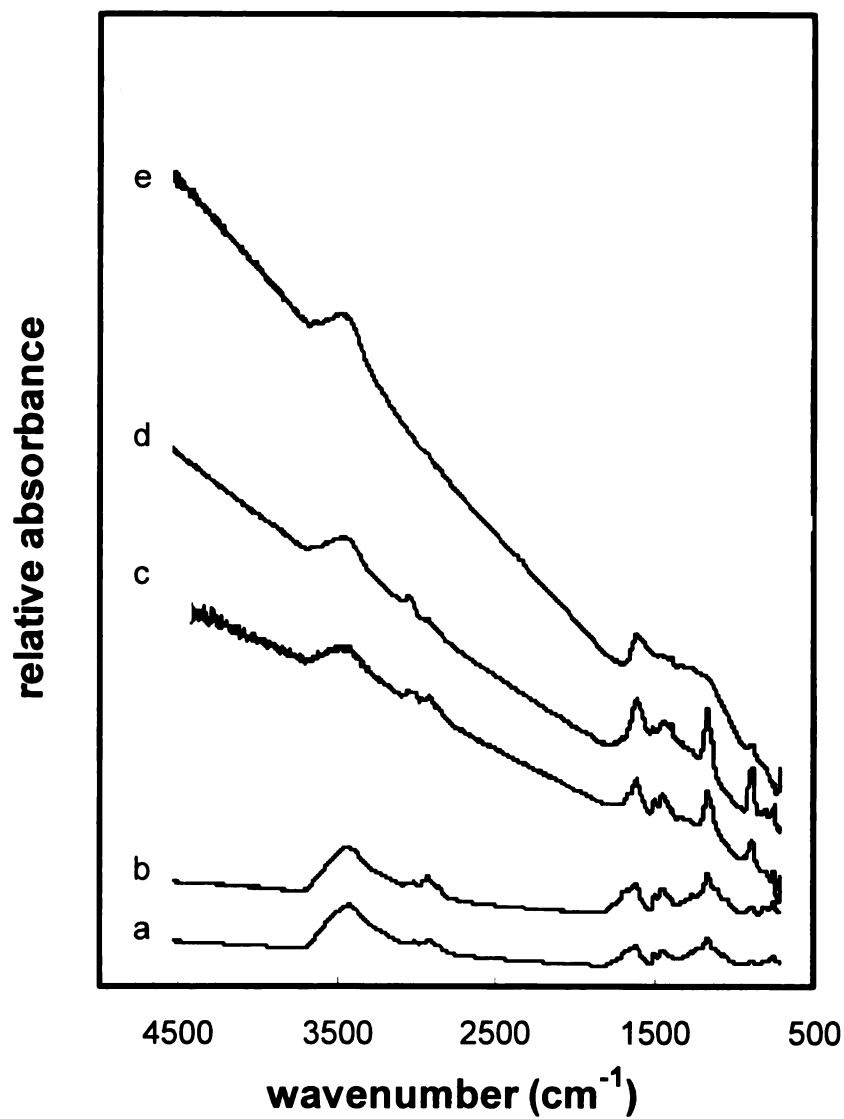


Figure 3.5. Infrared absorption spectra of the polybenzyl network formed from monomer **1** heated in nitrogen at 10 °C/min to a) 30 °C, b) 380 °C, c) 500 °C, d) 600 °C, and e) 800 °C.

but with the retention of aromatic C-H bonds. From the IR spectra, we find that samples taken at 500 and 650 °C have a strong electronic absorption that tails into the infrared region, indicating extensive π conjugation. In addition, we note that the IR bands corresponding to C-H stretching are retained. The bands due to aliphatic C-H bands (2900-3000 cm^{-1}) decrease in intensity while those due to aromatic C-H stretching (3000-3150 cm^{-1}) increase in intensity indicating the shift from aliphatic to aromatic C-H bonds as expected for the formation of acenes. Further treatment of the samples at 800 °C results in the near complete loss of C-H bonds and presumably the formation of a graphite structure. The broad absorption at 3500 cm^{-1} is due to residual moisture in the KBr and the amount was assumed to be constant for all samples.

An alternative method to dehydrogenate dihydroanthracenes is by using chemical dehydrogenation reagents, such as 2,3-dichloro-5,6-dicyano-1,4-benzoquinone (DDQ). The DDQ was refluxed with the polybenzyls in xylenes for 2 days. The product was collected by filtration, washed, and dried. Analysis by IR spectroscopy and TGA show little evidence for the success of the chemical treatment. It is quite possible that the extent of dehydrogenation was limited due to the insolubility of the polybenzyl networks.

Acene/poly(*p*-phenylene) hybrids. If a polymer containing the reactive methoxymethyl functionalities was synthesized, it is logical that it should exhibit the same type of chemistry as the bis(methoxymethyl) benzenes in the presence of

strong acids such as concentrated sulfuric acid. If the same type of reaction occurs when the polymer is exposed to the strong acid, it should result in a network in which the polymer backbones are cross-linked *via* benzyl bridges. Furthermore, if the polymer backbone exhibited extremely limited bond rotation, it seems reasonable that the most probable cross-linking of adjacent reactive functionalities would result in cyclized products. If this network propagates, it would result in a structure resembling a sheet of graphite, and should have high thermal stability.

The monomer was synthesized from readily available starting materials as shown in Figure 3.6. The free-radical bromination of 2,5-dibromo-*p*-xylene using N-bromosuccinimide led to 1,4-bis(bromomethyl)-2,5-dibromobenzene (**4**). The overall yield of this reaction was only ~30% due to the difficulty of separating the product from impurities. Although two equivalents of the brominating agent were used, the bromination exhibited no selectivity and the reaction resulted in a statistical distribution of non-, mono-, and di-brominated methyl groups. Due to the symmetry

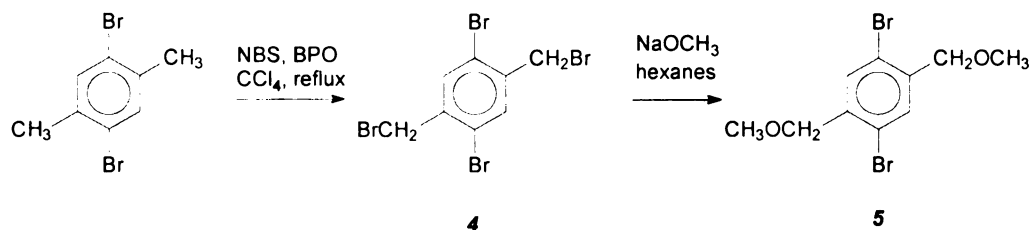


Figure 3.6. Synthesis of 1,4-bis(methoxymethyl)-2,5-dibromobenzene.

of the desired product **4**, it could be recovered by repeated recrystallization. Compound **4** was then reacted with 2 equivalents of sodium methoxide to form the bis(methoxymethyl)benzene **5**. When run in tetrahydrofuran, this reaction leads to a substantial amount of low molecular weight poly(phenylene vinylene). This side reaction was avoided by running the reaction in non-polar, non-coordinating solvents such as hexanes.

Methoxymethyl substituted poly(*p*-phenylene) was synthesized from the corresponding dibromobenzene monomer **5** using a nickel catalyzed coupling reaction (Figure 3.7). The resulting polymer was insoluble in DMF and precipitated from solution during the course of the polymerization. The polymer was collected by filtration and washed repeatedly with water and ethanol to remove any polymerization reagents. After drying, the polymer was obtained as a finely powdered, pale yellow solid. GPC analysis of the THF soluble fraction (5 wt.%) indicated a degree of polymerization less than 10 (relative to polystyrene standards).

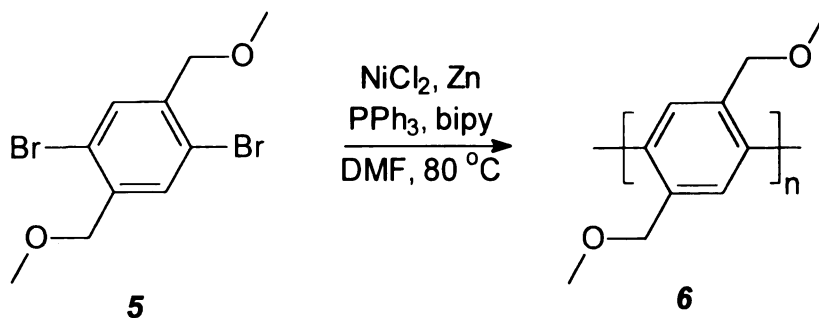


Figure 3.7. Synthesis of substituted poly(*p*-phenylene) **6**.

Polymer **7** was reacted with sulfuric acid following the same procedure as for the polymerization of bis(methoxymethyl)benzenes **1-3**. Due to the rigid nature of the PPP backbone, intramolecular cyclization leading to the formation of acene precursors should be favored (Figure 3.8). Figure 3.9 shows the thermal stabilities of the polymer and that of the network resulting from the acid catalyzed cross-linking. The polymer is thermally stable to 350 °C at which point the side chains are evolved as volatile products leaving behind the polyphenylene backbone which is stable to 700 °C. The weight loss observed in the TGA scans of the cross-linked network at lower temperatures is most likely due to the evolution of methanol resulting from the reaction of residual acid and methoxymethyl groups. Even though the product from the cross-linking reaction was neutralized with base and rinsed repeatedly with

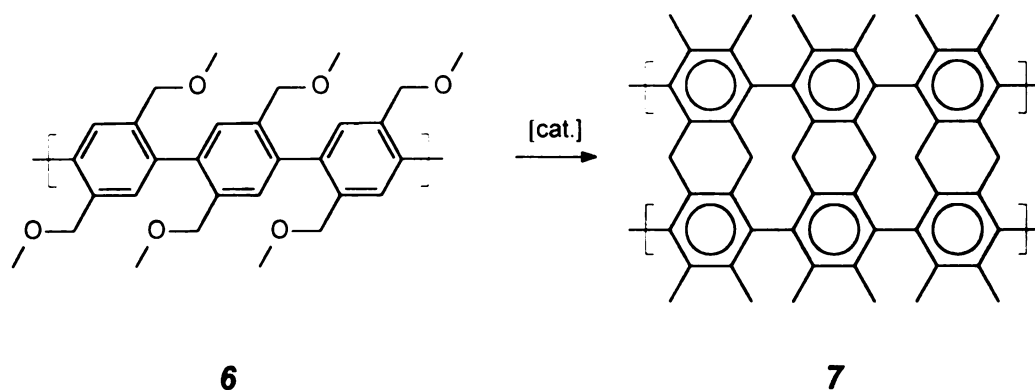


Figure 3.8. Cross-linking of substituted PPP **6**.

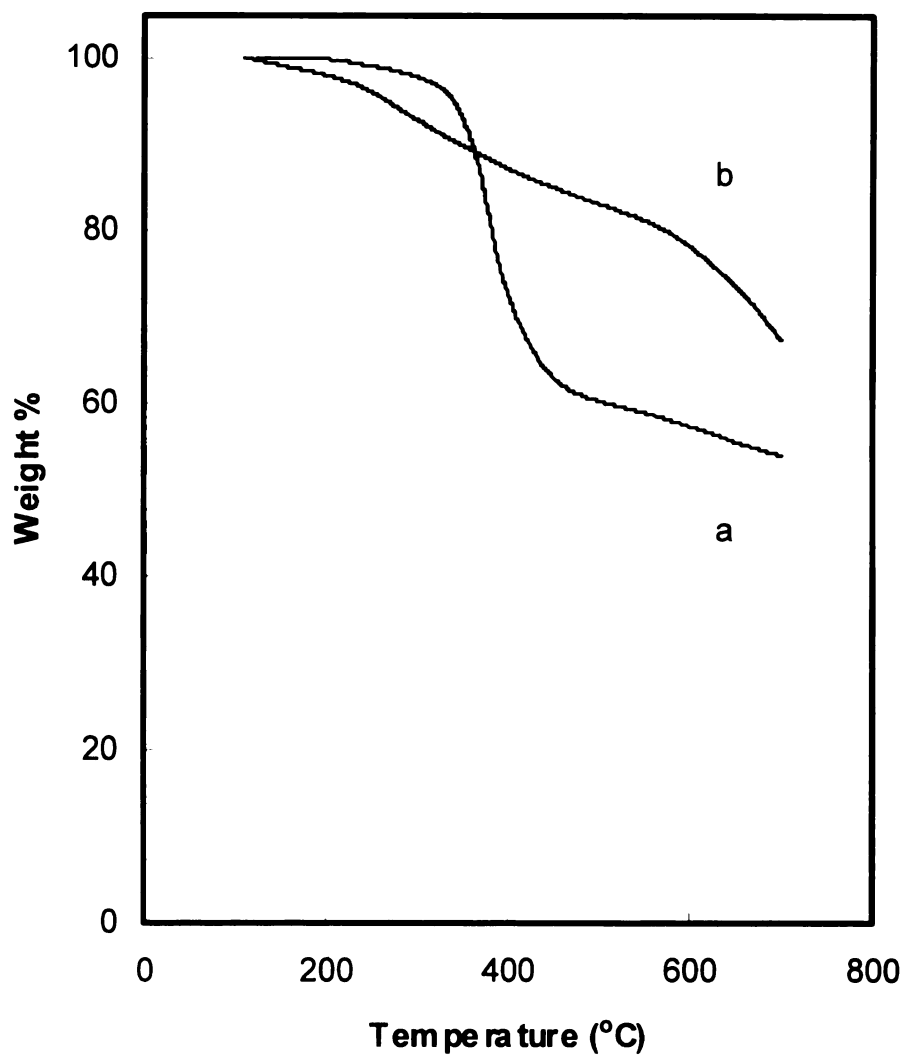


Figure 3.9. Thermogravimetric analysis of a) substituted polymer **6**, and b) cross-linked network **7** in nitrogen heated at 10 °C/min.

water, some sulfuric acid did remain in the tacky solid. Despite the early weight loss, the network exhibits excellent thermal stability, producing a 70% char yield at 700 °C.

These materials were also analyzed by IR spectroscopy, shown in Figure 3.10. The most noticeable evidence of the structural changes brought on by the acid catalyzed cross-linking of the polymer can be seen by the decreases in the C-H and C-O stretching intensities at 2900-3000 and 1100 cm^{-1} , respectively, due to the loss of the methoxy groups. As seen in the pyrolysis of the network formed from bis(methoxymethyl)benzene **1**, high temperature treatment of network **7** at 700 °C also results in the near complete loss of C-H bonds and the tailing of the electronic absorption into the IR. The results from IR and thermal analysis indicate that thermal treatment of the cross-linked network structure also leads to materials with extensive π -conjugation and low H content.

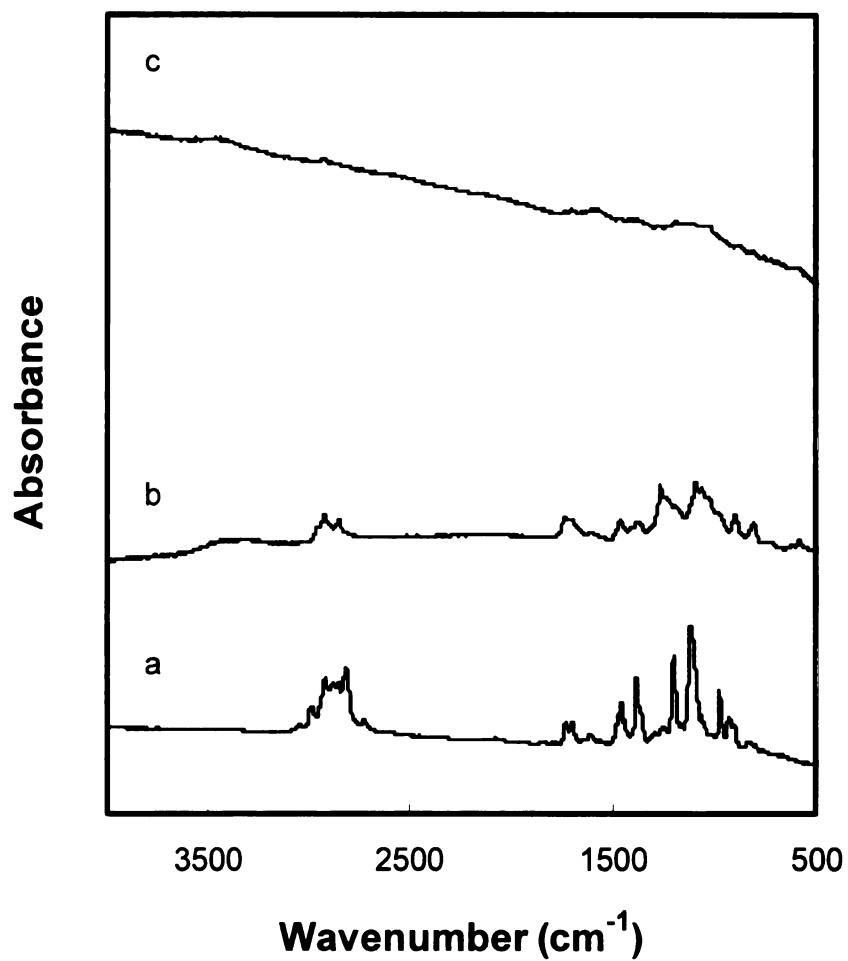


Figure 3.10. Infrared spectra of a) polymer 6, b) network 7, and c) carbon char of network 7 after thermal treatment at 700 °C.

3.4. Discussion

The synthesis of a perfectly linear polyacene is difficult due to the lack of synthetic control of the electrophilic aromatic substitution reaction used to prepare the polyacenic materials. All of the unsubstituted aromatic sites have the same reactivity. Selectivity could be obtained by polymerizing monomers or cross-linking polymers in a pre-ordered state. Highly ordered graphite sheets could be prepared from the cross-linking of assembled alkoxymethyl substituted PPP's. If a soluble PPP polymer with longer side chains were synthesized in high molecular weight, the polymer would likely form a nematic liquid crystalline phase at some temperature, as described in Chapter 2. Formation of the network could be initiated by the photogeneration of a strong Lewis acid that cross-links the substituted PPP polymer in an organized liquid crystalline state.

The intrinsic insolubility of a linear polyacene also hinders its synthesis. Both acenes and poly(*p*-phenylene)s (PPP) are rod-like polymers with extended π conjugation and both become insoluble at low degrees of polymerization. The problem of poor solubility for PPP has been overcome by attaching side chains to the polymer backbone. Soluble, high molecular weight PPP can be obtained by polymerizing a monomer substituted with *n*-hexyl side chains.¹⁸ A similar approach can be used to solubilize polyacenes. As shown in Figure 3.11, alkyl chains attached to the polyacene backbone to give "hairy rods" that like the polyphenylenes should also have enhanced solubility. These materials have the potential of forming very interesting

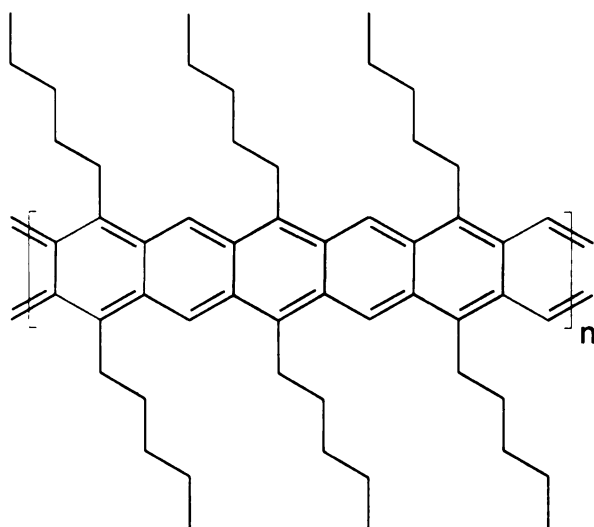


Figure 3.11. Alkyl substituted polyacene.

macromolecular architectures. If the linear, alkyl substituted polyacene could be synthesized in high molecular weight free of structural defects, this board-like polymer should exhibit smectic liquid crystallinity.^{19,20} Unlike other smectic polymers, these polymers should remain soluble due to the long alkyl side chains that act as spacers to disrupt the π -stacking of the polymer backbones.

To obtain a substituted polyacene, a monomer containing both methoxymethyl functionalities and unsubstituted aromatic sites capable of undergoing electrophilic aromatic substitution must be designed. Unlike monomers **1-3** however, these monomers would also have to possess solubilizing side chains. Strategies shown in Figure 3.12 could be easily used to synthesize the monomers from available

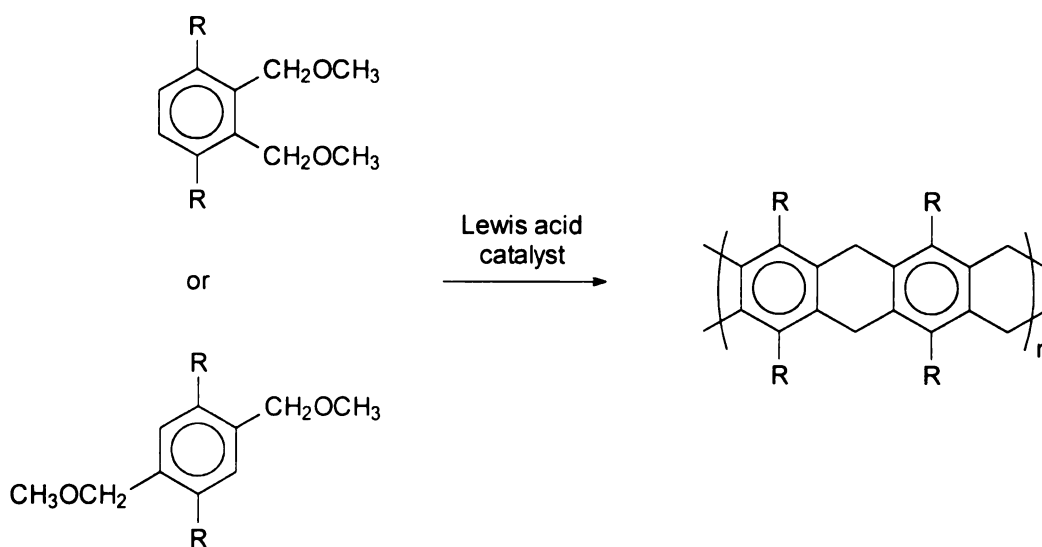


Figure 3.12. Synthesis of a soluble polyacene precursor.

starting materials, such as compound **5**. The long alkyl side chains ($R = n$ -hexyl or n -octyl) may help the monomers to align into lamellar phases, as seen with other similar compounds. Designing monomers capable of organizing into an ordered phase may increase the probability of intramolecular cyclization.

In order to obtain linear polymer, it is necessary to control the chemistry such that intramolecular cyclization reactions are favored over intermolecular reactions that lead to branching and cross-linking. Examples of similar cyclization reactions involving polymeric structures have appeared in the literature. Polyphenylenes with pendant secondary alcohols undergo an acid-catalyzed intramolecular cyclization to yield soluble planarized polyphenylenes.²¹ A similar

cyclization that leads to an S-substituted ladder polymer has also been reported.²¹ Certainly one factor favoring these reactions' success was carrying out the reaction in dilute solution.

Once polymerized, dehydrogenation of the polyacene precursor (Figure 3.13) could be performed using common dehydrogenation reagents, such as DDQ or Pd/C. Although an advantage of using Pd/C is that it is easy to remove from the reaction by filtration, longer reaction times may be necessary to reach high conversions since the mechanism of dehydrogenation requires the polymeric precursor to come in contact with the catalyst surface.

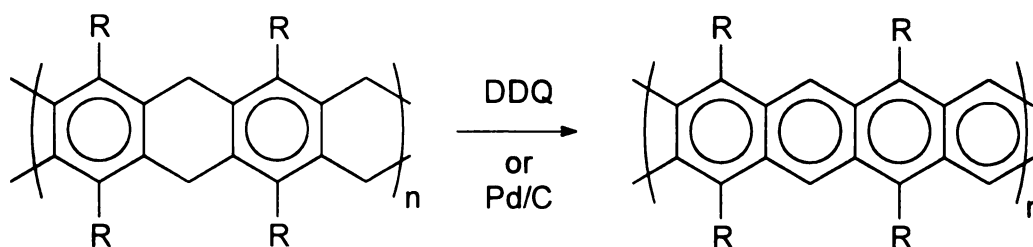


Figure 3.13. Chemical dehydrogenation of polyacene precursor.

Dehydrogenation of the precursor would alter the physical conformation of the polymer into a completely planar backbone. The extent of conjugation in the soluble polymer could then be characterized by UV/Vis spectroscopy. The predicted electronic absorption of the polymer backbone will extend into the far IR and possibly IR if the extent of conjugation is large. The properties of this soluble polyacene could then be compared to those predicted by theory.²²⁻²⁴

3.5. Conclusion

The high temperatures needed for the pyrolysis of phenolic and cellulose resins allows little control of the acene-like structural elements that are the precursors to graphite. If elements of the acene structure are designed into the starting material, it is possible to obtain partially graphitized structures at much lower temperatures that still retain some memory of the chemical structure before pyrolysis. Two types of polyacene syntheses based on a Lewis acid catalyzed electrophilic aromatic substitution reaction were investigated. The first targeted simple routes to acene-like materials that contain a substantial fraction of acene subunits. We found that bis(methoxymethyl)benzenes undergo acid-catalyzed polymerization to yield network structures. The idealized chemical structure for the polymerization of 1,2-bis(methoxymethyl)benzene is a linear polyacene precursor, that after elimination of H_2 , yields polyacenic materials with an extended p electron system. The second route targeted the synthesis of a methoxymethyl substituted poly(*p*-phenylene) that when chemically cross-linked, ideally formed a two-dimensional network closely resembling a graphite sheet. The IR and thermal analysis measurements indicate that much lower temperatures are required to pyrolyze these materials into partially graphitized structures. A synthetic route to a novel, soluble linear polyacene based on the same acid catalyzed electrophilic aromatic substitution reaction was also proposed. Once synthesized, the electronic properties of this material could be compared to those predicted by theory.

3.6. References

- 1) Megahed, S.; Scrosati, B. *J. Power Sources* **1994**, *51*, 79-104.
- 2) Salomon, M.; Scrosati, B. *Gazz. Chim. Ital.* **1996**, *126*, 415-427.
- 3) Brandt, K. *Solid State Ion.* **1994**, *69*, 173-183.
- 4) Zhang, S. S.; Liu, Q. G.; Yang, L. L. *J. Electrochem. Soc.* **1993**, *140*, L107-L108.
- 5) Yata, S.; Hato, Y.; Kinoshita, H.; Ando, N.; Anekawa, A.; Hashimoto, T.; Yamaguchi, M.; Tanaka, K.; Yamabe, T. *Synth. Met.* **1995**, *73*, 273-277.
- 6) Wang, T.; Kang, E. T.; Neoh, K. G.; Tan, K. L. *Synth. Met.* **1997**, *84*, 405-406.
- 7) Ago, H.; Nagata, K.; Yoshizawa, K.; Tanaka, K.; Yamabe, T. *Bull. Chem. Soc. Jpn.* **1997**, *70*, 1717-1726.
- 8) Tanaka, K.; Yata, S.; Yamabe, T. *Synth. Met.* **1995**, *71*, 2147-2149.
- 9) Yata, S.; Kinoshita, H.; Komori, M.; Ando, N.; Kashiwamura, T.; Harada, T.; Tanaka, K.; Yamabe, T. *Synth. Met.* **1994**, *62*, 153-158.
- 10) Yazami, R.; Guerard, D. *J. Power Sources* **1993**, *43*, 39-46.
- 11) Yamabe, T.; Tanaka, K.; Ago, H.; Yoshizawa, K.; Yata, S. *Synth. Met.* **1997**, *86*, 2411-2414.
- 12) Xing, W. B.; Xue, J. S.; Zheng, T.; Gibaud, A.; Dahn, J. R. *J. Electrochem. Soc.* **1996**, *143*, 3482-3491.
- 13) Zheng, T.; McKinnon, W. R.; Dahn, J. R. *J. Electrochem. Soc.* **1996**, *143*, 2137-2145.

- 14)Buiel, E.; George, A. E.; Dahn, J. R. *J. Electrochem. Soc.* **1998**, *145*, 2252-2257.
- 15)Ortiz, B.; Walls, F.; Yuste, F.; Barrios, H.; Sanchez-Obregon, R.; Pinelo, L. *Synth. Commun.* **1993**, *23*, 749-756.
- 16)Otsubo, T.; Kohda, T.; Misumi, S. *Bull.Chem.Soc.Jpn.* **1980**, *53*, 512-517.
- 17)Bedard, T. C.; Moore, J. S. *J. Amer. Chem. Soc.* **1995**, *117*, 10662-10671.
- 18)Rehahn, M.; Schluter, A. D.; Wegner, G.; Feast, W. J. *Polymer* **1989**, *30*, 1060-1062.
- 19)Voigt-Martin, I. G.; Simon, P.; Bauer, S.; Ringsdorf, H. *Macromolecules* **1995**, *28*, 236-242.
- 20)Voigt-Martin, I. G.; Simon, P.; Yan, D.; Yakimansky, A.; Bauer, S.; Ringsdorf, H. *Macromolecules* **1995**, *28*, 243-254.
- 21)Scherf, U.; Mullen, K. *Synthesis* **1992**, 23-38.
- 22)Whangbho, M. H.; Hoffmann, R.; Woodward, R. B. *Proc. R. Soc. London, Ser. A* **1979**, *366*, 23.
- 23)Salem, L.; Longuett-Higgins, H. C. *Proc. R. Soc. London, Ser. A* **1960**, 255, 435.
- 24)Li, Z. J.; Xu, H. B.; Yao, K. L. *Mod. Phys. Lett. B* **1997**, *11*, 477-483.

Chapter 4

Synthesis and Characterization of Cross-linkable Poly[(1-trimethylsilyl-1-propyne)-*co*-(1-(4-azidobutyldimethylsilyl)-1-propyne)] Copolymers

4.1. Introduction

Since it was first synthesized,¹ poly(1-trimethylsilyl-1-propyne) (PTMSP) has been a material of particular interest for gas separations. Its oxygen permeability is roughly ten times that of poly(dimethylsiloxane), the polymer typically used as a benchmark for high permeability.² Rubbery polymers, such as poly(dimethylsiloxane) around room temperature, usually have a high gas permeability attributed to its flexible backbone and resultant high free volume.³ On the other hand, typical glassy polymers have low gas permeabilities. The reason for PTMSP's unusually high permeability can be traced directly to its rigid random coil backbone. With its rigid coiled backbone structure and the presence of the large bulky substituents, inter-segmental packing is hindered and thus the polymer has a large free volume.

Unfortunately a major drawback of PTMSP is that the permeability declines with time,⁴ an effect that has been attributed to aging or densification. We propose that if the polymer chains were cross-linked, the interdiffusion of chains would be prevented and the decline in the desired physical properties could be avoided.

To accomplish this, we chose organic azides as cross-linking moieties. Organic azides are widely used for cross-linking polymers⁵⁻¹¹ and have three

advantages as cross-linking agents. They are easily synthesized, most commonly via S_N2 substitution chemistry using sodium azide and a phase transfer agent, but preparation from a large number of other functional groups has also been reported.¹² Azides are latent cross-linking agents and can be activated by thermal, photochemical, or chemical means when cross-linking is desired, increasing the flexibility of material processing. Finally, azide functional groups decompose to nitrogen gas and reactive nitrenes that undergo insertion reactions.¹³ Thus, no low molecular weight by-products are formed that could contaminate the material.

Azide-based cross-linking is particularly attractive for the stabilization of membranes used for gas and liquid separations. In a recent publication, the preparation of cross-linked PTMSP membranes using bis(aryl azide)s was explored.¹¹ Cross-linking PTMSP membranes with aryl azides stabilized their permeability and rendered the membranes insoluble. However, one limitation of the bis(aryl azide) cross-linking approach is that the azides phase separate from PTMSP at relatively low concentrations (≈ 5 wt%), and thus the cross-link density is limited by the solubility of the cross-linking agents in the polymer matrix. Increased cross-link densities are needed for better control of the pore size in PTMSP and to minimize polymer swelling in liquid separation schemes.

Higher cross-link densities could be obtained by preparing bis(azide)s that are more compatible with PTMSP, or by directly attaching azides to the polymer backbone. A disadvantage of the former approach is that the added azides occupy

much of the free volume in the polymer, leading to a large drop in permeability.¹¹ Direct attachment of azides to the polymer eliminates the phase separation problem and minimizes the size of the cross-linking agent. The structure of PTMSP suggests three strategies for incorporating azides into PTMSP: reactions involving the main chain double bonds, substitution reactions at allylic methyl sites, or copolymerization with an acetylenic comonomer having either an azide group or a suitable azide precursor. In this chapter, strategies for the direct attachment of azides to the PTMSP framework and characterization of the cross-linking behavior of the resulting polymers are explored.

4.2. Experimental Section

Materials. Tetrahydrofuran (THF) and toluene were purified by distillation from calcium hydride followed by a second distillation from sodium/benzophenone ketyl. Unless otherwise specified, all other ACS reagent grade starting materials and solvents were used as received from commercial suppliers without further purification.

Characterization. Proton nuclear resonance (^1H NMR) spectra were measured using a Varian Gemini-300 spectrometer at 300 MHz. All samples were run at room temperature in CDCl_3 . Chemical shifts were calibrated using residual CHCl_3 and are reported in ppm (δ) relative to tetramethylsilane. Infrared spectra of polymers were obtained under nitrogen at room temperature on a Nicolet Magna-IR 550 Fourier Transform IR spectrometer. IR measurements of samples before and after thermal treatment were carried out on films cast on NaCl disks. A Hitachi U-4001 UV-visible spectrometer was used to obtain the UV-visible spectra of cyclohexane solutions of the polymers. Molecular weights of the polymers were determined by gel permeation chromatography (GPC) using a PLgel 20 μ Mixed A column and a Waters R401 Differential Refractometer detector at room temperature with THF as eluting solvent at a flow rate 1 mL/min. Monodisperse polystyrene standards were used to calibrate the molecular weights. The concentration of the polymer solutions used for GPC measurements was 1 mg/mL. Differential scanning calorimetry (DSC) data were obtained under a He environment using a Perkin-Elmer

DSC 7 instrument at a heating rate of 10 °C/min. The DSC 7 temperature was calibrated with an indium standard. Thermogravimetric analyses (TGA) were performed under nitrogen and air atmospheres at a heating rate of 10 °C/min on a Perkin-Elmer TGA 7 instrument. Elemental analyses were performed at the Microanalysis Laboratory at the University of Illinois, Urbana-Champaign, using a CE440 Carbon, Hydrogen, Nitrogen Analyzer (Exeter Analytical, Inc) and conventional Br analysis (titration).

Poly[1-trimethylsilyl-1-propyne]. PTMSP was prepared according to the literature procedure.¹⁴⁻¹⁶ A solution of 1-trimethylsilyl-1-propyne (0.64 g, 5.7 mmol) in dry toluene (10 mL) was degassed by three freeze/pump/thaw cycles. The monomer solution was then added via cannula to a mixture of tantalum pentachloride (120 mg, 0.34 mmol) and triphenylbismuth (150 mg, 0.34 mmol). The reaction mixture was heated to 80 °C and stirred for 16 hours. The resulting gel-like product was dissolved by adding more toluene, centrifuged to remove catalyst residues and precipitated by slow addition into an excess of methanol with rapid stirring. Redissolving in toluene and reprecipitating into methanol yielded 0.51 g (80%) of poly(1-trimethylsilyl-1-propyne). GPC: M_n = 750,000. M_w/M_n = 2.3. ¹H NMR: δ 0.25 (br, 9H), 1.75 (br, 3H).

Allylic bromination of PTMSP. Partially brominated PTMSP (50%) was prepared following the literature procedure¹⁷ by reacting PTMSP (1.0 g) with N-bromosuccinimide (0.79 g, 4.5 mmol) in refluxing CCl₄ (100 mL) in the presence of

benzoyl peroxide (100 mg). Conversion to the brominated product was determined by monitoring the formation of a signal at 2.2 ppm in the ^1H NMR and an absorption band at 1219 cm^{-1} in the IR spectra due to the introduction of C-Br stretching. The yield was nearly quantitative.

Azidization of brominated PTMSP. Brominated PTMSP (0.50 g, 2.2 mmol Br) was dissolved in either 25 mL benzene or THF under a nitrogen atmosphere. The phase transfer reagent (18-crown-6 ether, 29 mg, 0.11 mmol), and NaN_3 (0.58 g, 8.9 mmol) or LiN_3 (0.44 g, 8.9 mmol) were added at the desired temperature (50 °C for THF and 60 °C for benzene). The reaction mixture was sampled at different times, precipitated into methanol, and the conversion determined by ^1H NMR and IR spectroscopy. For reactions using ZnCl_2 , the same procedure was used except that ZnCl_2 (0.18 g, 0.73 mmol) and pyridine (0.18 g, 2.2 mmol) were used in place of the phase transfer reagent.

4-Bromo-1-butene (2). 4-Bromo-1-butene was prepared according to the literature procedure¹⁸ in 37% yield (21 g); bp 98-100 °C (lit.¹⁸ 98-100 °C). ^1H NMR: δ 2.7 (m, 2H), 3.3 (t, 2H), 5.1 (m, 1H), 5.8 (m, 2H).

4-Bromobutyldimethylchlorosilane (3). Compound **3** was prepared following the procedure of Kunzler and Percec¹⁹ in 85% yield (17.9 g); bp 90-95 °C/23 mm Hg (lit.¹⁹ 92-95 °C/5 mmHg). ^1H NMR: δ 0.4 (s, 6H), 0.8 (t, 2H), 1.5 (m, 2H), 1.9 (m, 2H), 3.4 (t, 2H).

1-(4-Bromobutyldimethylsilyl)-1-propyne (4). A solution of propynyllithium was prepared by the drop-wise addition of *n*-BuLi (2.5 M in hexanes, 12 mL) to a cold propyne-ether solution obtained by bubbling propyne gas through cold diethyl ether (-78 °C). To the solution of propynyllithium was added 4-bromobutyldimethylchlorosilane (6.7 g, 29 mmol) dropwise at 0 °C. The reaction mixture then was stirred overnight at room temperature and then poured into 400 mL of ice water. The ether layer was collected and washed with distilled water, dried over MgSO₄, filtered and the solvent removed by rotoevaporation. The remaining oil was purified by vacuum distillation at 59-65 °C/3 mmHg to yield 4.6 g (68%) of 1-(4-bromobutyldimethylsilyl)-1-propyne (lit.¹⁹ 70-75 °C/15 mmHg). ¹H NMR: δ 0.15 (s, 6H), 0.6 (t, 2H), 1.5 (m, 2H), 1.85 (s, 3H), 1.9 (m, 2H), 3.4 (t, 2H).

Poly[(1-trimethylsilyl-1-propyne)-*co*-(1-(4-bromobutyldimethylsilyl)-1-propyne)] (5a-5g). The following procedure, illustrated for the synthesis of the copolymer containing 20 mol% of the 1-(4-bromobutyldimethylsilyl)-1-propyne comonomer, was used to prepare all of the copolymers. A mixture of 1-trimethylsilyl-1-propyne (5.23 g, 0.047 mol) and 1-(4-bromobutyldimethylsilyl)-1-propyne (2.72 g, 0.012 mol) was dissolved in dry toluene (100 mL) and degassed by three freeze/pump/thaw cycles. The monomer solution was then added via cannula to a mixture of tantalum pentachloride (0.835 g, 2.33 mmol) and triphenylbismuth (1.025 g, 2.33 mmol). The reaction mixture was heated to 80 °C and stirred for 16 hours. The resulting gel-like product was diluted with toluene, centrifuged to remove residual

catalyst, and precipitated by slow addition into an excess of methanol with rapid stirring. Redissolving in toluene and reprecipitating into methanol yielded 6.54 g (83%) of poly[(1-trimethylsilyl-1-propyne)-*co*-(1-(4-bromobutyl-dimethylsilyl)-1-propyne)]. GPC: $M_n = 432,000$. $M_w/M_n = 2.4$. ^1H NMR: δ 0.2 (br), 1.6 (br), 1.8 (br), 3.4 (br).

Poly[(1-trimethylsilyl-1-propyne)-*co*-(1-(4-azidobutyldimethylsilyl)-1-propyne)] (6a-6g). Sodium azide (0.65 g, 10 mmol) and a catalytic amount of tetrabutylammonium hydrogen sulfate (TBAH, 100 mg) were added to a stirred solution of 1.0 g of poly[(1-trimethylsilyl-1-propyne)-*co*-(1-(4-bromobutyl-dimethylsilyl)-1-propyne)] (**5g**) in 100 mL of THF. The reaction mixture was stirred for 120 hours at 60 °C. The resulting polymer was dissolved in additional THF and centrifuged to remove most of the catalyst and other undissolved solids. The cloudy polymer solution was washed with water to remove salts not removed by centrifugation. The resulting clear solution was precipitated into methanol, filtered, redissolved in THF and again precipitated in methanol. The collected polymer was vacuum dried at 50 °C overnight to obtain 0.90 g (90%) of poly[(1-trimethylsilyl-1-propyne)-*co*-(1-(4-azidobutyldimethylsilyl)-1-propyne)]. GPC: $M_n = 410,000$, $M_w/M_n = 2.6$. ^1H NMR: δ 0.2 (br), 1.6 (br), 1.8 (br), 3.25 (br).

Film casting and cross-linking. Viscous casting solutions were obtained by dissolving the copolymer (200 mg) in toluene (10 mL). Polymer films were prepared by pouring the casting solutions onto a flat glass plate and drying for 48 hours. The films were then completely dried in a vacuum oven at 50 °C overnight. Thermal cross-linking of the resulting free standing copolymer films was achieved by heating the samples in a vacuum oven at 250 °C for 3 hours.

Swelling experiments. Cross-linked copolymer films were cut into 2 cm × 2 cm pieces, weighed, and immersed in solvents with solubility parameters (δ) ranging from 14-20 × 10³ (J/m³)^{1/2}. After 24 hours, the films were removed from the solvent, blotted dry, weighed, and placed back into the solvent. This procedure was repeated until the samples reached a constant weight. The reported swelling values are the average of three individual film measurements.

4.3. Results

Despite numerous attempts and the use of various reaction conditions, it has been shown that the double bonds of the PTMSP backbone are unreactive.¹⁹ Low reactivity for these double bonds is not unexpected because of the severe steric effects caused by the methyl and trimethylsilyl side groups.

Incorporation of azides at allylic sites. Direct attachment of azides to the allylic methyl groups of PTMSP is an attractive strategy for accessing PTMSP polymers with high azide contents and high degrees of cross-linking because the small size of the azide group should result in minimal structural changes compared the parent polymer. As shown in Figure 4.1, brominated PTMSP was prepared using

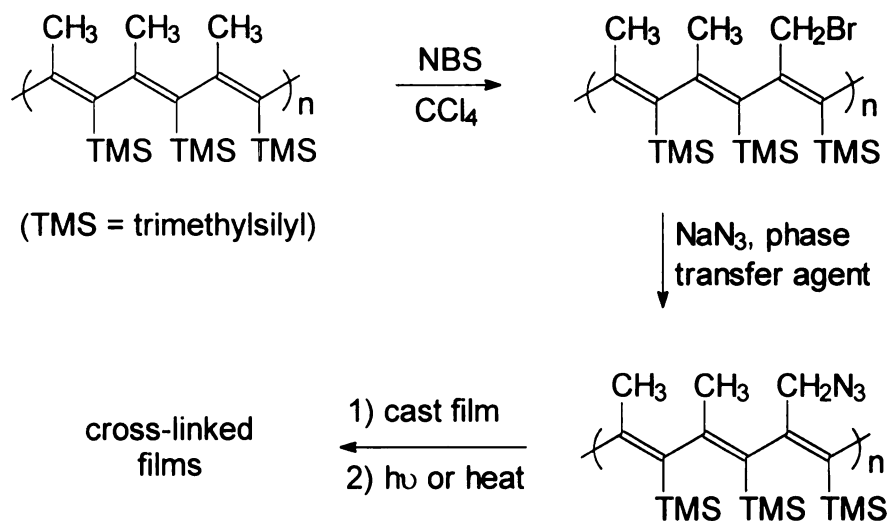


Figure 4.1. Synthesis of azide-containing PTMSP via allylic bromination.

standard free-radical conditions,^{17,20} and various methods were examined for nucleophilic displacement of the bromide by azide. Allyl azides are easily prepared from allyl bromides by reaction with NaN_3 or trimethylsilyl azide,²¹ and similar methods have been used to partially convert halogen-containing polymers such as poly(vinyl chloride)²²⁻²⁴ and poly(epichlorohydrin)²⁵ to polymeric azides. However, we found that substitution chemistry at the allylic methyl group in PTMSP is highly hindered. Both IR and ^1H NMR spectroscopy showed no evidence for incorporation of azide into the polymer.

Since $\text{S}_{\text{N}}2$ chemistry failed, we followed the procedure of Ravindranath *et al.*²⁶ and used Lewis acids to form allylic carbocations that could be trapped by the azide anions. The product from the azidization reaction of 50% brominated PTMSP showed a small peak at 2100 cm^{-1} in the IR spectra indicating the presence of the N_3 group, but a strong BrCH_2^- vibrational band at 1219 cm^{-1} was still evident. Proton NMR also indicated only partial introduction of the azide. Our best results show only limited success, with less than 5% conversion to the azido derivatives after five days.

Incomplete conversion to the azide is a serious problem since brominated PTMSP degrades rapidly in the presence of UV light and oxygen.²⁰ Before these polymers can be cross-linked into insoluble films, the remaining bromide must be removed while retaining the azides. We tried to replace the remaining bromine with hydrogen by treating the azido derivatives with $\text{Bu}_3\text{SnH/AIBN}$. After reacting in

toluene at 75 °C for 2 hours, IR spectra showed the disappearance of both the $-N_3$ and the $BrCH_2-$ bands, indicating that the reaction was not selective and that hydride replaced the bromide and reduced the azide group.

We also examined anionic methods for substitution at the methyl group. For example, brominated PTMSP treated with either BuLi or Li metal generated the allylic anion, but gelation was observed in these reactions and the resulting polymers became insoluble and unprocessable. Presumably, slow formation of the anion allowed the coupling of anions with residual allyl bromides to give a cross-linked network.

Incorporation of azides via copolymerization. Because steric hindrance at the allylic methyl group resulted in only partial conversion of the allylic bromide to the azide, we decided to increase the reactivity of the halide by moving it away from the polymer backbone. While the tether could be connected to either the allylic methyl or trimethylsilyl group of the monomer, attachment through the trimethylsilyl group should have the least effect on the polymerization rate since the site of the substitution is farther from the triple bond. Following the approach of Kunzler and Percec,¹⁹ we prepared copolymers of 1-trimethylsilyl-1-propyne and 1-(4-bromobutyldimethylsilyl)-1-propyne. Azide groups can be introduced into these copolymers by simple nucleophilic displacement reactions. Because monomers containing azides are unlikely to survive the polymerization conditions, we did not explore the direct polymerization of an azide-containing monomer.

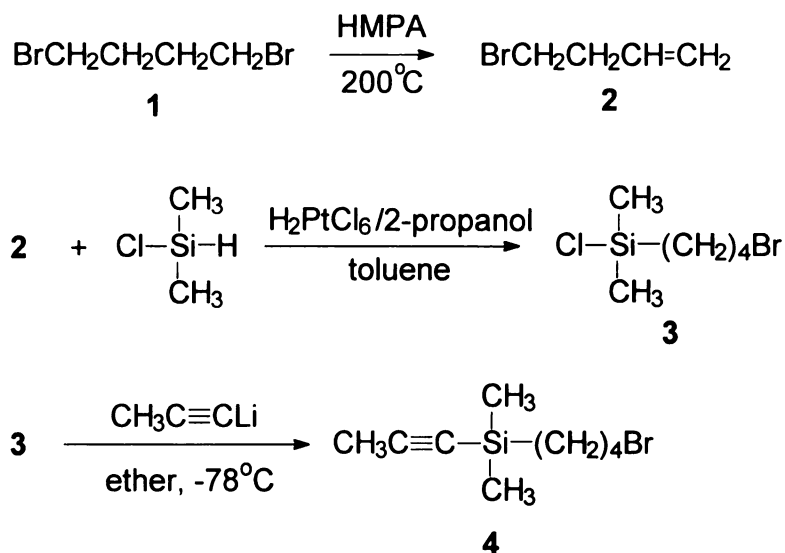


Figure 4.2. Synthetic route to 1-(4-bromobutyldimethylsilyl)-1-propyne.

The comonomer, prepared by the route outlined in Figure 4.2, was copolymerized with 1-trimethylsilyl-1-propyne to give a series of copolymers that contain 2-20 mol% of 1-(4-bromobutyldimethylsilyl)-1-propyne (Figure 4.3). GPC measurements showed that the molecular weights of the copolymers were similar to those of PTMSP, ranging from $4\text{-}5 \times 10^5$ g/mol with a polydispersity of 2.5. Treatment of the copolymer with sodium azide and a phase transfer agent smoothly converted the bromobutyl side chain to the corresponding azide. The reaction was sampled at different times and analyzed by ^1H NMR and FTIR spectroscopy to determine the conversion. In the IR spectra, the intensity of the band at 1219 cm^{-1} decreased (CH_2

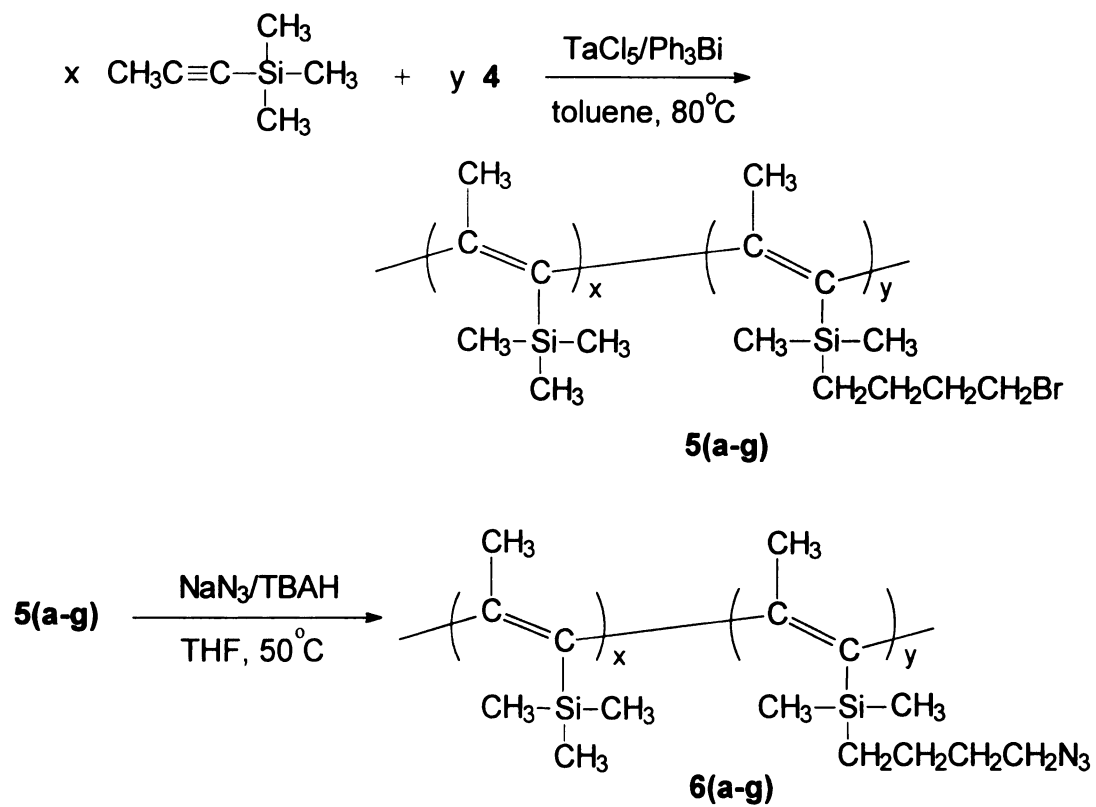


Figure 4.3. Synthetic route to copolymers **6a-6g**.

wagging, CH₂Br group), and a new band grew in at 2100 cm⁻¹ that corresponds to the -N₃ group²⁷ in poly[(1-trimethylsilyl-1-propyne)-*co*-(1-(4-azidobutyldimethylsilyl)-1-propyne)]. Corresponding changes were seen in the ¹H NMR data. The peak at 3.4 ppm from the -CH₂Br segment in poly[(1-trimethylsilyl-1-propyne)-*co*-(1-(4-bromobutyldimethylsilyl)-1-propyne)] decreased as a new resonance at 3.25 ppm for -CH₂N₃ in poly[(1-trimethylsilyl-1-propyne)-*co*-(1-(4-azidobutyldimethylsilyl)-1-propyne)] increased. The peak at 3.4 ppm in the ¹H NMR spectra and the absorption band at 1219 cm⁻¹ in the IR spectra both decreased to baseline, demonstrating that complete displacement of the bromide was achieved after 5 days.

Polymer characterization. Elemental analyses (Table 4.1) of the copolymers showed no bromine detectable by titration, confirming the high degrees of bromide to azide conversion indicated in the ¹H NMR and IR data. The absolute azide content in the copolymers can also be calculated from the experimental C/N ratios. We found that the azide contents of copolymers calculated from elemental analyses data result in ≈20% lower values than expected. The deviations from the expected values may be due to PTMSP's tendency to form refractory oxides in oxidizing environments.²⁸

Shown in Figure 4.4 are the IR spectra of the series of copolymers with increasing azide contents. The spectra are normalized relative to the intensity of the C=C absorption (1600 cm⁻¹) of the polymer backbone. The most prominent feature

Table 4.1. Elemental analyses of poly[(1-trimethylsilyl-1-propyne)-*co*-(1-(4-azido-butyldimethylsilyl)-1-propyne)] copolymers.

Theoretical N₃ (mol%)^a	5		10		20	
	theo.	exp.	theo.	exp.	theo.	exp.
C%	63.46	63.26	62.76	62.80	61.52	60.61
H%	10.61	10.02	10.45	10.25	10.17	7.68
N%	1.80	1.36	3.49	2.71	6.52	5.45
Si%	24.13	b	23.30	27.79	21.79	24.95
Experimental N₃ (mol%)^{c,d}	3.8		7.8		17.0	

- a. calculated by assuming 100% conversion from poly[(1-trimethylsilyl-1-propyne)-*co*-(1-(4-bromobutyldimethylsilyl)-1-propyne)]
- b. not analyzed
- c. calculated from elemental analysis results
- d. Br was not detected using titration method

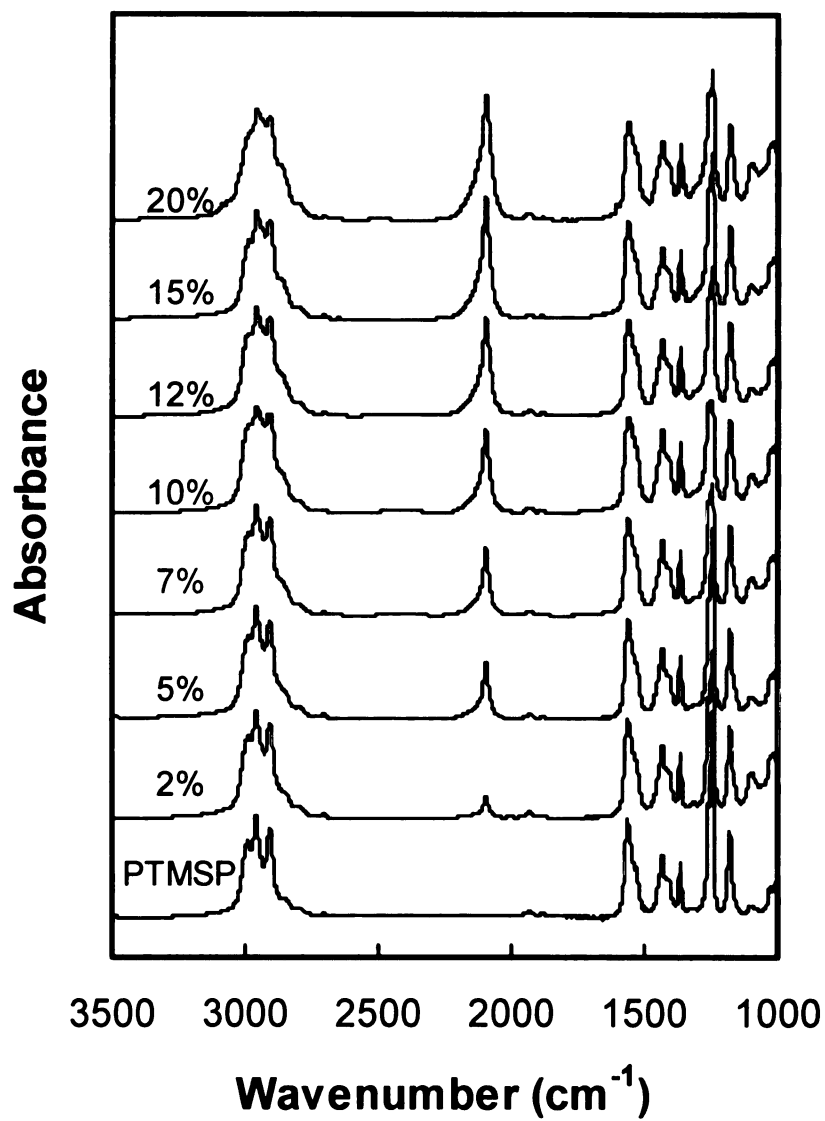


Figure 4.4. FTIR spectra of PTMSP and copolymers **6a-6g**.

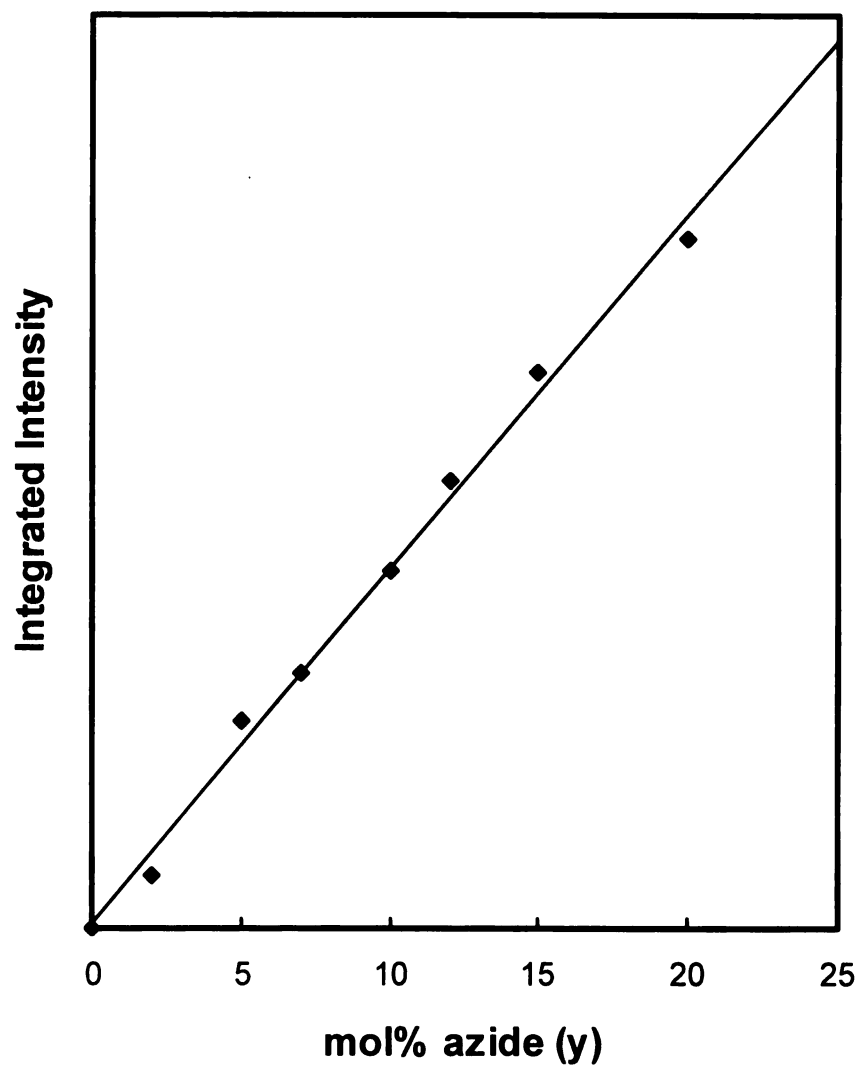


Figure 4.5. Integrated azide absorbance intensity at 2100 cm^{-1} versus the azide content in copolymers **6a-6g** as calculated from the comonomer feed ratios.

in the spectra is the increase in the intensity of the absorption band for the alkyl azide at 2100 cm^{-1} . This increase is mirrored by a growth in the intensity of the aliphatic C-H stretching bands ($2800\text{-}3000\text{ cm}^{-1}$) caused by the increase in the concentration of alkyl side chains in the higher azide-content copolymers. When the integrated intensities of the azide absorption bands are plotted versus the theoretical azide calculated from the comonomer feed ratios (Figure 4.5), we obtain a linear relationship indicating that the overall composition of the samples are comparable to the initial monomer ratios.

UV-visible spectra of cyclohexane solutions of poly[(1-trimethylsilyl-1-propyne)-*co*-(1-(4-azidobutyldimethylsilyl)-1-propyne)] show no absorption above 300 nm. Absorption bands of alkyl azides²⁷ typically occur at $\lambda_{\text{max}} = 287\text{ nm}$ ($\epsilon = 25$) and $\lambda_{\text{max}} = 216\text{ nm}$ ($\epsilon = 500$), but the strong C=C absorption of the polymer backbone masks the azide absorption in these samples. Like PTMSP, the azide-containing copolymers are snow-white solids after precipitation into methanol and form clear, colorless films when cast from solvents such as THF or toluene.

Thermogravimetric analyses (Figure 4.6) of poly[(1-trimethylsilyl-1-propyne)-*co*-(1-(4-azidobutyldimethylsilyl)-1-propyne)] under nitrogen show the onset of a weight loss at $225\text{ }^{\circ}\text{C}$ due to the decomposition of the azide groups and the release of nitrogen from the polymer. Depending upon the density of the original sample, the subsequent cross-linking reactions result in a 10-20 % char yield at $600\text{ }^{\circ}\text{C}$. In contrast, PTMSP is thermally stable to $350\text{ }^{\circ}\text{C}$ and then rapidly decomposes

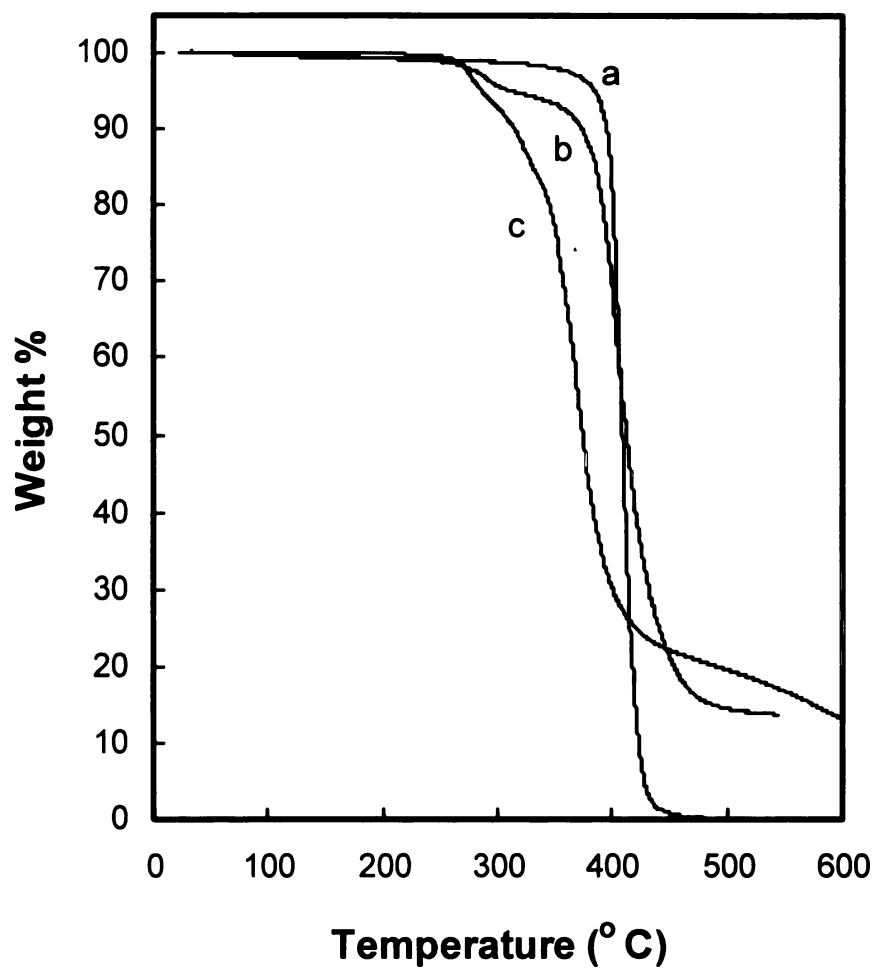


Figure 4.6. TGA of a) PTMSP in nitrogen; b) copolymer **6g** in nitrogen; and c) copolymer **6g** in air.

to monomer, yielding no residue. When run in air, the copolymers again evolve nitrogen at 225 °C, but the resulting products are less stable and decompose more rapidly. The weight loss due to evolution of nitrogen could, in principle, be used to quantitate the N₃ contents in the copolymers. However, the weight loss from nitrogen evolution partially overlaps with a weight loss associated with a slow degradation of the polymer, and consistent values could not be obtained.

DSC measurements on poly[(1-trimethylsilyl-1-propyne)-*co*-(1-(4-azidobutyl)dimethylsilyl)-1-propyne)] copolymers show no thermal transitions below the azide decomposition temperature (< 225 °C) indicating that like PTMSP,²⁹ the copolymers do not exhibit a glass transition. We interpret the similarity of the PTMSP and copolymer DSC scans as evidence that the added side chains did not drastically alter the physical properties of the PTMSP backbone. The exothermic transition for azide decomposition is centered at 270 °C in the DSC thermograms (Figure 4.7) and can be quantitatively related to the azide content in the copolymers. Figure 4.8 shows that the enthalpy change associated with the exotherm is linearly related to the azide content in the copolymers calculated from the original co-monomer feed ratios. The plot yields a positive y-intercept since the DSC exotherm also includes a contribution from the change in heat capacity (ΔC_p) of the cross-linked networks.

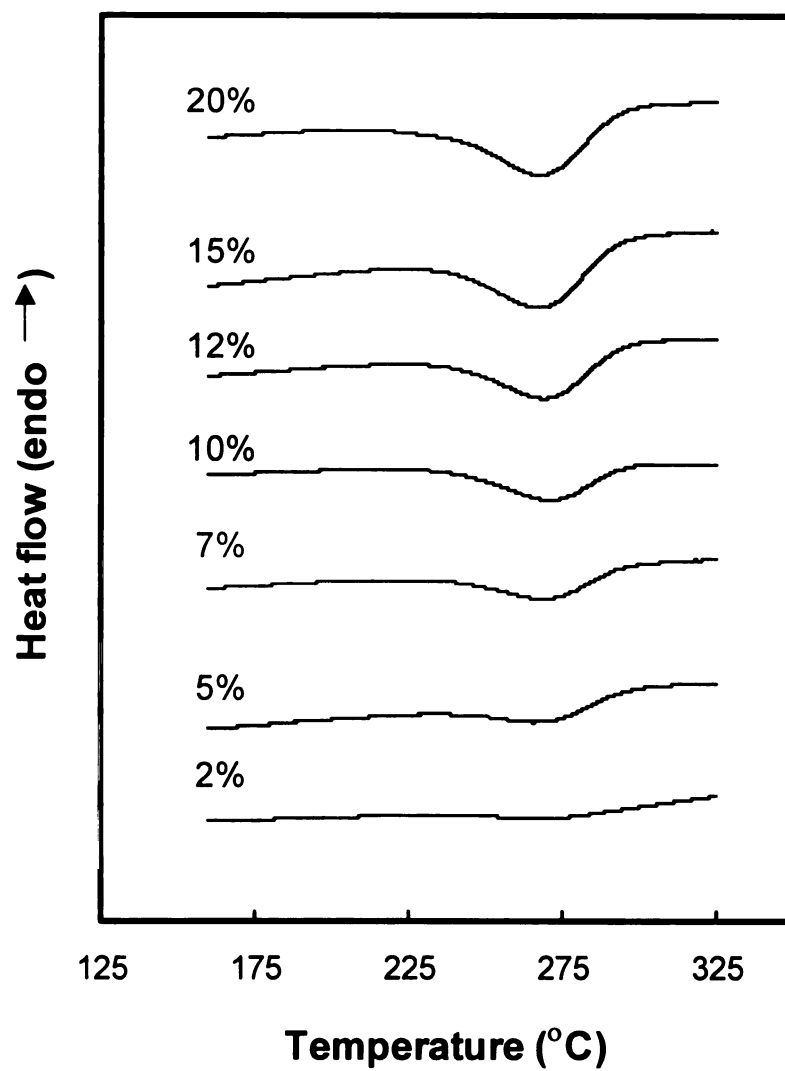


Figure 4.7. DSC results for copolymers **6a-6g**.

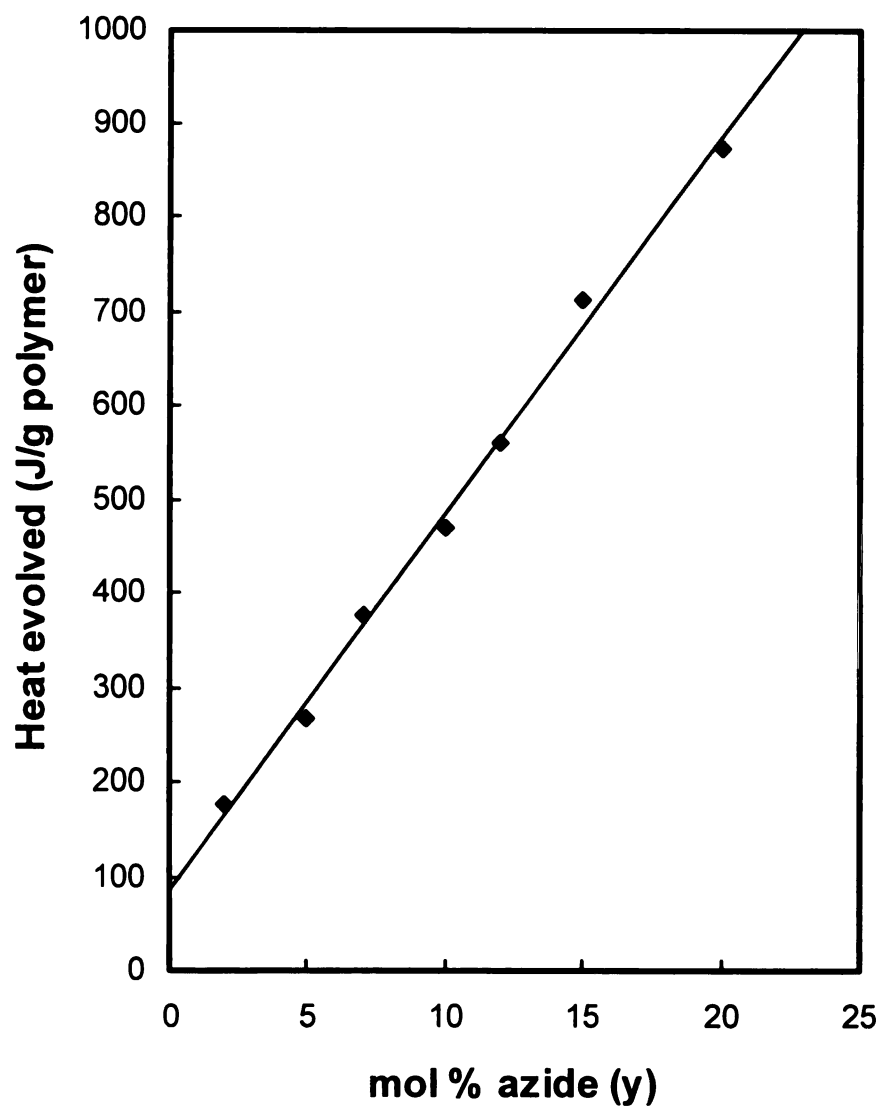


Figure 4.8. Heat evolved during thermal decomposition of azide copolymers **6a-6g** measured by DSC.

Thermal cross-linking of copolymer films. We studied the thermal decomposition of the azide-containing copolymers from 225-275 °C, the temperature range that corresponds to the exotherm measured in the DSC curves (Figure 4.7) and the nitrogen weight loss seen in the TGA thermograms (Figure 4.6). The rate of the reaction was determined by monitoring the decrease in the intensity of the N₃ absorption at 2100 cm⁻¹ in the IR (Figures 4.9 – 4.11). We assumed that the azide concentrations in the films are proportional to the integrated absorption intensities in the normalized IR spectra. Using Equation 1, where [N₃]_o and [N₃]_t are the azide

$$-\ln \left(\frac{[\text{N}_3]_t}{[\text{N}_3]_o} \right) = k_d t \quad (1)$$

concentrations in a film before cross-linking and a film at time *t*, respectively, the azide degradation rate constant (*k_d*) were obtained for each temperature studied (Figure 4.12). An Arrhenius plot (Figure 4.13) of the resulting *k_d* values gave the activation energy for azide decomposition (*E_a*) in the copolymer. For copolymer **6f**, the activation energy was calculated to be 130 kJ/mol.

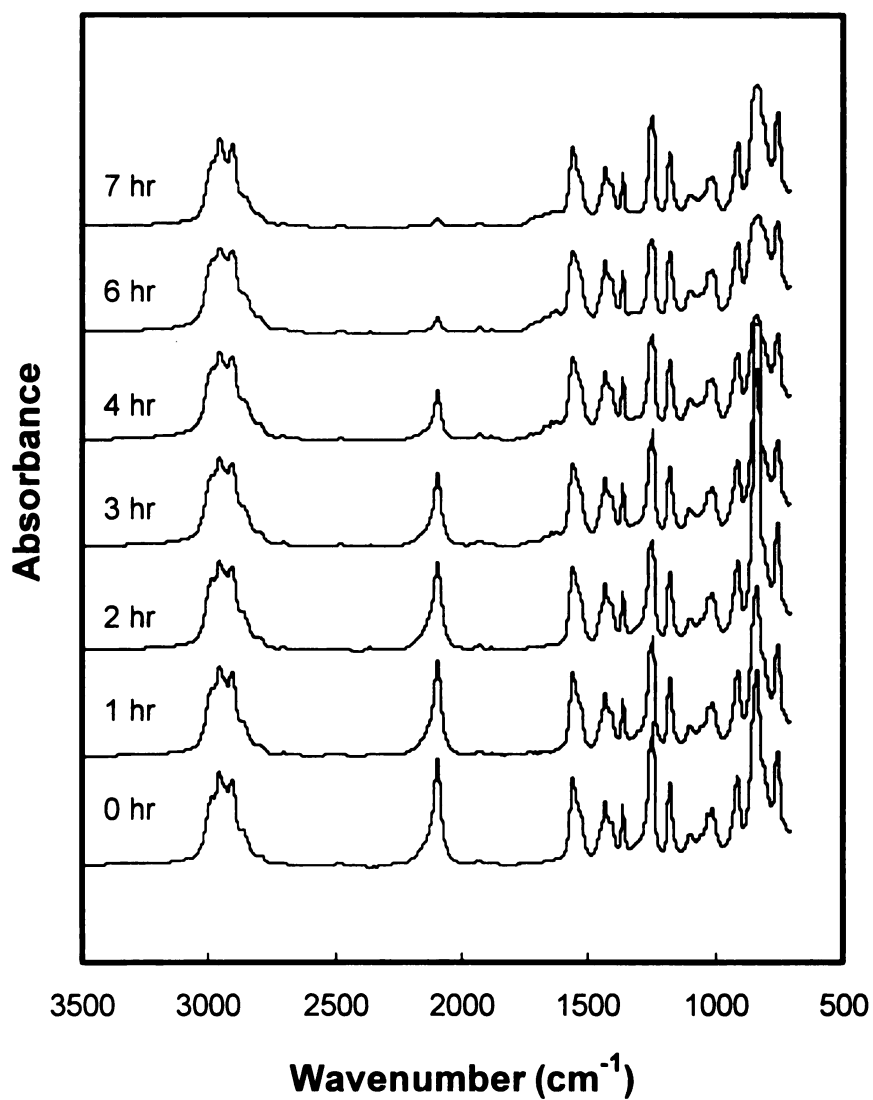


Figure 4.9. FTIR spectra showing the thermal decomposition of copolymer **6f** at 225 °C under vacuum.

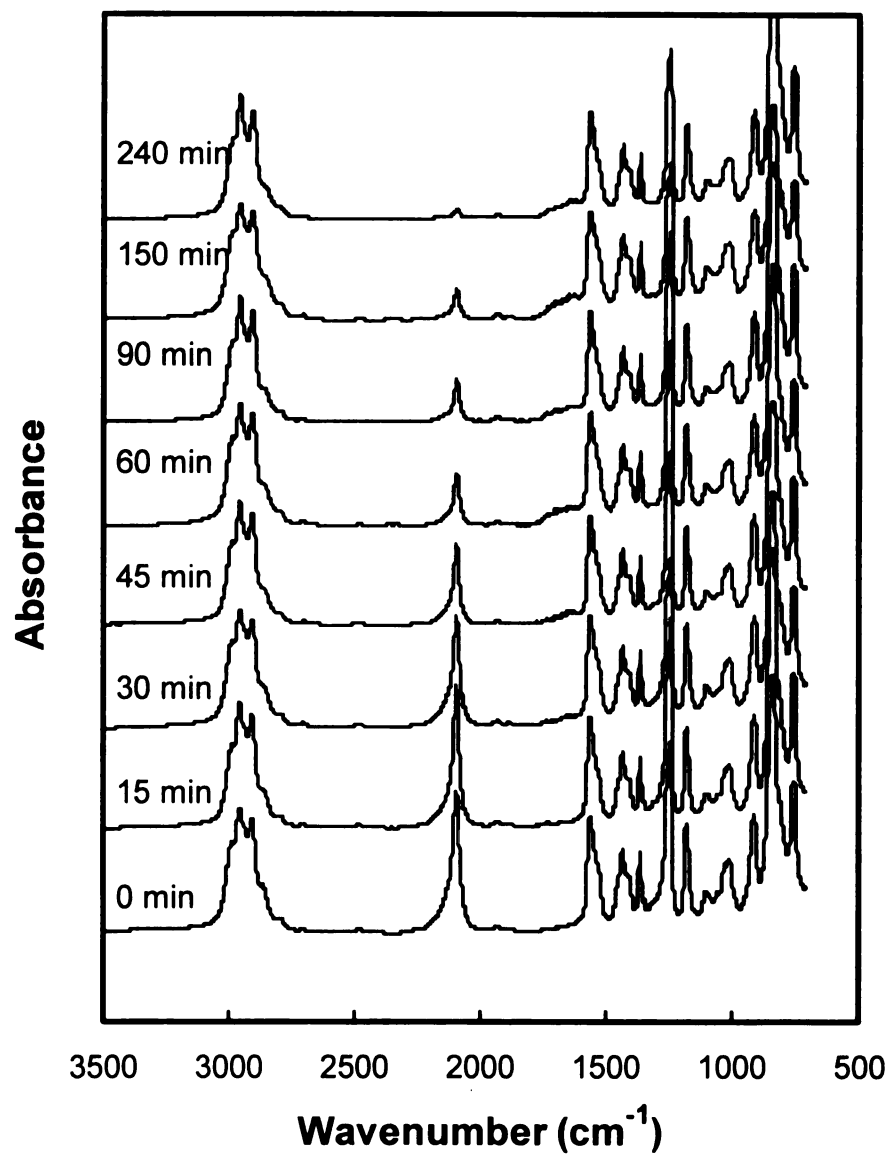


Figure 4.10. FTIR spectra showing the thermal decomposition of copolymer **6f** at 250 °C under vacuum.

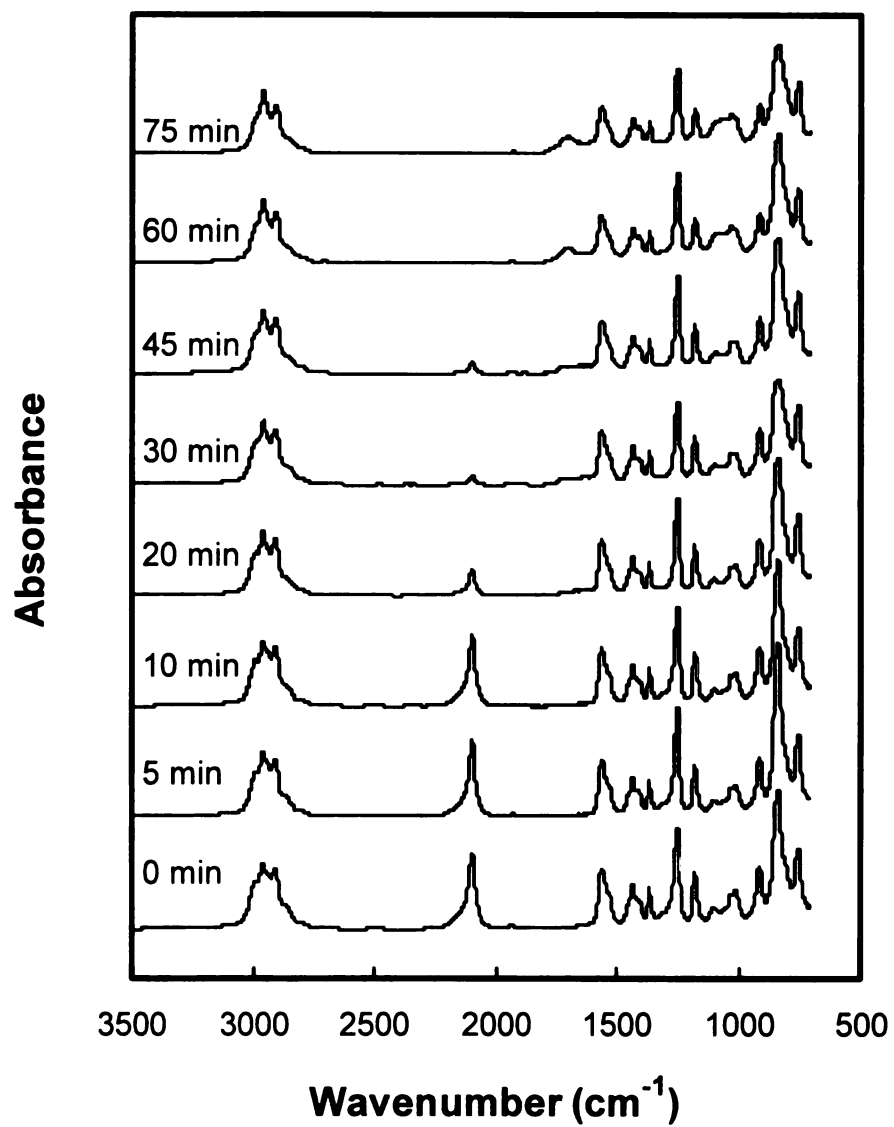


Figure 4.11. FTIR spectra showing the thermal decomposition of copolymer **6f** at 275 °C under vacuum.

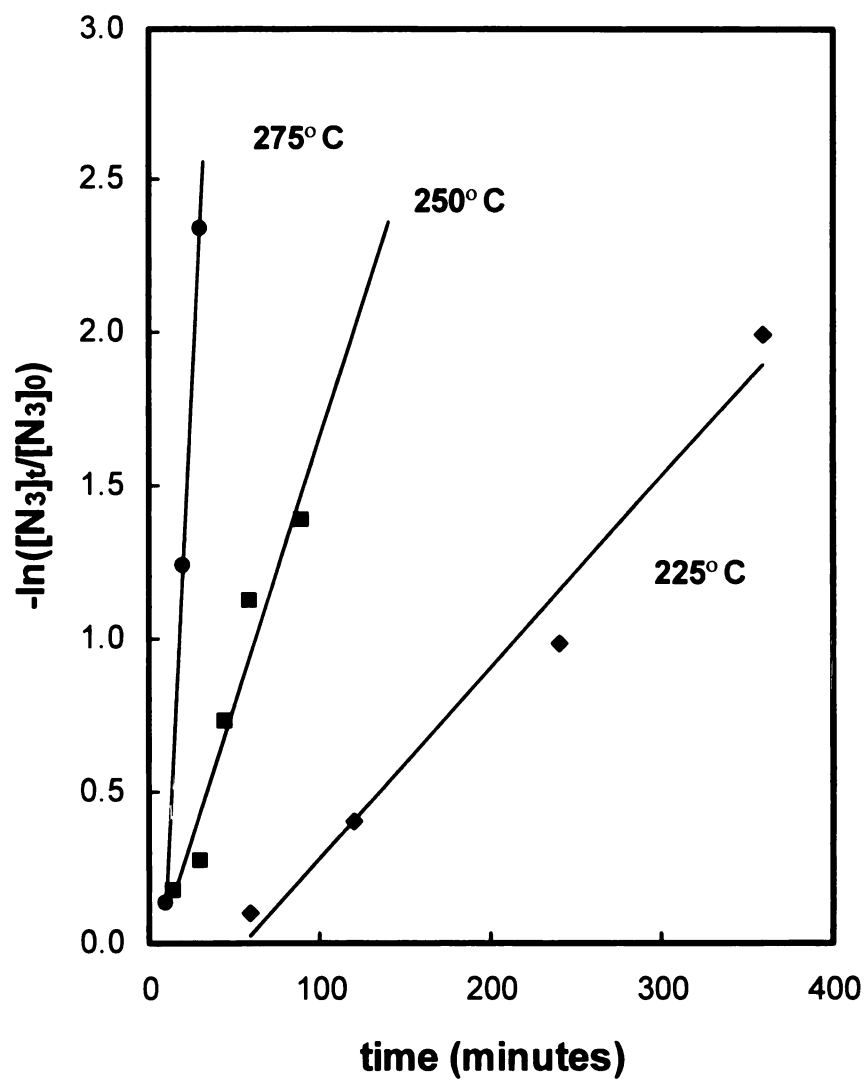


Figure 4.12. Loss of $[N_3]$ in copolymer **6f** versus time at the indicated temperatures.

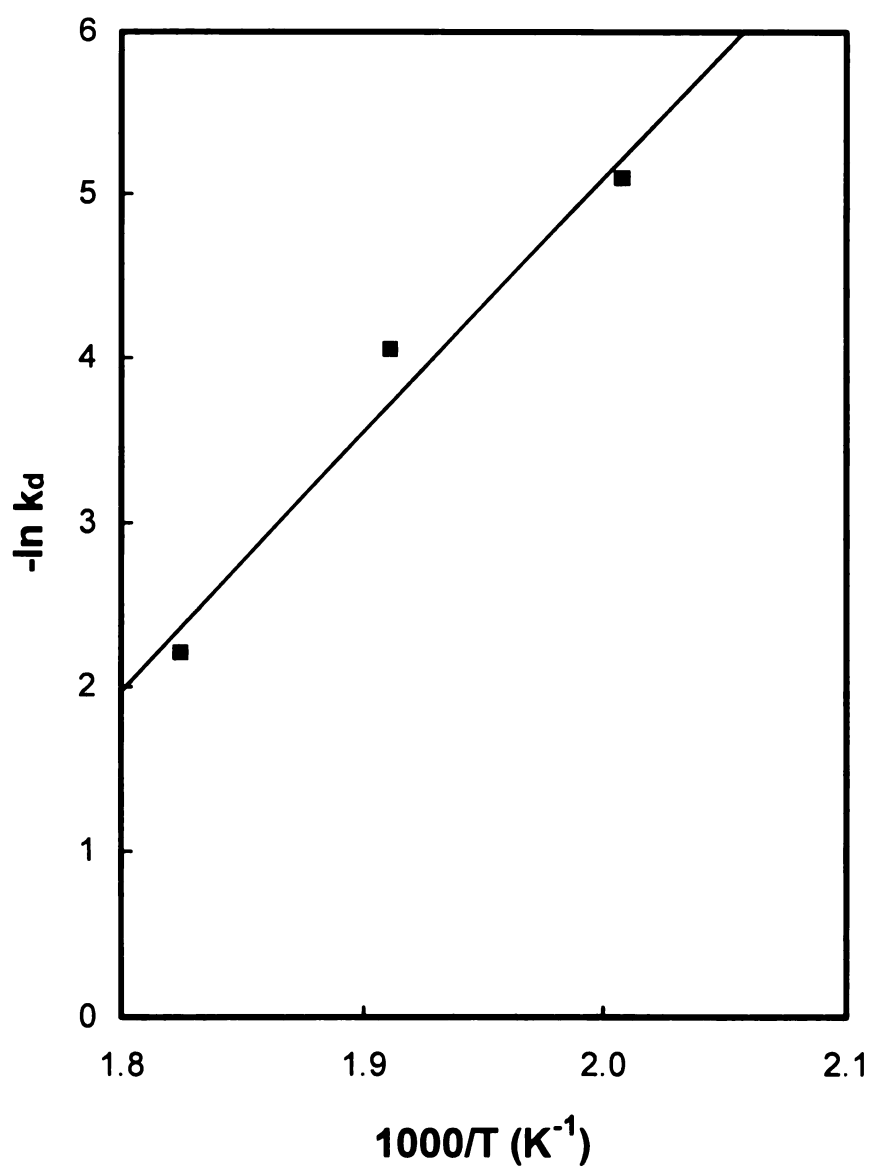


Figure 4.13. Arrhenius plot of the rates of thermal decomposition of copolymer **6f**.

Swelling measurements. Polymer films used for swelling experiments were cast from toluene solutions and were dried under vacuum at 50 °C. The conditions selected for cross-linking the copolymer films (250 °C, 3 hours) were chosen to maximize the extent of cross-linking while minimizing thermal degradation. Thermal decomposition shows up as a visible yellowing of the samples and the appearance of new bands in the IR spectra at $\sim 1700\text{ cm}^{-1}$. Swelling measurements were performed on cross-linked copolymers that contained 2 mol% (**6a**) and 15 mol% azide (**6f**) before cross-linking. Pieces of the cross-linked copolymer films were cut and immersed in a series of poor H-bonding solvents that are good solvents for PTMSP. After 24 hours, the films were removed from the solvent, blotted dry, weighed, and returned to the solvent. After an additional 24 hours, the procedure was repeated to ensure that the films had reached equilibrium. Figure 4.14 shows the results for these two cross-linked networks. Cross-linked copolymer **6a** swells significantly in octane, cyclohexane, and toluene, while cross-linked copolymer **6f** exhibits minimal swelling over the entire solvent range, with only a slight preference for octane, cyclohexane, and toluene. Cross-linked films of the entire series of azide copolymers (**6a-6g**) were placed into toluene ($\delta = 18.2\text{ (J/m}^3)^{1/2} \times 10^{-3}$) and the degree of swelling measured. Figure 4.15 shows a dramatic decrease in swelling as the cross-linking density increases, with copolymers with azide contents greater than 5 mol% showing negligible swelling in toluene.

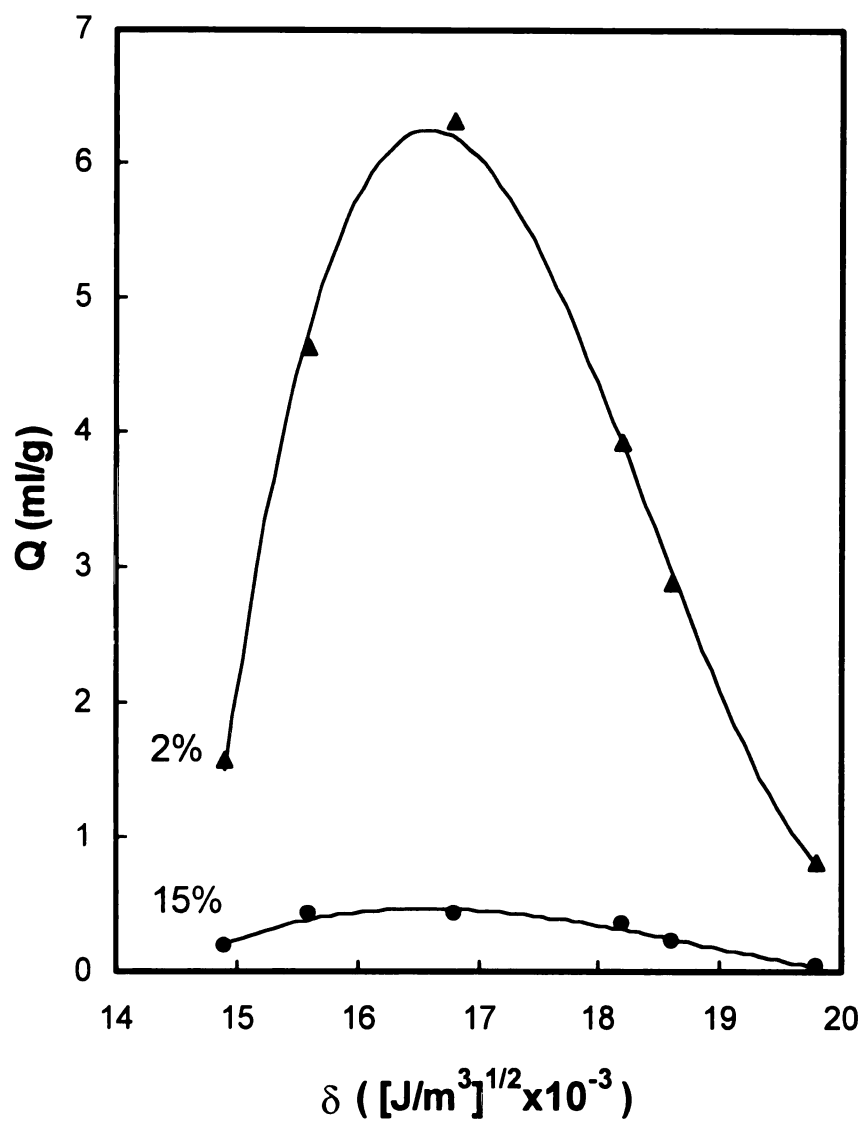


Figure 4.14. Swelling of thermally cross-linked films of copolymers **6a** and **6f** in solvents with different solubility parameters, δ ($[\text{J/m}^3]^{1/2} \times 10^{-3}$).

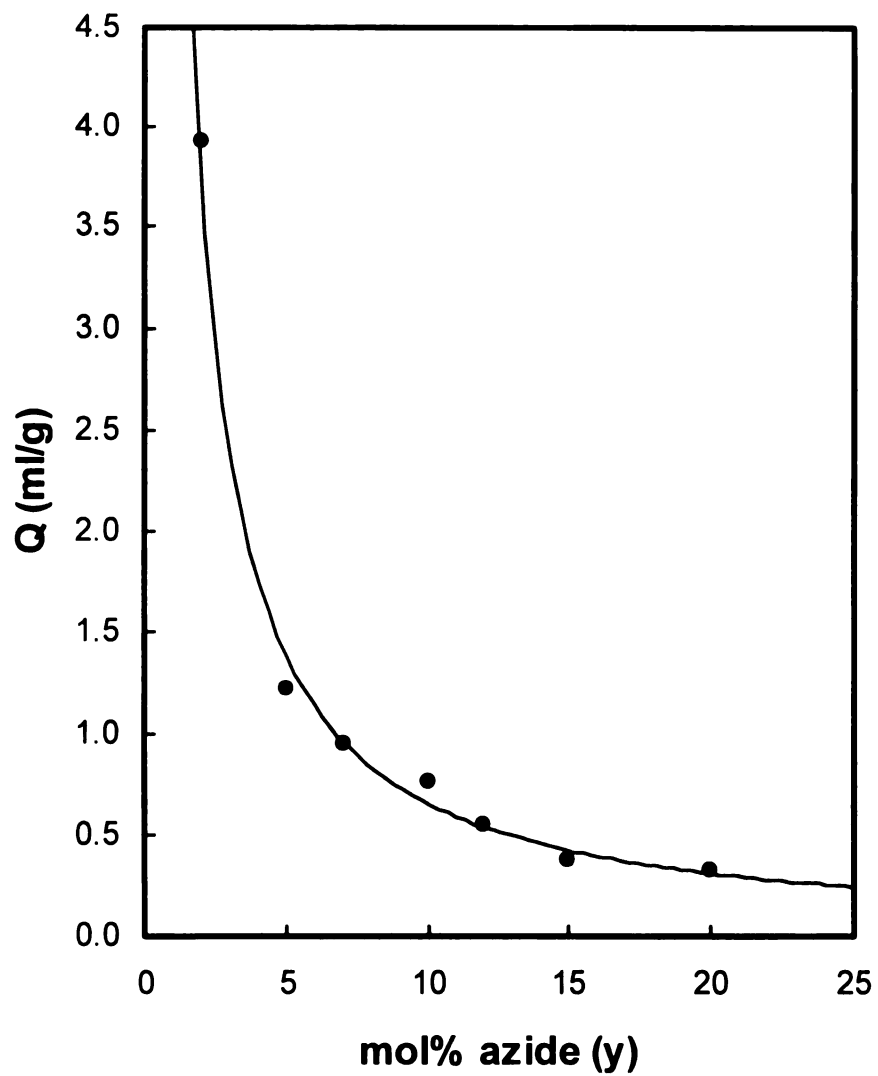


Figure 4.15. Swelling of thermally cross-linked films of copolymers **6a-6g** in toluene.

4.4. Discussion

Synthetic strategy. In a previous report, we explored the use of aryl azides as polymer cross-linking agents.¹¹ Cross-linkable PTMSP films were easily prepared by casting from polymer solutions containing added bis(aryl azide), but a major limitation of this scheme is that only low levels of aryl azide can be incorporated into most polymers before the onset of phase separation. In principle, the compatibility of aryl azides with polymer hosts could be improved through chemical modifications of the aryl azide structure. In similar fashion, alkyl azides could also be used in the form of an additive. The higher decomposition temperature of alkyl azides means that the processing window for polymers containing alkyl azides is wider than for those with aryl azides. One potential drawback, however, is that the higher temperatures needed for cross-linking might lead to some loss of the cross-linking agent from the polymer due to the volatility of the low molecular weight alkyl azide.

Our goal of reaching higher azide contents (and higher degrees of cross-linking) was achieved by directly attaching the azide group to the polymer backbone. In most polymers this would be an easy task since azides are good nucleophiles and can be introduced using simple S_N2 chemistry. However, the steric hindrance associated with the PTMSP backbone blocked our attempts to introduce the azide group. Copolymerization with a functional acetylenic comonomer followed by its conversion to the azide using a nucleophilic displacement reaction was necessary to incorporate larger amounts of azide functionality into PTMSP.

The addition of the tethered side chains does not appear to drastically alter

the physical properties of the PTMSP backbone. The UV-vis absorption spectra of the copolymers are nearly identical to that of PTMSP. Neither PTMSP nor the copolymers strongly absorb above 280 nm, indicating that the C=C bonds are not conjugated and the rigid polymer backbone is retained. This conclusion is also supported by DSC data that indicate that the copolymers, like PTMSP, do not exhibit a glass transition below its thermal decomposition temperature.

The copolymerization route enabled us to overcome the problem of phase of separation at low azide contents and reach high degrees of cross-linking. While the highest azide content we explored in this work was 20 mol%, much higher levels are accessible by changing the monomer feed ratios during the synthesis of PTMSP copolymers.

Cross-linking. Both aryl and alkyl azides can be activated using thermal or photochemical processes. The UV-vis spectra of PTMSP films containing bis(aryl azide)s have two absorption maxima, one from PTMSP and a second from the bis(aryl azide) (*e.g.* 300 nm for 4,4'-diazidobenzophenone).¹¹ Because their absorption maximum occurs at lower energies, aryl azides can be photochemically decomposed selectively in optically clear substrates like PTMSP. Thus, the irradiation of PTMSP containing bis(aryl azide)s at 300 nm led to cross-linked films with no discernable damage to the host polymer. For alkyl azides, the absorption maximum is shifted to shorter wavelengths and coincides with the absorption band for PTMSP. Irradiation of the alkyl azide groups in poly[(1-trimethylsilyl-1-propyne)-*co*-(1-(4-

azidobutyldimethylsilyl)-1-propyne)] may lead to photochemistry that alters the structure of the polymer backbone. In addition, thick samples or those with high azide contents may be difficult to cure by UV.

DSC data show that polymers containing either alkyl or aryl azides thermally decompose, leading to cross-linked products. The limited compositional range available for aryl azide additives prevented us from examining the relationship between thermal decomposition and azide content in detail, but the data reported in this paper for alkyl azides indicate that the thermal properties show a linear dependence on composition over the entire range studied. Although the conditions required to cross-link alkyl azide substituted PTMSP are more severe than those required for the activation of bis(aryl azide)s, mechanically stable optically clear cross-linked networks with low levels of degradation were obtained. We also observed that copolymer films cast on glass exhibit excellent adhesive properties after cross-linking, either through chemical or physical interactions with the surface. Only after prolonged immersion in good solvents and sonication did a cross-linked film of copolymer **6f** fragment and dislodge from the glass surface.

Cross-linking the rigid polymer chains before they have a chance to interdiffuse results in stabilized low-density open structures with high amounts of free volume. Swelling measurements made on the series of cross-linked copolymer films (**6a-6g**) show that a low level of cross-linking yields materials impervious to solvent. Flexible polymers, such as polysiloxanes, typically require higher degrees

of cross-linking to yield non-swelling films,³¹ but the low levels of swelling observed in lightly cross-linked PTMSP networks could be anticipated from the known rigidity of the PTMSP chains. The slight swelling of PTMSP networks with greater than 10 mol% cross-linking, as measured by weight gain, is presumably due to solvent molecules occupying the free volume of the polymer.

Permeability and temporal stability of cross-linked membranes. The oxygen and nitrogen permeability coefficients of freshly prepared and cross-linked membranes were measured.³² As shown in Tables 4.2 and 4.3, the permeability coefficient of uncross-linked films decreases slightly as the amount of azide incorporated in the copolymer increases, presumably due to the side chains occupying the free volume of the membranes.

Cross-linked membranes exhibit vastly different properties depending upon the mode of cross-linking employed. The different behavior of thermal and photo cross-linked films may be due to more free volume in the thermally cross-linked membranes. During the thermal process, thermal expansion of the membranes initially creates a dilated network with high free volume. Cross-linking then interlocks the chains, maintaining the high free volume (Table 4.2). Unlike flexible polymers, which could easily relax at these relatively low cross-linking densities, the rigidity of the PTMSP backbone prevents bond rotations that would enable interdiffusion of the polymer chains leading to decreased free volume, and therefore decreased permeability.

Table 4.2. Permeability coefficients of oxygen, $P(O_2)$, and the oxygen/nitrogen separation factor (α) at 23 ± 1 °C of thermally cross-linked poly[(1-trimethylsilyl-1-propyne)-*co*-(1-(4-azidobutyldimethylsilyl)-1-propyne)] copolymer membranes. $P(O_2)$ is in units of $10^{-7} \text{ cm}^3(\text{STP}) \cdot \text{cm}/\text{cm}^2 \cdot \text{s} \cdot \text{cm Hg}$.

mol% N ₃ in copolymer	before cross-linking		after cross-linking	
	P(O ₂)	$\alpha(O_2/N_2)$	P(O ₂)	$\alpha(O_2/N_2)$
PTMSP	7.4	1.7	6.0	1.6
2	5.4	1.7	3.5	1.7
3	5.2	1.7	3.0	1.9
5	3.5	1.7	2.1	2.1
7	3.3	1.5	2.1	2.1
10	3.7	1.6	2.2	2.1

Table 4.3. Permeability coefficients of oxygen, $P(O_2)$, and the oxygen/nitrogen separation factor (α) at 23 ± 1 °C of photo cross-linked poly[(1-trimethylsilyl-1-propyne)-*co*-(1-(4-azidobutyldimethylsilyl)-1-propyne)] copolymer membranes. $P(O_2)$ is in units of $10^{-7} \text{ cm}^3(\text{STP}) \cdot \text{cm}/\text{cm}^2 \cdot \text{s} \cdot \text{cm Hg}$.

mol% N ₃ in copolymer	before cross-linking		after cross-linking	
	$P(O_2)$	$\alpha(O_2/N_2)$	$P(O_2)$	$\alpha(O_2/N_2)$
PTMSP	7.4	1.7	0.70	3.2
2	5.6	1.8	0.46	3.8
5	4.2	1.5	0.37	3.7
7	3.4	1.5	0.30	3.9

In contrast, membranes cross-linked photochemically are not dilated and cross-linking leads to densification of the network (Table 4.3). The high energy required to activate the alkyl azides also leads to photo-oxidative cross-linking of the irradiated surface due to residual oxygen in the irradiation chamber. Consistent with this interpretation are the measured pycnometric densities of the copolymer membranes. Thermal cross-linking results in only a small change in density, while photo cross-linking results in significant densification.

Ideally, a greater content of azide groups in the copolymer should also produce higher degrees of cross-linking. However, higher azide contents did not lead to higher separation factors. We believe that for azide contents >5%, the cross-linked network is too rigid to allow further densification and losses in free volume. This observation shows that there is a limit of modification beyond which the selectivity is not affected.

The permeabilities of cross-linked membranes, unlike PTMSP membranes, did not decline when stored under vacuum.³² If we assume that interchain diffusion leads to densification and causes the decreases in the free volume and permeability, this suggests that cross-linking of PTMSP inhibits the interchain diffusion and stabilizes the gas permeability.

Comparison to energetic materials. Finally, we need to address the potential application of azide-containing PTMSP as an energetic material. For copolymer **6f**, an activation energy of 130 kJ/mol was calculated from IR data using

the Arrhenius equation. This value compares well to the reported activation energy of another azide containing polymer, GAP, which has an $E_a = 120$ kJ/mol.³³ The copolymers are stable under ambient conditions and are not nearly as “shock sensitive” as trinitrotoluene (TNT) or nitroglycerine, which have activation energies of approximately 30 kJ/mol and 2 kJ/mol respectively.³⁴

The heat released during the thermal decomposition of azide in the copolymers is comparable to that of other azide-based materials. The enthalpy of azide decomposition for the copolymer with the highest azide content in the series, **6g**, is -1.2 kJ/g, as measured by DSC. Two other azide containing materials, GAP³⁵ and poly(vinyl nitrate) partially substituted with azide (PVAZ),³⁶ have reported enthalpies of -1.8 and -2.7 kJ/g, respectively. The higher enthalpies for these two polymers are due to the higher azide content incorporated in the structures. PTMSP with increased azide contents (>20 mol%) could easily be prepared by increasing the co-monomer feed ratio or by homopolymerization of the functional co-monomer. The molar enthalpies for thermal decomposition of copolymers **6a-6g** were also calculated from the DSC results. All copolymers in this series evolved approximately -800 kJ/mol N_3 . This value is comparable to the measured molar decomposition enthalpy of a sample of PTMSP containing a known amount of non-volatile dodecyl azide. Thus, the data indicate that the azide groups decompose independently and the thermochemistry of the copolymers is additive.

4.5. Conclusions

Copolymers of 1-(4-azidobutyldimethylsilyl)-1-propyne and 1-trimethylsilyl-1-propyne were prepared by functionalizing the bromobutyl side chain of poly[(1-trimethylsilyl-1-propyne)-*co*-(1-(4-bromobutyldimethylsilyl)-1-propyne)] copolymers. The amount of N₃ in the copolymers was determined quantitatively by elemental analysis, DSC, and IR spectroscopy. Compared to the cross-linking of PTMSP by the physical addition of bis(aryl azide)s, copolymerization allowed incorporation of a higher concentration of cross-linking sites without phase separation. The measured activation energy and enthalpies of thermal decomposition of azide contained in the series of copolymers are comparable to other reported azide containing materials. Thermally induced cross-linking of the copolymer films resulted in rigid, non-swelling materials at relatively low cross-link densities. Mechanically stable membranes were prepared by thermal and photochemical cross-linking of azide-functionalized PTMSP copolymers. The separation properties of the cross-linked membranes are dependent upon the method of cross-linking and can be ascribed to the amount of free volume in the cross-linked membranes. Measurements taken after one month of storage under vacuum indicate that all cross-linked membranes exhibit no decline in permeability.

4.6. References

- 1) Masuda, T.; Isobe, E.; Higashimura, T.; Takada, K. *J. Am. Chem. Soc.* **1983**, *105*, 7473.
- 2) Shimomura, H.; Nakanishi, K.; Odani, H.; Kurata, M.; Masuda, T.; Higashimura, T. *Kobunshi Ronbunshu* **1986**, *43*, 747.
- 3) Takada, K. M., H.; Masuda, T.; Higashimura, T. **1985**, *30*, 1605.
- 4) Masuda, T.; Higashimura, T. *Silicon Based Polymer Science*; Ziegler, J. M. and Fearon, F. W. G., Ed.; American Chemical Society: Washington, DC, 1990; Vol. 224, pp 641.
- 5) Morita, H.; Mori, S.; Uchino, N.; Yokoyama, S. *Z. Phys. Chemie-Int. J. Res. Phys. Chem. Chem. Phys.* **1993**, *182*, 209-216.
- 6) Murray, K. A.; Holmes, A. B.; Moratti, S. C.; Friend, R. H. *Synth. Met.* **1996**, *76*, 161-163.
- 7) Gonzalez, L.; Rodriguez, A.; deBenito, J. L.; Marcos Fernandez, A. *J. Appl. Polym. Sci.* **1997**, *63*, 1353-1359.
- 8) Yan, M. D.; Cai, S. X.; Wybourne, M. N.; Keana, J. F. W. *J. Mater. Chem.* **1996**, *6*, 1249-1252.
- 9) Naito, I.; Morihara, H. *J. Imaging Sci. Technol.* **1996**, *40*, 50-55.
- 10) Yamamoto, J.; Uchino, S.; Hattori, T.; Yoshimura, T.; Murai, F. *Jpn. J. Appl. Phys. Part 1 - Regul. Pap. Short Notes Rev. Pap.* **1996**, *35*, 6511-6516.

- 11)Jia, J. P.; Baker, G. L. *J. Polym. Sci. Pt. B-Polym. Phys.* **1998**, *36*, 959-968.
- 12)Scriven, E. F. V.; Turnbull, K. *Chem. Rev.* **1988**, *88*, 297-368.
- 13)Abramovitch, R. A.; Kyba, E. P. *The Chemistry of the Azido Group*; Patai, S., Ed.; Interscience Publishers: London, 1971, pp 221-330.
- 14)Nagai, K.; Higuchi, A.; Nakagawa, T. *J. Polym. Sci. Pt. B-Polym. Phys.* **1995**, *33*, 289-298.
- 15)Nagai, K.; Nakagawa, T. *J. Membr. Sci.* **1995**, *105*, 261-272.
- 16)Masuda, T.; Isobe, E.; Higashimura, T. *Macromolecules* **1985**, *18*, 841.
- 17)Baker, G. L.; Klausner, C. F.; Gozdz, A. S.; Shelburne, J. A.; Bowmer, T. N. *Adv. Chem. Ser.* **1990**, 663-678.
- 18)Kraus, G.; Landgrebe, K. *Synthesis* **1984**, *10*, 885.
- 19)Kunzler, J.; Percec, V. *New Polym. Mater.* **1990**, *1*, 271.
- 20)Bowmer, T. N.; Baker, G. L. *Polym. Prepr., ACS Div. Polym. Chem.* **1986**, *27*, 218.
- 21)Nishiyama, K.; Karigomi, H. *Chem. Lett.* **1982**, *9*, 1477.
- 22)Gilbert, E. E. *J. Polym. Sci.; Polym. Chem. Ed.* **1984**, *22*, 3603.
- 23)Hidalgo, M.; Gonzalez, L.; Mijangos, C. *J. Appl. Polym. Sci.* **1996**, *61*, 1251-1257.
- 24)Jayakrishnan, A.; Sunny, M. C.; Rajan, M. N. *J. Appl. Polym. Sci.* **1995**, *56*, 1187-1195.
- 25)Cohen, H. L. *J. Polym. Sci. Poly. Chem. Ed.* **1981**, *19*, 1337-1347.

- 26) Ravindranath, B.; Srinivas, P. *Ind. J. Chem.* **1985**, *24B*, 1178.
- 27) Gurst, J. E. *The Chemistry of the Azido Group*; Patai, S., Ed.; Interscience Publishers: London, 1971, pp 191-202.
- 28) Gozdz, A. S.; Baker, G. L.; Klausner, C.; Bowden, M. J. *Proc. SPIE* **1987**, *771*, 18.
- 29) Tang, B. Z.; Masuda, T.; Higashimura, T.; Yamaoka, H. *J. Polym. Sci. Pol. Chem.* **1989**, *27*, 1197-1209.
- 30) Burrell, H. *Polymer Handbook*; 2nd ed.; Brandrup, J. and Immergut, E. H., Ed.; John Wiley & Sons: New York, 1975, pp IV-337.
- 31) Pleshakov, D. V.; Lotmentsev, Y. M. *Vysokomol. Soedin.* **1994**, *36*, 2026-2030.
- 32) Jia, J. *Cross-linked Poly[1-trimethylsilyl-1-propyne]*; Michigan State University: East Lansing, Michigan, 1997.
- 33) Eroglu, M. S. *Polym. Bull.* **1998**, *41*, 69-76.
- 34) Johansson, C. H.; Persson, P. A. *Detonics of High Explosives*; 1st ed.; Academic Press Inc.: New York, 1970.
- 35) Arisawa, H.; Brill, T. B. *Combust. Flame* **1998**, *112*, 533-544.
- 36) Mishra, S. C.; Pant, J.; Dutta, P. K.; Durgapal, U. C. *Def. Sci. J.* **1997**, *47*, 131-137.

Chapter 5

PTMSP as a Permeable Solid Support in Oxygen Sensor Applications

5.1. Introduction

Quantitative detection of oxygen is important for medical applications, control of industrial processes, and combustion. Electrochemical cells are commonly used to detect oxygen at high temperatures,¹⁻³ while ambient temperature sensors are often based on the quenching of luminescence from organic and organometallic chromophores.^{4,5} Optical schemes are particularly attractive since they can be adapted for use in fiber optic geometries that are robust and insensitive to electronic noise. However, a drawback of these schemes is that the chromophores often decompose and have limited temperature ranges.

In contrast, the physical properties and photophysics of $\text{Mo}_6\text{Cl}_{12}$ and related metal clusters are well suited for oxygen sensing schemes. The photosensitive $\text{Mo}_6\text{Cl}_{12}$ cluster, shown in Figure 5.1, is composed on an octahedral core of molybdenum atoms with eight face bridging chlorides and four axial chlorides, which are shared among neighboring cluster subunits to form a $(\text{Mo}_6\text{Cl}_{12})_n$ polymeric structure.⁶ Pumping the clusters with 300 to 400 nm radiation generates a strong red luminescence that is efficiently quenched by ground state $^3\text{O}_2$. The clusters show no signs of degradation and are thermally stable to 600 °C. The observed emission intensity (I) from the clusters is related to the concentration of quencher, $[\text{O}_2]$, by the

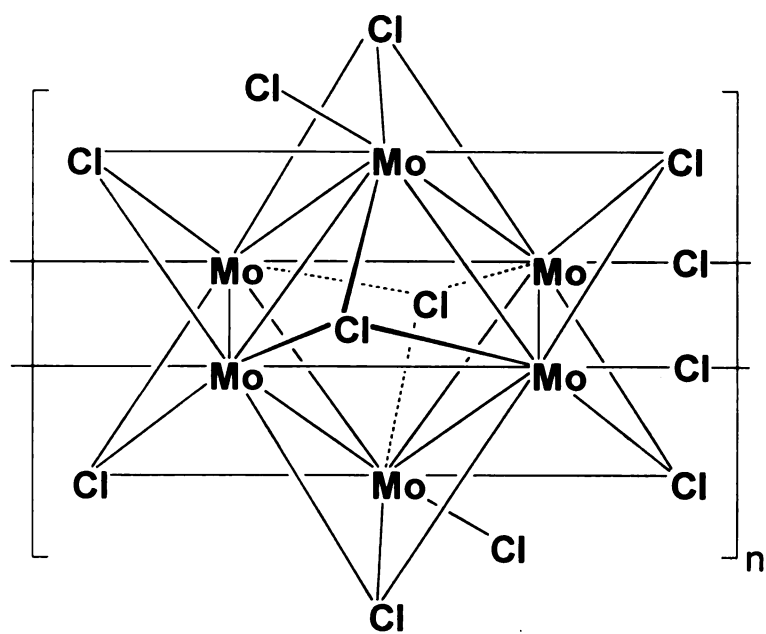


Figure 5.1. Structure of $(\text{Mo}_6\text{Cl}_{12})_n$ clusters.

Stern-Vollmer equation (Equation 1), where K_q is the product of the fluorescence lifetime and the quenching rate constant of the cluster.⁷ Shown in Figure 5.2 is the relationship between signal intensity and quencher concentration for the molybdenum

$$\frac{I_o}{I} = 1 + K_q[O_2] \quad (1)$$

clusters in solution.⁸ The large changes in signal intensity with small changes in the oxygen concentration indicate that these clusters would be ideal probes for sensing oxygen in the range of 10^{-4} to 10^{-1} M.

To adapt Mo_6Cl_{12} to fiber optic sensing, the clusters need to be immobilized at the end of a silica optical fiber. Polymers and silica have been used to immobilize Mo clusters for oxygen detection and as sensitizers for 1O_2 generation,⁸⁻¹⁰ but for gas sensing applications, the polymer matrix needs to have a high permeability to ensure fast response times.

Because of its attractive physical properties and high oxygen permeability, poly(1-trimethylsilyl-1-propyne) (PTMSP) should be an excellent support for fiber optic based sensing applications. PTMSP is an amorphous polymer with a low density and a large free volume caused by the inefficient packing of its rigid random coil backbone. Its permeability coefficient for oxygen is ten times greater than poly(dimethylsiloxane), the polymer typically used as the benchmark for high

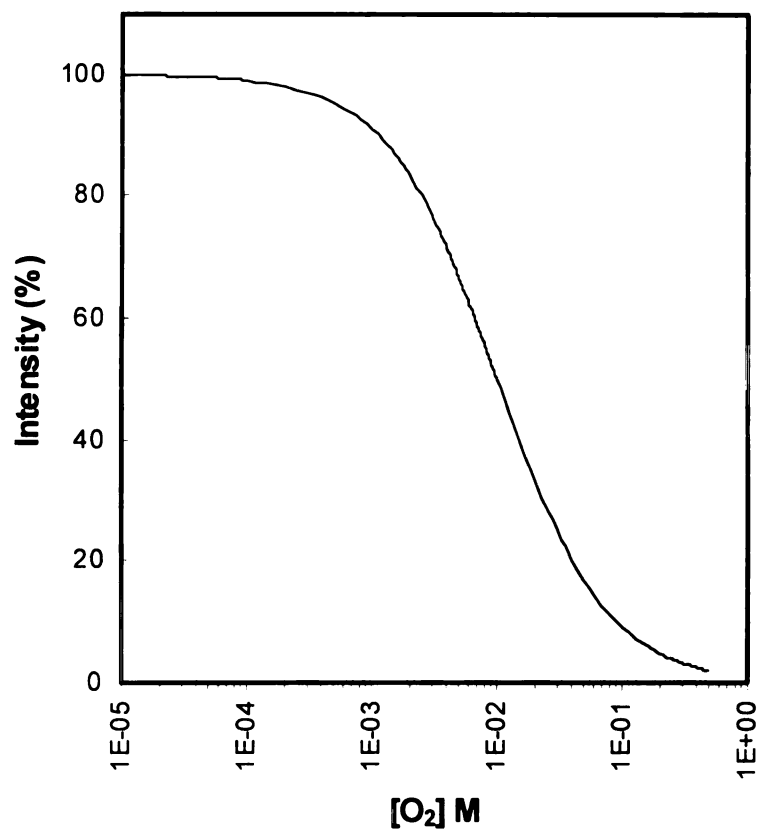


Figure 5.2. Stern-Vollmer plot of emission intensity versus $[O_2]$.

permeability.¹¹ PTMSP is tough and mechanically stable, with a modulus between that of typical amorphous materials and rubbery polymers. PTMSP exhibits no glass transition below its degradation temperature (350 °C), is relatively chemically inert, and is optically clear with no absorption above 280 nm. Transparent films can be produced by spin casting or solvent evaporation

Combining the optical properties of $\text{Mo}_6\text{Cl}_{12}$ clusters with the physical properties of PTMSP should lead to a composite ideal for fiber optic based oxygen sensing applications. This chapter describes the effectiveness and stability of PTMSP as a solid support, and the procedure used to prepare and bind the PTMSP/ $\text{Mo}_6\text{Cl}_{12}$ composite to the end of a large core silica optical fiber. This work led to the development of a reflection mode fiber optic capable of the real time monitoring of oxygen in 0 - 21% gaseous environments.

5.2. Experimental Section

Materials. The preparation of PTMSP, poly[(1-trimethylsilyl-1-propyne)-*co*-(1-(4-bromobutyldimethylsilyl)-1-propyne)] and poly[(1-trimethylsilyl-1-propyne)-*co*-(1-(4-azidobutyldimethylsilyl)-1-propyne)] copolymers are described in Chapter 4. $\text{Mo}_6\text{Cl}_{12}$ was prepared according to literature procedures.^{2,6,12} Tetrahydrofuran (THF) and toluene were purified by distillation from calcium hydride followed by a second distillation from sodium/benzophenone ketyl. Unless otherwise noted, all other reagent grade materials were purchased from commercial suppliers and used without further purification.

Characterization. Proton nuclear resonance (^1H NMR) spectra were measured using a Varian Gemini-300 spectrometer at 300 MHz. All samples were run at room temperature in CDCl_3 . Chemical shifts were calibrated using residual CHCl_3 and are reported in ppm (δ) relative to tetramethylsilane. Infrared spectra were obtained under nitrogen at room temperature on a Nicolet Magna-IR 550 Fourier Transform IR spectrometer. A Hitachi U-4001 UV-visible spectrometer was used to obtain the UV-visible spectra of cyclohexane solutions of the polymers and acetonitrile solutions of $\text{Mo}_6\text{Cl}_{12}$. Fluorescence spectra of the molybdenum clusters dissolved in acetonitrile were obtained using a Hitachi F-4500 fluorescence spectrophotometer. Molecular weights of the polymers were determined by gel permeation chromatography (GPC) using a PLgel 20 μ Mixed A column and a Waters R401 Differential Refractometer detector at room temperature with THF as eluting solvent

at a flow rate 1 mL/min. Monodisperse polystyrene standards were used to calibrate the molecular weights. The concentration of the polymer solutions used for GPC measurements was 1 mg/mL. Thermogravimetric analyses (TGA) were performed under nitrogen and air atmospheres at a heating rate of 10 °C/min on a Perkin-Elmer TGA 7 instrument.

Poly[(1-trimethylsilyl-1-propyne)-*co*-(1-(4-cyanobutyldimethylsilyl)-1-propyne)]. Poly[(1-trimethylsilyl-1-propyne)-*co*-(1-(4-bromobutyldimethylsilyl)-1-propyne)] (80 mg, 0.6 mmol Br) was dissolved in toluene (5 mL). Sodium cyanide (NaCN, 0.294g, 6 mmol) and a catalytic amount of tetra-*n*-butylammonium iodide (*n*-Bu₄NI, 0.022g, 0.06 mmol) were dissolved in 1 mL distilled water and added to the polymer solution. The flask was fitted with a water condenser and placed into an oil bath heated to 105 °C. The mixture was stirred vigorously overnight. Upon cooling, water (50 mL) was added and the polymer was extracted with methylene chloride (3 x 50 mL). The combined organic layers were dried over magnesium sulfate, filtered, and the solvent removed under reduced pressure. The polymer was redissolved in toluene and precipitated dropwise into an excess of methanol. The polymer was collected by filtration to yield 48 mg (60%). GPC: $M_n = 400,000$. $M_w/M_n = 2.3$. ¹H NMR: δ 0.2 (br), 1.6 (br), 1.8 (br), 2.3 (br). IR: C \equiv N, 2250 cm⁻¹. Anal. Calcd. for (C_{6.8}H₁₃N_{0.2}Si)_n: C, 64.99; H, 10.43; N, 2.23; Si, 22.35. Found: C, 63.23; H, 10.67; N, 1.91; Si, not determined.

Casting/dipping solutions. Solutions used to coat fibers and cast films were prepared by dissolving $\text{Mo}_6\text{Cl}_{12}$ (300 mg, 0.3 mmol) in 300 mL of spectroscopic grade acetonitrile. The solution was concentrated to give a yellow oil, presumably the corresponding acetonitrile adduct of the molybdenum complex. A solution of PTMSP in tetrahydrofuran was added to the yellow oil. After filtration through a 2 μm filter, the solution was concentrated to the desired viscosity (typically 1-2 wt %) with a steady stream of dry nitrogen and gentle heating.

Film casting. Films used for measuring the optical properties of the composites were spin cast from the previously described solutions onto Suprasil™ high-purity quartz slides (1x2 cm^2) inside a He atmosphere drybox. Spinning rates ranged from 1000 to 2000 rpm depending upon the viscosity of the sample. Film thickness was measured using a Dektak SFM instrument.

Fiber coating. The sensor was fabricated from a commercially available multimode fiber, FT-1.5-UMT from 3M Specialty Optical Fibers, which is designed for UV to visible transmission. The large core diameter (1500 μm) and high numerical aperture (0.39) of the fiber allows for efficient excitation and collection of the luminescence from clusters immobilized at the back face of the fiber. The exposed surfaces of the cleaved 1.5-meter length fibers were cleaned in a UV-ozone photoreactor for 30 min, and then immediately transferred into a He-atmosphere drybox. A thin primer layer of poly[(1-trimethylsilyl-1-propyne)-*co*-(1-(4-azidobutyldimethylsilyl)-1-propyne)] (azide content 15%) was applied by dip coating

the fiber tip into a 1 wt% solution in toluene. After drying, the primer layer was cross-linked at 250 °C for 3 hours. A transparent, uniform bead (~ 100 μm) of Mo₆Cl₁₂/polymer composite was then applied by dipping the primed fiber tip into a 2 wt% casting solution. The composite bead was allowed to dry overnight and then was dried under vacuum at ambient temperature for 1 hour.

Detection apparatus. The coated fiber tip was secured in a glass cell by a rubber septum that was fed through from the front end of the fiber. The “flow-through” cell was equipped with a gas inlet and outlet in order to control the environment around the sensor. Radiation from a 325 nm He/Cd laser was coupled via a microscope objective into the front end of the fiber to provide the incident pump beam. A maximum of 2.5 mW could be coupled into the fiber. The reflected luminescence was collected at the front end of the fiber with either a photodiode or photomultiplier tube. Separation of the signal and pump beams was accomplished using a 45° long wave pass (LWP) dichroic beamsplitter and a 630nm LWP filter.

5.3. Results

To use PTMSP as a permeable support for $\text{Mo}_6\text{Cl}_{12}$ clusters, it is necessary that the polymer does not interfere with the optical properties of the clusters. As shown in Figure 5.3, PTMSP does not absorb above 280 nm.¹³ Therefore, the support matrix will not absorb the excitation energy of the molybdenum clusters at 325 nm. Separation of the emission radiation from the initial excitation energy is also simplified due to the large red shift of the cluster emission.

PTMSP and $\text{Mo}_6\text{Cl}_{12}$ must be miscible in order to form homogeneous composites that possess good optical properties. However, PTMSP is soluble in non-polar solvents while $\text{Mo}_6\text{Cl}_{12}$ clusters are only soluble in polar solvents such as methanol and acetonitrile. Only THF was found to efficiently dissolve both. Our initial scheme involved physically dispersing and suspending $\text{Mo}_6\text{Cl}_{12}$ in the polymer by mixing solutions of the polymer and salt in THF and concentrating the solutions until viscous. The casting solutions were prepared to yield composites with ~10% of the volume occupied by the clusters. Unfortunately, during film formation, $\text{Mo}_6\text{Cl}_{12}$ clusters precipitated in the polymer matrix creating heterogeneous films with poor optical properties. In THF, two of the bridging chlorides are replaced by solvent, and the $(\text{Mo}_6\text{Cl}_{12})_n$ polymer clusters dissolve as discrete clusters. But in the absence of suitable ligands, the clusters reassemble through the bridging chlorides as the solvent evaporates. Attempts to kinetically control the crystallization by speeding up the evaporation rate (i.e. increasing the spinning rate) resulted in films which were too thin with salt concentrations below limits of detection.

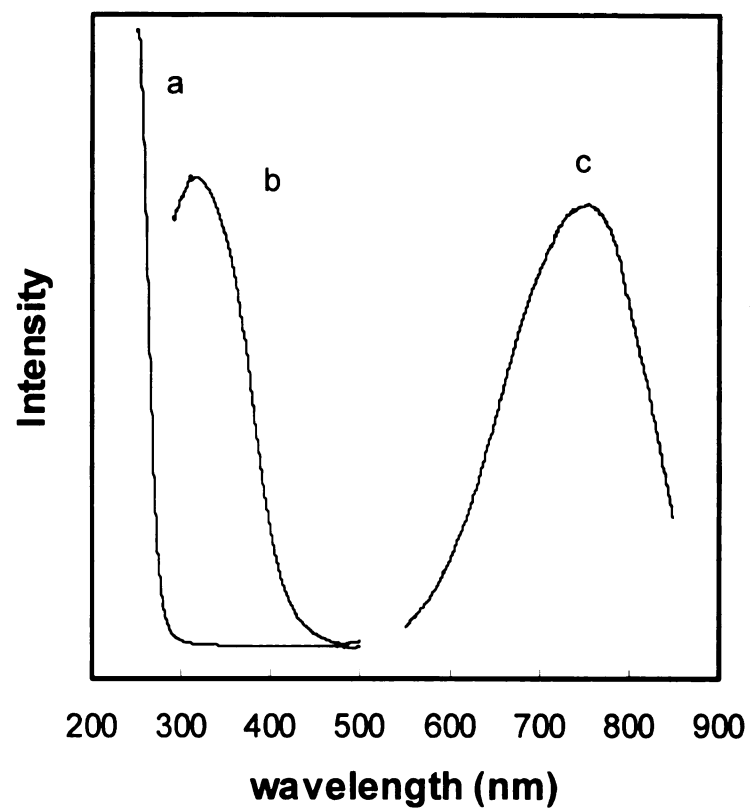


Figure 5.3. The UV/Vis absorption spectra of a) PTMSP and b) $\text{Mo}_6\text{Cl}_{12}$, and the fluorescence spectra of c) $\text{Mo}_6\text{Cl}_{12}$.

Similar metal clusters have been dissolved in various polymers by utilizing the axial coordination sites to ligate the cluster core to the polymeric backbone.^{8-10,14,15} Dissolving the clusters in PTMSP could be accomplished by using a PTMSP copolymer with side chains that contain polar ligands capable of solvating the molybdenum salt. Since the photophysics of interest is due to electronic transitions in the core of the cluster, attachment of the cluster to a polymer matrix does not add non-radiative pathways to the lumophore. Of the ligand-containing copolymers that were investigated, a nitrile containing copolymer proved to be the most chemically stable and easiest to synthesize.

The nitrile-containing copolymer was synthesized from a brominated PTMSP copolymer, poly[(1-trimethylsilyl-1-propyne)-*co*-(1-(4-bromobutyl-dimethylsilyl)-1-propyne)], with 20% of the repeat units having bromobutyl side chains.¹⁶ As shown in Figure 5.4, treatment of the copolymer with sodium cyanide and a phase transfer agent smoothly converted the bromobutyl side chain to the corresponding nitrile. The reaction was analyzed by ¹H NMR and FTIR spectroscopy to determine the conversion. In the IR spectra, the intensity of the band at 1219 cm⁻¹ decreased (CH₂Br group), and a new band grew in at 2250 cm⁻¹ corresponding to the -C≡N group in poly[(1-trimethylsilyl-1-propyne)-*co*-(1-(4-cyanobutyl-dimethylsilyl)-1-propyne)]. Corresponding changes were seen in the ¹H NMR data. The peak at 3.4 ppm from the -CH₂Br segment in poly[(1-trimethylsilyl-1-propyne)-*co*-(1-(4-bromobutyl-dimethylsilyl)-1-propyne)] decreased as a new resonance at 2.3 ppm for

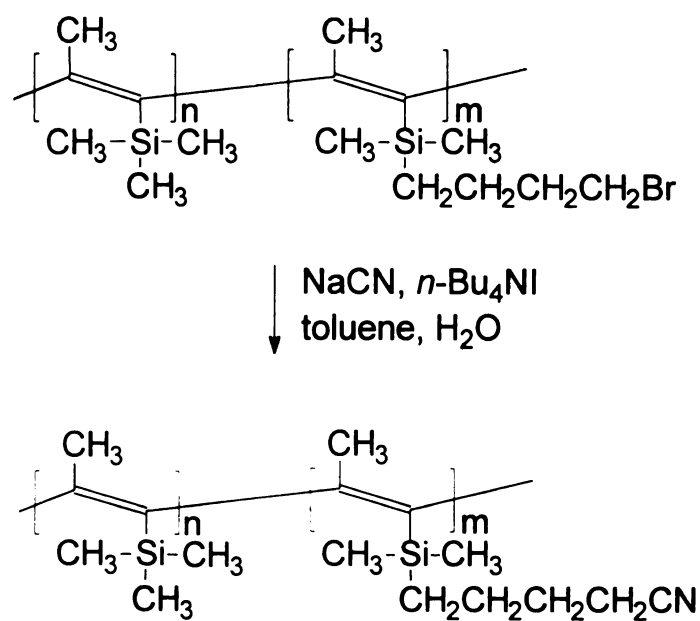


Figure 5.4. Synthesis of poly[(1-trimethylsilyl-1-propyne)-*co*-(1-(4-cyanobutyl)dimethylsilyl)-1-propyne)].

-CH₂CN in poly[(1-trimethylsilyl-1-propyne)-*co*-(1-(4-cyanobutyldimethylsilyl)-1-propyne)] increased. The peak at 3.4 ppm in the ¹H NMR spectra and the absorption band at 1219 cm⁻¹ in the IR spectra both decreased to baseline, demonstrating that complete displacement of the bromide was achieved.

The copolymer was redissolved in toluene and stirred over powdered molybdenum clusters for several days. The solution was then filtered to remove the undissolved clusters and concentrated to a viscous solution. The luminescent properties of the Mo₆Cl₁₂/nitrile copolymer composites were characterized by fluorescence measurements of films spin cast onto quartz slides. The amount of cluster dissolved in the copolymers was too low to be detected, indicating that either the nitrile ligands were not strong enough to displace the bridging chloride ligands or the concentration of the pendant nitriles was too low to ligate a useful quantity of cluster. IR spectra of the composite films indicated no shift in the frequency of the nitrile absorption band due to coordination with the cluster.

A casting solution of the nitrile copolymer containing a higher concentration of clusters was prepared in THF as was previously done for PTMSP/Mo₆Cl₁₂ composites. Although films cast from this solution still exhibited some phase separation, modulation of the fluorescence from the clusters was observed in air and argon environments (Figure 5.5). Quenching of the fluorescence by oxygen in air resulted in a 5x decrease in the luminescence intensity.

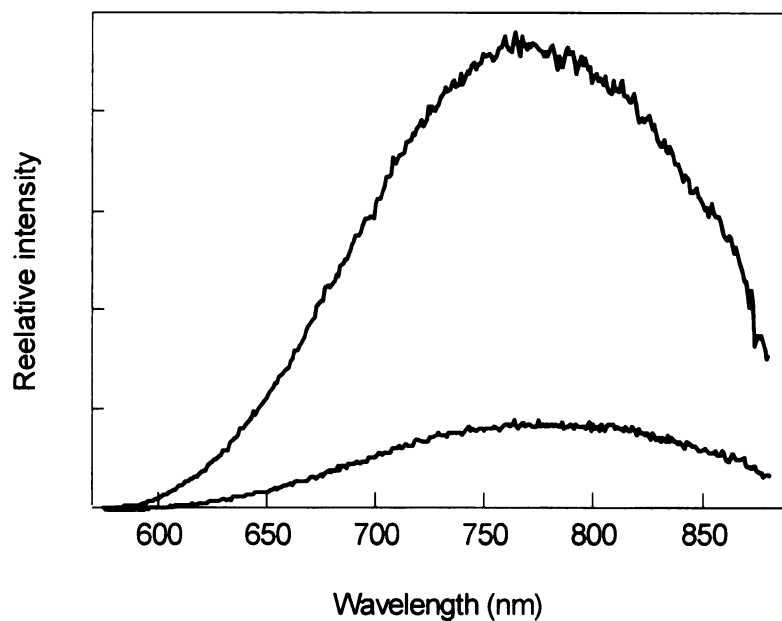


Figure 5.5. Luminescence spectra from a $\text{Mo}_6\text{Cl}_{12}$ /nitrile-PTMSP copolymer composite film in laboratory air (bottom curve) and under Ar (top curve).

The problems of low cluster concentration and phase separation in the composites were overcome by preparing a soluble derivative of $(\text{Mo}_6\text{Cl}_{12})_n$ that can co-dissolve with PTMSP in high concentration. Although the clusters are soluble in both THF and acetonitrile, the clusters precipitate from THF after evaporation reforming a yellow powder. However after evaporation of acetonitrile, a soluble yellow oil formed. The ideal structure of the adduct is $\text{Mo}_6\text{Cl}_{12}(\text{CH}_3\text{CN})_2$, but it is unlikely that acetonitrile efficiently forms single solvated clusters. The only reported examples of isolated single clusters were synthesized by replacing the bridging chlorides with covalently bound ligands.^{10,17} We assume that acetonitrile merely acts as a temporary ligand, solvating small domains of clusters that once dispersed in the PTMSP framework are unable to phase separate. Films prepared on quartz slides using casting solutions containing the acetonitrile solvated clusters exhibited high intensity emission due to the high cluster loading and minimal loss of signal due to scattering caused by phase separation.

The composites showed poor adhesion to freshly cleaved fiber tips, and peeled off the fiber upon drying. To achieve better adhesion to the fiber, we first applied a primer layer to the fiber tip to enable better wetting by the composite. The primer layer consisted of a cross-linkable PTMSP derivative, poly[(1-trimethylsilyl-1-propyne)-*co*-(1-(4-azidobutyldimethylsilyl)-1-propyne)], which after heating, adhered to the fiber surface. Uniform beads of the PTMSP/ $\text{Mo}_6\text{Cl}_{12}$ composite were then applied to the fiber tip by repeated dipping of the tip into the viscous solutions.

After drying, the beads of $\text{Mo}_6\text{Cl}_{12}$ /PTMSP composite were mechanically stable and adhered well to the fiber end.

The measured emission intensity from the coated fiber (Fiber 1) in varying oxygen concentrations is shown in Figure 5.6. Although steps in the observed intensity are seen as the atmosphere is changed from pure oxygen to nitrogen, re-introduction of nitrogen into the cell resulted in a positive spike in the signal that decayed to the previous intensity level after a short period of time. We propose that this is due to the presence of additional quenching species. As shown in Figure 5.7, the PTMSP backbone is susceptible to radical chain oxidation, and the degradation by-products may act as efficient quenchers of the excited clusters. The degradation pathway can be initiated by a radical source generated either chemically or photochemically. Upon irradiation of the composite in nitrogen, a steady state amount of photooxidation products in the polymer is generated, causing a decay of the observed emission intensity. Introduction of oxygen accelerates the chain degradation process, forming additional quenching species that further lower the emission intensity. Although reintroduction of nitrogen into the cell results in the maximum emission intensity, continued chain degradation reforms the steady state amount of quenchers, decreasing the observed intensity.

Investigation of the casting solutions revealed that the tetrahydrofuran used to dissolve the composite tested positive for peroxides. After evaporation of the solvent, a ~4% non-volatile weight residue remained consisting of peroxidized and

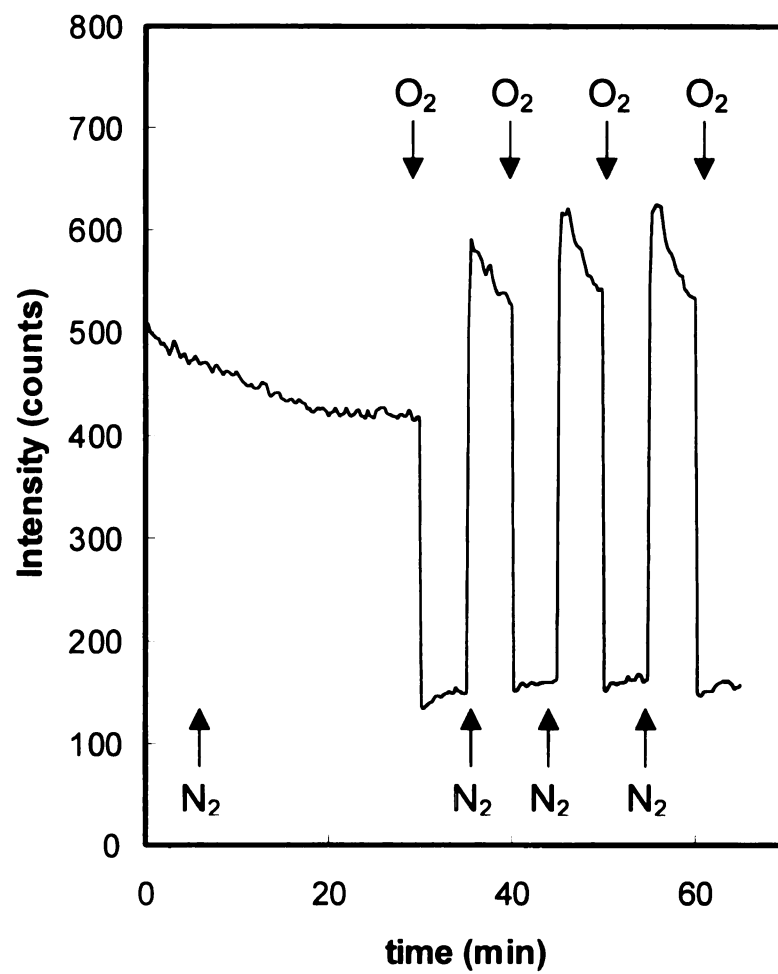


Figure 5.6. Observed emission from Fiber 1 in varying oxygen/nitrogen environments.

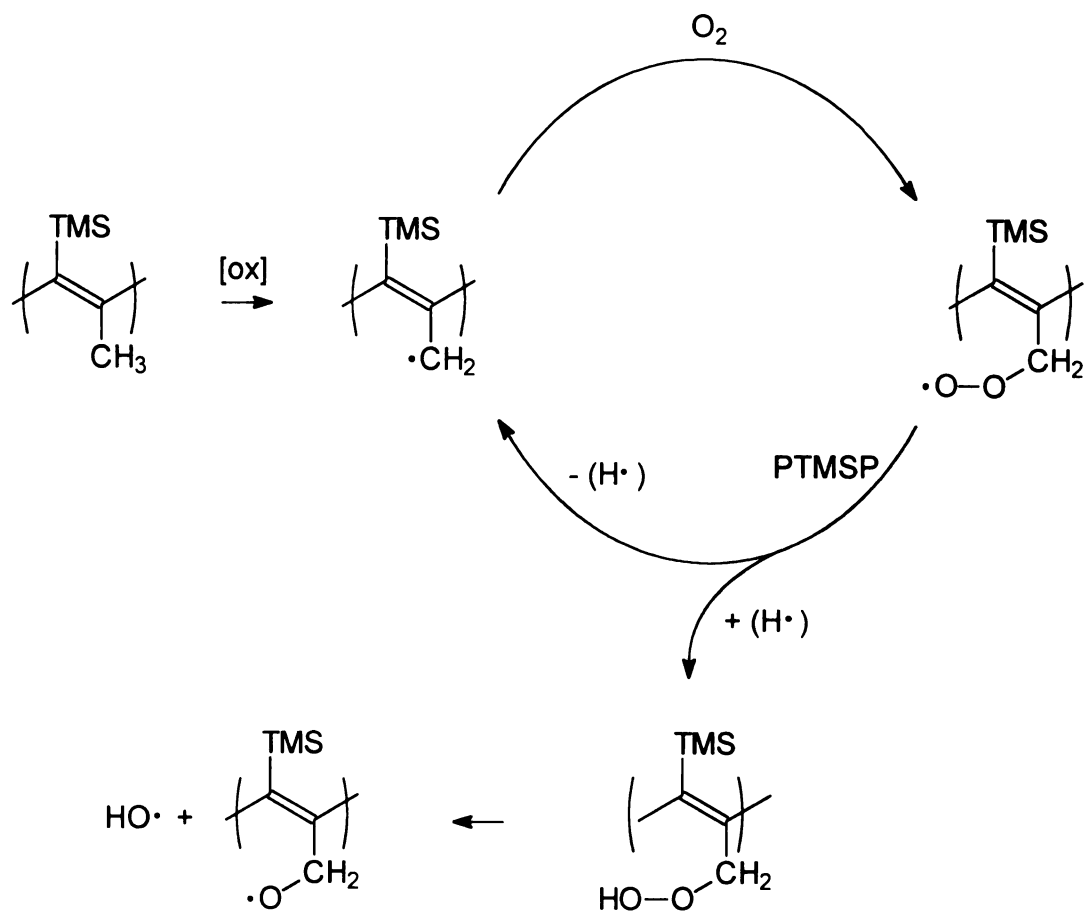


Figure 5.7. Peroxide induced chain degradation of PTMSP.

polymerized THF. When used for the preparation of the composites, this non-volatile material remained in the composite after drying, aiding in the degradation. To avoid this contamination, freshly distilled THF was passed through an activated alumina column immediately before use.

New composite coated fibers prepared using peroxide-free solvent were tested in varying oxygen concentration environments (Fiber 2). The intensity of the observed emission decreased in a stepwise manner as the concentration of oxygen surrounding the probe was systematically increased over time (Figures 5.8 and 5.9). The emission intensity stepped up to its original level upon reintroduction of pure nitrogen into the cell. The data indicated no spiking due to peroxide formation and polymer degradation, as was seen in the previous samples. When the raw data is fitted to the Stern-Vollmer equation, the value of K_q extracted from the experimental data from the solid state sensor probe is comparable to the quenching constants calculated from solution data,⁷ indicating that the clusters behave similarly in PTMSP (Figure 5.10).

To determine the sensor's operating temperature range, thermogravimetric analysis was performed on the components of the fiber sensors. Pieces of the fiber jacket and inner cladding were removed from the fiber core. The outer jacket is thermally stable to 325 °C under nitrogen, at which point it begins to yellow and becomes brittle. The inner cladding is slightly less thermally stable, rapidly degrading at 275 °C under nitrogen. The PTMSP/Mo₆Cl₁₂ composites are thermally stable to

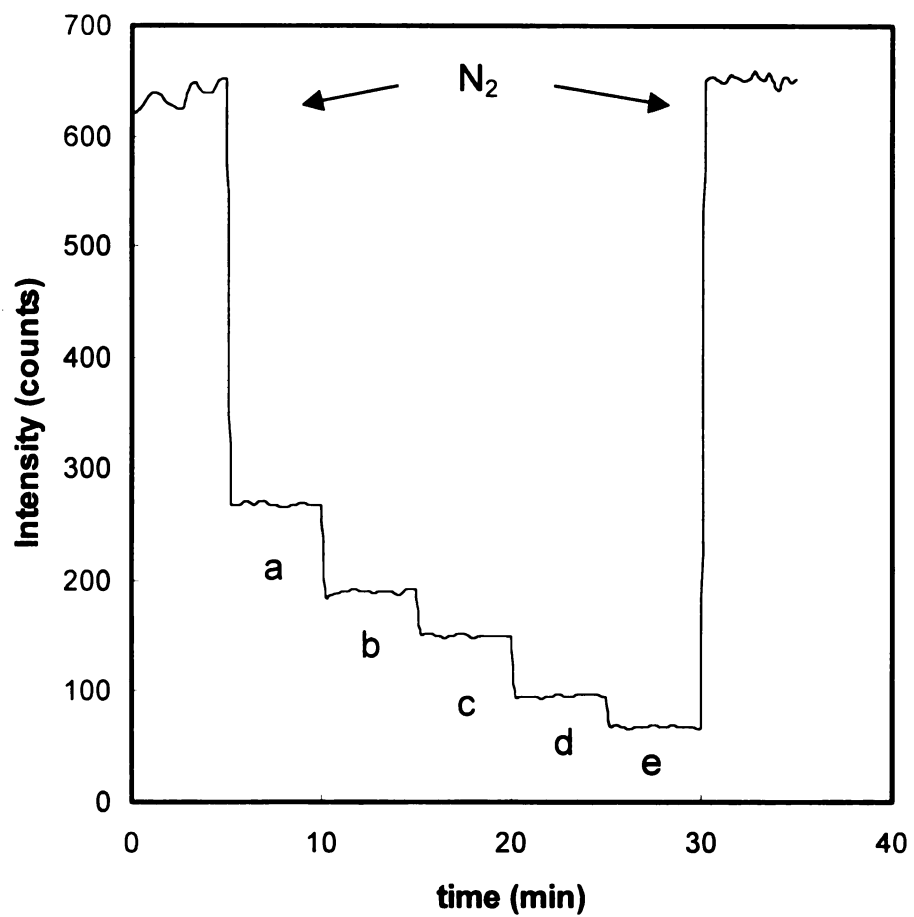


Figure 5.8. Observed emission intensity from Fiber 2 in nitrogen and a) 2.1%, b) 4.1%, c) 6.2%, d) 12.4%, and e) 20.6% oxygen containing environments.

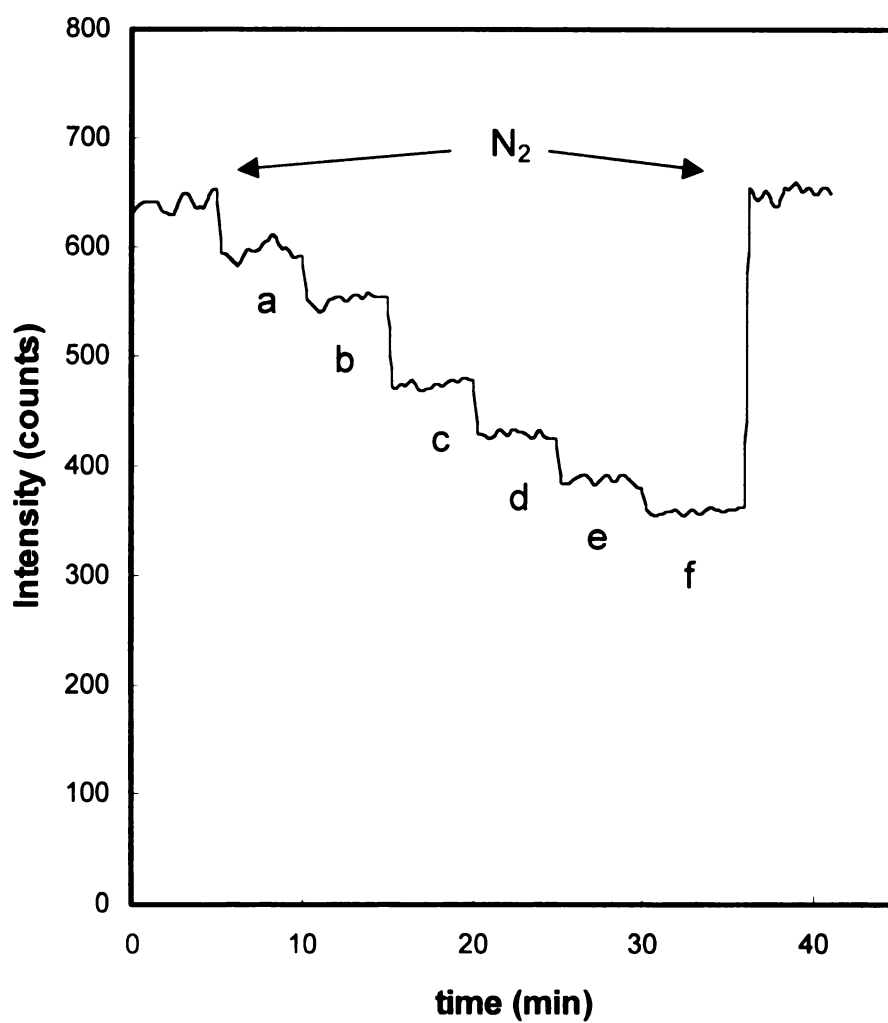


Figure 5.9. Observed emission intensity from Fiber 2 in nitrogen and a) 0.1%, b) 0.2%, c) 0.4%, d) 0.6%, e) 0.8% and f) 1.0% oxygen containing environments.

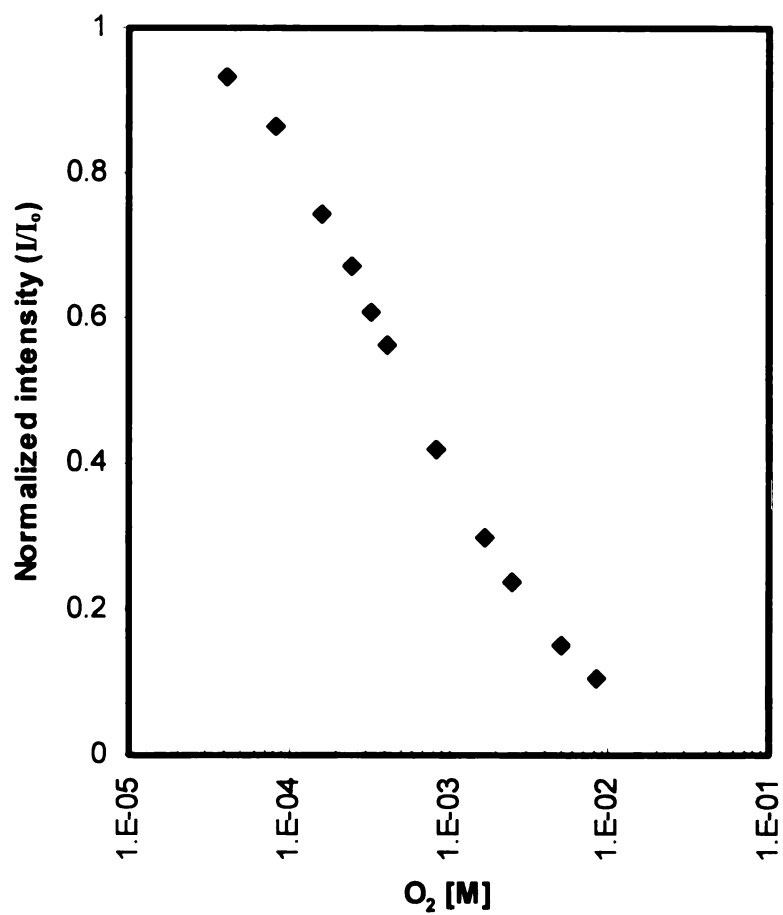


Figure 5.10. Stern-Vollmer plot of emission data from Fiber 2.

~350 °C under nitrogen, but begin to degrade about 10 degrees lower in air. Interestingly, the composites form significant amounts of residue (15-20 wt%) that are thermally stable past 400 °C. Under nitrogen, PTMSP alone completely degrades by 400 °C, leaving no residue. In air however, PTMSP exhibits only a 10 wt% residue at 400 °C, presumably due to the formation of cross-linked material. These data indicate that the added $\text{Mo}_6\text{Cl}_{12}$ clusters provide an alternative degradation pathway leading to thermally cross-linked material.

The stability of the composites at elevated temperatures was also investigated over an extended period of time. PTMSP and the PTMSP/ $\text{Mo}_6\text{Cl}_{12}$ composites were isothermally heated at 200 °C under nitrogen and air for 4 hours. Under inert conditions PTMSP undergoes a minor weight loss (0.7 wt%), but in air the weight loss increases (2.5 wt%) and the sample shows signs of yellowing. The composites lose 1.4 wt% under nitrogen, of which a small portion of this weight loss could be attributed to the loss of acetonitrile ligands. In air, the composite loses 2.6 wt% and begins to brown. From the thermal analysis results, the upper temperature limit of the sensor is 200 °C, currently limited by the stability of the composite matrix.

5.4. Discussion

Phase separation. A major problem encountered during the design of the fiber optic sensor was the phase separation of the molybdenum clusters from the polymer matrix. The molybdenum clusters favor reforming its polymeric structure after removal of solvent. Incorporation of the clusters into a PTMSP copolymer containing nitrile ligands proved ineffective, but preparation of a soluble adduct that could be physically dispersed in PTMSP allowed the formation of transparent samples. By replacing the bridging chlorides with acetonitrile ligands, the clusters did not phase separate from the matrix after removal of solvent. Transmission electron microscopy (TEM) was performed on the samples to determine the size of the clusters imbedded in the composite. However, the concentration of clusters was too high to yield useful data.

Permeability of composite. PTMSP was chosen as the polymer support due to its mechanical properties and high gas permeability. The addition of molybdenum clusters will no doubt occupy some of the free volume of the matrix, and as a result, lower the permeability. The oxygen permeability of the composite was not measured because of the difficulty of preparing large, uniform membranes free of defects. An estimate of the permeability can be made by comparing the composite to the PTMSP membranes containing added bis(aryl azide).¹³ Since the clusters and the bis(aryl azide)s are roughly the same size and the wt% amounts added are similar, the permeability through the composite should be comparable.

Degradation of composite matrix. The radical chain degradation process of PTMSP is a serious limitation to the lifetime of the composite based sensor. Small traces of oxidation in the polymer can lead to significant decreases in the molecular weight after a short period of time. After approximately 2 hours of testing, a sample of polymer was extracted off a sensor fiber tip. The molecular weight of the sample, as measured by GPC, dropped from 1,000,000 g/mol to 50,000 g/mol after testing. The sample still possessed good mechanical properties, but extended exposure would likely decrease the molecular weight below a usable level. More importantly, this degradation pathway introduces additional quenching species that interfere with the optical properties of the clusters. Sensor aging could be seen after prolonged cycling between oxygen and nitrogen. The signal intensity weakened and the depth of modulation needed to detect small changes in oxygen concentration decreased. The use of peroxide-free solvents to prepare the samples decreased the rate of sensor aging, but residual peroxides can lead to significant degradation over time.

Cross-linking. To expand the number of potential applications of these sensors, schemes to make the composite impervious to solvents would be desirable. This could be accomplished by using a cross-linkable polymer support. Fibers were prepared using composite solutions of poly[(1-trimethylsilyl-1-propyne)-*co*-(1-(4-azidobutyldimethylsilyl)-1-propyne)] and $\text{Mo}_6\text{Cl}_{12}$. We were able to adhere transparent beads of composite to the fiber tips, but during the cross-linking procedure, the samples severely darkened. The emission from these composite coated fibers

lacked the depth of modulation previously observed in the $\text{Mo}_6\text{Cl}_{12}$ /PTMSP composite coated fibers.

Although we are unable to cross-link the composite using azide chemistry, the sensors made from the PTMSP/ $\text{Mo}_6\text{Cl}_{12}$ composites may also operate in aqueous conditions. Since PTMSP does not swell in water, the large molybdenum clusters are unlikely to leach out of polymer matrix. This may expand the potential uses of the sensor to biological and biomedical applications, such as monitoring oxygen levels in blood.

5.5. Conclusions

A fiber optic oxygen sensor based on oxygen quenching of the red emission from molybdenum halide clusters was developed. PTMSP served as a mechanically stable, permeable support for the luminescent probes. Phase separation of the molybdenum clusters from the polymer matrix was overcome by forming a soluble acetonitrile adduct that dissolved in the polymer. Distinguishable steps in the emission intensity from the $\text{Mo}_6\text{Cl}_{12}$ /PTMSP composite coated fiber probes were observed in varying oxygen concentration environments ranging from 0.1 to 20%. Fast response times due to the highly permeable matrix were observed. The sensors do exhibit limited operating lifetimes however due to the photooxidation of the polymer matrix.

Sensors capable of detecting oxygen at lower concentrations could be fabricated using other molybdenum clusters (i.e. $\text{Mo}_6\text{Cl}_{14}^{-2}$) that have different quenching constants (K_q). Theoretically, a family of sensors capable of monitoring a wide gamut of gaseous oxygen concentrations could be produced by this method.

The present probe is thermally stable to at least 200 °C, limited by the polymer matrix. Since the $\text{Mo}_6\text{Cl}_{12}$ clusters are synthesized at 1000 °C, immobilization of the clusters in an inert, thermally stable sol-gel matrix is an attractive alternative.^{18,19} This would enable oxygen sensing in gaseous environments at elevated temperatures as well as liquid environments with varying salinity and pH.

5.6. References

- 1) Yamamoto, K.; Kasuga, T.; Nogami, M. *Appl. Phys. Lett.* **1998**, *73*, 3297-3299.
- 2) Mussell, R. D.; Nocera, D. G. *J. Phys. Chem.* **1991**, *95*, 6919-6924.
- 3) Azad, A. M.; Akbar, S. A.; Mhaisalkar, S. G.; Birkefeld, L. D.; Goto, K. S. *J. Electrochem. Soc.* **1992**, *139*, 3690-3704.
- 4) McNamara, K. P.; Li, X. P.; Stull, A. D.; Rosenzweig, Z. *Anal. Chim. Acta* **1998**, *361*, 73-83.
- 5) McNamara, K. P.; Rosenzweig, Z. *Anal. Chem.* **1998**, *70*, 4853-4859.
- 6) Schafer, V. H.; Schnering, H. G.; Tillack, J.; Kuhn, F.; Wohrle, H.; Baumann, H. *Z. Anorg. Chem.* **1967**, *353*, 281.
- 7) Jackson, J. A.; Turro, C.; Newsham, M. D.; Nocera, D. G. *J. Phys. Chem.* **1990**, *94*, 4500-4507.
- 8) Jackson, J. A.; Newsham, M. D.; Worsham, C.; Nocera, D. G. *Chem. Mat.* **1996**, *8*, 558-564.
- 9) Robinson, L. M.; Shriver, D. F. *J. Coord. Chem.* **1996**, *37*, 119-129.
- 10) Robinson, L. M.; Lu, H.; Hupp, J. T.; Shriver, D. F. *Chem. Mat.* **1995**, *7*, 43-49.
- 11) Shimomura, H.; Nakanishi, K.; Odani, H.; Kurata, M.; Masuda, T.; Higashimura, T. *Kobunshi Ronbunshu* **1986**, *43*, 747.
- 12) Mussell, R. D.; Nocera, D. G. *Inorg. Chem.* **1990**, *29*, 3711-3717.
- 13) Jia, J. P.; Baker, G. L. *J. Polym. Sci. Pt. B-Polym. Phys.* **1998**, *36*, 959-968.

- 14)Sergeev, G. B.; Petrukhina, M. A. *Prog. Solid State Chem.* **1996**, *24*, 183-211.
- 15)Golden, J. H.; Deng, H. B.; Disalvo, F. J.; Frechet, J. M. J.; Thompson, P. M. *Science* **1995**, *268*, 1463-1466.
- 16)Ruud, C. J.; Jia, J.; Baker, G. L. submitted to *Macromolecules* **1999**.
- 17)Ehrlich, G. M.; Warren, C. J.; Haushalter, R. C.; Disalvo, F. J. *Inorg. Chem.* **1995**, *34*, 4284-4286.
- 18)McDonagh, C.; MacCraith, B. D.; McEvoy, A. K. *Anal. Chem.* **1998**, *70*, 45-50.
- 19)Lin, J.; Brown, C. W. *Trac-Trends Anal. Chem.* **1997**, *16*, 200-211.